CHAPTER 15: THE OCEANS AS A CHEMICAL SYSTEM

INTRODUCTION

Antoine Lavoisier* called seawater "the rinsings of the Earth." Given the tenuous understanding of geological processes existing at the time (the late 18th century), this is a remarkably insightful observation. Most of the salts in the oceans are derived from weathering of the continents and delivered to the oceans by rivers. But the story of seawater is more complex than this. Some components of seawater are derived from hydrothermal metamorphism of the oceanic crust. Other components in seawater, most notably the principal anions as well as water itself, are derived from neither weathering nor hydrothermal reactions. These so-called "excess volatiles" are derived from volcanic degassing. Furthermore, salts do not simply accumulate in seawater. This point was overlooked by John Jolly in his attempt to estimate the age of the Earth, described in Chapter 8, from the mass of salts in the sea and the amount added annually by rivers. His result, 90 million years, is a factor of 50 less than the actual age of the Earth. The ocean is a dynamic, open system, and it is ultimately the balance between addition and removal of an element that dictates it concentration in the ocean. This was recognized by Georg Forschhammer in 1865 when he wrote: "*The quantity of different elements in seawater is not proportional to the quantity of elements which river water pours into the sea, but is inversely proportional to the facility with which the elements are made insoluble by general chemical or organo-chemical actions in the sea*." One of our objectives in this chapter will be to examine the budget of dissolved matter in the oceans; that is, to determine the sources and sinks and the rates at which salts are added and removed from the oceans.

Elements also cycle between different forms within the oceans; these include both organic and inorganic solids as well as various dissolved species. This internal cycling is intimately tied to the various physical, geological, and biological processes occurring within the ocean. The biota plays a particularly crucial role both in internal chemical cycling and in controlling the overall composition of seawater. A second objective of this chapter will be to examine how elements and compounds are distributed within the ocean, and how they cycle between various forms.

Lavoisier's statement also reminds us that the oceans are part of a grander geochemical system. Sediments deposited in the ocean provide a record of that system. On human time scales at least, the ocean appears to be very nearly in steady state. It is tempting to apply Lyell's principal of uniformitarianism and assume that the composition of the seawater has also been constant on geologic time scales. There is, however, strong evidence that some aspects of seawater composition do change over time, as we found in Chapters 8 and 9. Precisely because these variations are related to changes in other geological processes, such as plate tectonics, climate, life, and atmospheric chemistry, they can tell us much about the Earth's history and the workings of the planet. Interpreting these past changes begins with an understanding of how the modern ocean works and the controls on its composition. This understanding is our main goal for this chapter.

SOME BACKGROUND OCEANOGRAPHIC CONCEPTS

SALINITY, CHLORINITY, DENSITY, AND TEMPERATURE

A useful concept in oceanography is *salinity*. Salinity can be thought of as the total dissolved solids in seawater. More precisely, salinity is defined as: *the weight in grams of the dissolved inorganic matter in one kilogram of water after all the bromide and iodide have been replaced by the equivalent amount of chloride and all carbonate converted to oxide* (CO_2 driven off). This unfortunate defi-

*Antoine Lavoisier, born in France in 1843, is often called the father of modern chemistry. He died at the guillotine in 1794.

nition has an interesting historical basis. Robert Boyle† found that he could not reproduce total dissolved solid measurements by drying and weighing. The salinity definition is due to Thorensen, who would bubble Cl_2 gas, which substitutes for Br and I, through seawater. The salt could then be heated, converting carbonate to oxide, and a constant weight achieved. Salinity is now determined by measuring electrical conductivity, which increases in direct relation to the concentrations of ions in water, and hence with salinity. Another useful definition is *chlorinity*, which is *the halide concentration in grams per kilogram measured by titration with silver and calculated as if all the halide were chloride* (total halides are actually 0.043% greater than chlorinity). Chlorinity can also be measured by conductivity. As we shall see, Cl is always present in seawater as a constant proportion of total salt, and therefore there is a direct relationship between chlorinity and salinity. By definition:

$$S‰ = 1.80655\ Cl‰ \qquad 15.1$$

"Standard seawater", which is close to average seawater, has a salinity of 35.000 parts per thousand (ppt or ‰) and a chlorinity of 19.374 ‰. Open ocean water rarely has a salinity greater than 38‰ or less than 33‰.

Temperature, along with salinity, determines the density of seawater. Since density differences drive much of the flow of ocean water, these are key oceanographic parameters. Temperature in the oceans can be reported as *potential*, or *in situ* temperature, but the former is the most commonly used. In situ temperature is the actual temperature of a parcel of water at depth. Potential temperature, denoted θ, is the temperature the water would have if brought to the surface. The difference between the two is thus the temperature difference due to adiabatic expansion. Since water cools when it expands, potential temperature is always less than *in situ* temperature (except for surface water, where there is not difference). The difference is small, on the order of 0.1°C. While this difference is important to oceanographers, it is generally negligible for our purposes. Temperature and salinity, and therefore also density, are conservative properties of seawater, which is to say that they can be changed only at the surface.

The density of seawater is 2 to 3 percent greater than that of pure water. Average seawater, with a salinity of 35‰ and a temperature of 20°C, has a density of 1.0247 g/cc. Density is usually reported as the parameter σ, which is the per mil deviation from the density of pure water (1 g/cc). Thus if density is 1.0247 g/cc, σ is 24.7. Again, one can distinguish between *in situ* and potential density, potential density being the density water would have if brought to the surface, and is always lower than *in situ* density. The difference is small, a few percent, and generally negligible for our purposes.

Circulation of the Ocean and the Structure of Ocean Water

The concentrations of dissolved elements vary both vertically and horizontally in the ocean. To fully understand these variations, we need to know something about the circulation of the ocean. This circulation, like that of the atmosphere, is ultimately driven by differential heating of the Earth: solar energy is gained principally at low latitudes and lost at high latitudes. Because the mechanisms of surface and vertical circulation in the oceans are somewhat different, it is convenient to treat them separately.

Surface Circulation

Surface circulation of the ocean is driven primarily by winds; hence the surface circulation is sometimes also called the *wind-driven circulation*. Figure 15.1 is a simplified map of the wind-driven circulation. The important features are as follows:

• Both north and south of the climatic equator, known as the Inter-Tropical Convergence, or ITC, water moves from east to west, driven by the Trade Winds. These currents are known as the North

† Robert Boyle (1627-91) was another of the founders of modern chemistry. He defined the chemical element as the practical limit of chemical analysis, and deduced the inverse relationship between the pressure and volume of gas, a version of the ideal gas law.

Chapter 15: Oceans

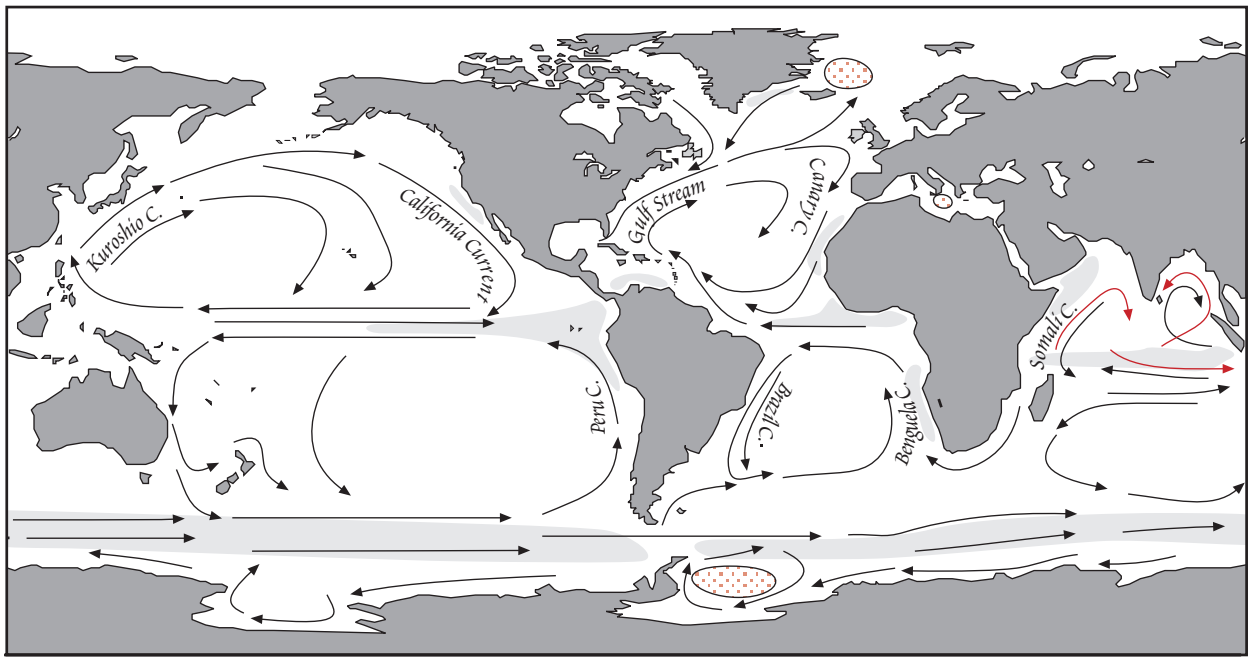

Figure 15.1. Surface and Deep Circulation of the oceans. Arrows show the direction of wind driven currents. Gray areas are regions of upwelling. Red stippled areas are regions of deep water production. In the Indian Ocean, black arrows show current directions in northern hemisphere winter, red arrows show current direction in northern hemisphere summer.

and South Equatorial Currents. Between these two currents, the Equatorial Counter Current runs from west to east.

• Two large gyres operate in both the Atlantic and Pacific Oceans, one in the northern and one in the southern hemisphere. Rotation is clockwise in the northern hemisphere and counter-clockwise in the southern hemisphere. The Coriolis Force, an apparent force that results from the Earth's rotation, is largely responsible for this circular current pattern. These currents are most intense in along the western boundaries of ocean basins, a phenomenon, also due to the Earth's rotation. Examples of intense western boundary currents are the Gulf Stream and Kuroshio Current.

• The circulation in the Indian Ocean is similar, but undergoes radical seasonal changes in response to the Monsoons. In northern hemisphere summer, the North Equatorial Current reverses and joins the equatorial countercurrent to become the Southwest Monsoon Current. The Somali Current, which flows to the southwest along the African Coast in northern hemisphere winter, reverses direction to flow northeastward in northern hemisphere summer.

• Water moves from west to east in Southern Ocean (the globe-encircling belt of ocean south of Africa and So. America). This is called the Antarctic Circumpolar Current or West Wind Drift. Directly adjacent the Antarctic coast, a counter current, called the Polar Current, runs east to west.

Density Structure and Deep Circulation

The deep circulation of the oceans is driven by density differences. Seawater density is controlled by temperature and salinity, so this circulation is also called the *thermohaline circulation*. Most of the ocean is stably stratified; that is, each layer of water is denser than the layer above and more dense than the layer below. Where this is not the case, a water mass will move up or down until it reaches a level of equilibrium density. *Upwelling* of deeper water typically occurs where winds or currents create a *divergence* of surface water. *Downwelling* occurs where winds or currents produce a *convergence* of surface water. Wind and current-driven upwelling and downwelling link the surface and deep circulation of the ocean.

CHAPTER 15: OCEANS

In the modern ocean, temperature differences dominate density variations and are principally responsible for deep circulation. This may not have always been the case, however. During warmer periods in the past, such as the Cretaceous, deep circulation may have been driven principally by salinity differences.

Figure 15.2 shows an example of how temperature, salinity, and density vary with depth in temperate and tropical regions. Both are usually nearly constant in the upper hundred meters or so as a result of mixing by waves (the actual depth of the mixed layer varied both seasonally and geographically, depend largely on wave height). Below the upper mixed layer is a region, called the *thermocline*, where temperature decreases rapidly. Salinity may also change rapidly in this region; a region where salinity changes rapidly is called a *halocline*. The temperature changes cause a rapid increase in density with depth, and this region of the water column is called the *pycnoline*. Below the pycnoline, temperature and salinity vary less with depth. Temperature and salinity are *conservative* properties of a water mass, which is to say that they can only be changed at the surface. Hence within the deep ocean, temperature and salinity vary only because of mixing of different water masses. In polar regions, water may be essentially isothermal throughout the water column.

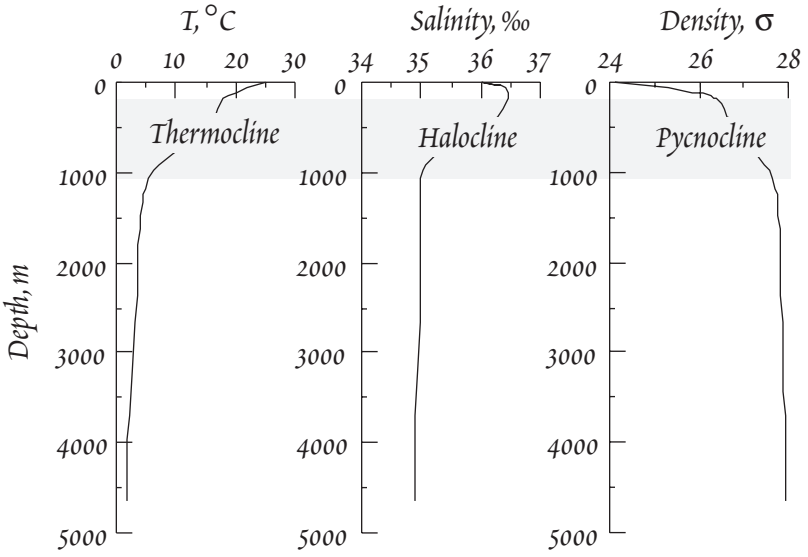

Figure 15.2. Temperature, salinity, and density variations at GEOSECS station 25 at 58° N in the North Atlantic. The station was occupied in September, and summer heating has extended the thermocline and pycnocline nearly to the surface. Gray area shows the position of the permanent thermocline and pycnocline. An inversion in the salinity profile near the surface indicates an excess of precipitation over evaporation.

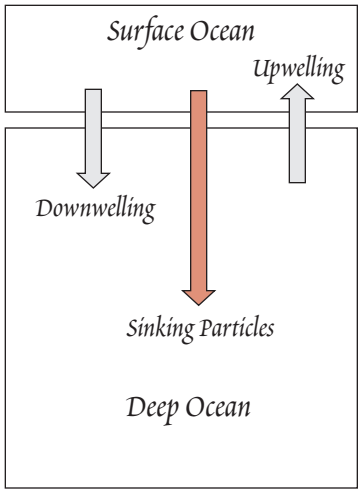

Figure 15.3. The two box model of the ocean and the fluxes between them.

The pycnocline represents a strong boundary to vertical mixing of water and effectively isolates surface water from deep water. This leads to a sometimes useful chemical simplification: the two-box model of the ocean. In this model, the ocean is divided into a box representing the surface water above the pycnoline, and one representing the deep water below it (Figure15.3). Fluxes between these boxes can occur both because of advection of water (upwelling and downwelling) and because of falling particles, both organic and inorganic. The upper box exchanges with the atmosphere and receives all the riverine input. All photosynthetic activity occurs in the upper box because light effectively does not penetrate below 100m (only 0.5% of the incident sunlight penetrates to a depth of 100 m, even in the clearest water). On the other hand, the flux out of the ocean of both particles and dissolved solids occurs through the lower box. Since the depth of the surface layer varies in the ocean and the density boundary is gradational rather than sharp, any definition of the size of the boxes is rather arbitrary. The depth of the boundary between the surface and deep layer may be variably defined, depending on the particular problem at hand. In Example 15.1, for

instance, we define it as 1000 m.

Water flows across the pycnocline only a few limited regions; we can divide these into regions of "intermediate water" formation and "deep water" formation (formation refers to a water mass acquiring its temperature and salinity characteristics at the surface and sinking through the pycnocline). Intermediate waters do not usually penetrate below depths of 1500 m; deep water may pene-

EXAMPLE 15.1. REPLACEMENT TIME OF DEEP OCEAN WATER

Use the simple two-box model in Figure 15.4 together with the following to estimate the residence time of water in the deep ocean. Take the boundary between the surface and deep water to be 1000m. Assume the system is at steady state and that $^{14}C/C$ ratio in deep water is 10% lower than in of surface water (Stuvier, et al., 1983).

Answer: Since we can assume the system is at steady state, the upward and downward fluxes of both water and carbon must be equal. Denoting the water flux by F_W we may write the mass balance equation for carbon in the deep water reservoir as:

$$F_W C_D = F_W C_S + F_{CP} \qquad 15.2$$

where C_D, C_S, and C_P are the concentrations of carbon in deep water and shallow water respectively, and F_{CP} is the flux of carbon carried by sinking particles. The sinking particle flux in thus just:

$$F_{CP} = F_W(C_D - C_S) \qquad 15.3$$

In other words, the sinking particle flux must account for the difference in carbon concentration between the surface and deep water.

We may now write a mass balance equation for ^{14}C in deep water by setting the loss of ^{14}C equal to the gain of ^{14}C. ^{14}C is lost through the upward flux of water and radioactive decay and gained by the downward flux of water and the sinking particle flux.

$$F_W C_D(^{14}C/C)_D - \lambda V_D C_D(^{14}C/C)_D = F_W C_S(^{14}C/C)_S + F_{CP}(^{14}C/C)_S \qquad 15.4$$

where $(^{14}C/C)_D$, and $(^{14}C/C)_S$ are the $^{14}C/C$ ratios in deep and shallow water respectively, V_D is the volume of deep water, and λ is the decay constant of ^{14}C. We have implicitly assumed that sinking particles have the same ^{14}C activity as surface water. Subsituting 15.3 into 15.4, we have

$$F_W C_D(^{14}C/C)_D + \lambda V_D C_D(^{14}C/C)_D = F_W C_S(^{14}C/C)_S + F_W(C_D - C_S)(^{14}C/C)_S \qquad 15.5$$

Rearranging and eliminating terms we have

$$\lambda V_D (^{14}C/C)_D = F_W (^{14}C/C)_S - F_W (^{14}C/C)_D \qquad 15.6$$

Another rearrangement and we arrive at:

$$V_D/F_W = [1 - (^{14}C/C)_D/(^{14}C/C)_S]/[\lambda(^{14}C/C)_D/(^{14}C/C)_S] \qquad 15.7$$

As we shall see later in this chapter, we define steady state residence time as the amount in a reservoir divided by the flux into it or out of it. Thus the above equation gives the residence time of water in the deep ocean (notice it has units of time). Substituting 0.1209×10^{-3} yr^{-1} for λ (Table 8.5) and 0.9 for $(^{14}C/C)_D/(^{14}C/C)_S$, we calculate a residence time of 920 years. This is somewhat longer than the residence time arrived at by Stuvier et al. (1983) through a more sophisticated analysis.

We can also use this equation to calculate the average upward velocity of water. Rearranging 15.7, we have:

$$F_W = V_D\lambda(^{14}C/C)_D/(^{14}C/C)_S/[1 - (^{14}C/C)_D/(^{14}C/C)_S] \qquad 15.8$$

If we express the volume of the deep ocean as the average depth, d, times area, A, we have:

$$F_W = Ad\lambda(^{14}C/C)_D/(^{14}C/C)_S/[1 - (^{14}C/C)_D/(^{14}C/C)_S] \qquad 15.9$$

Dividing both sides by A, we have:

$$F_W/A = d\lambda(^{14}C/C)_D/(^{14}C/C)_S/[1 - (^{14}C/C)_D/(^{14}C/C)_S] \qquad 15.10$$

F_W/A is the velocity. Taking d as 3000 m, we calculate F_W/A as 3.26 m/yr. (This calculation follows a similar one in Broeker and Peng, 1983).

trate to the bottom. There are four principal regions of intermediate water production. The first is in the Mediterranean where evaporation increases salinity of surface water to 37-38‰. Winter cooling further increases density causes this surface water to sink. It flows out of the Strait of Gibraltar and sinks in the Atlantic to a depth of about 1000 m where it spreads out. This water is known as Mediterranean Intermediate Water (MIW). Another intermediate water, known as Antarctic Intermediate Water, or AAIW, is produced at the convergence at the Antarctic Polar Front at about 50°S. North Pacific Intermediate Water is produced at the convergence Arctic Polar Front at about 50° N in the Pacific. North Atlantic Intermediate Water is also produced at the Arctic Polar Front at 50° to 60° N. Of these water masses, Antarctic Intermediate Water is the densest and most voluminous.

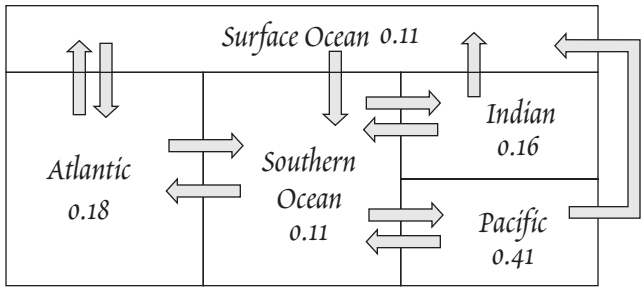

Figure 15.4. Simple two-dimensional box model of ocean circulation. The volumes of each reservoir are not given in units of 10^{18} m^3 (after Stuvier et al., 1983). In this case, the boundary between surface water and deep water is taken as 1500 m.

There are only two regions of deep water production, both at high latitudes. Antarctic Bottom Water (AABW), which is the densest and most voluminous deep water in the ocean, is produced primarily in the Weddell Sea. Cold winds blowing from Antarctica cool it, while freezing of sea ice increases its salinity. The other deep water mass, North Atlantic Bottom Water (NADW), is produced around Iceland in winter when winds cause upwelling and cooling of saline MIW. NADW then sinks and flows southward along the western boundary of the Atlantic. In the Southern Ocean it mixes with and becomes part of the AABW.

Mixing between deep water and water results in a slow, diffuse upward advection through the deep layer and then into the thermocline. Thus whereas the flux from the surface layer to the deep one is focused, the upward flux is diffuse. Final return from the thermocline to the surface occurs in localized zones of upwelling. The principal upwelling zones are those along the equator, where the trade winds create a divergence of surface water, along the west coasts of continents, where winds blowing along the coast drive the water offshore (this is a process known as Ekman transport and is related to the Coriolis force), and at the Antarctic divergence in the Southern Ocean.

With our knowledge of deep water circulation, we can extend our one dimensional model (Figure 15.3) to two dimensions (Figure 15.4). The model illustrates several important features of the deep circulation of the oceans. First, no deep water is produced in either the Pacific or Indian Oceans. Second, the Atlantic exports deep water and imports surface water. Both the Indian and Pacific import deep water and export surface water. Third, all exchanges of deep water take place via the Southern Ocean. This simple picture of deep water transport will allow us to easily understand some of the chemical differences between Pacific and Atlantic Ocean water. This model can also be used, together with ^{14}C activities, to determine the replacement time, or ventilation time, of deep water. Stuvier et al. (1983) used this model and ^{14}C activities measured at 124 stations occupied during the GEOSECS program from 1972 to 1978 to determine deep water residence times of 275, 250, and 510 years for the Atlantic, Indian, and Pacific Oceans respectively.

The Composition of Seawater

Table 15.1 lists the concentrations and chemical form of the elements in seawater. Concentrations range over 12 orders of magnitude (16 if H and O are included). From Figure 15.5 we see that the most abundant elements in seawater are those on the "wings" of the Periodic Table, the alkalis, the alkaline earths, and the halogens. In the terminology we introduced in Chapter 6, these elements form "hard" ions that have inert gas electronic structures. Bonding of these elements is predominately covalent; they have relatively small electrostatic energy and large radius (low Z/r ratio), so that in solution they are present mainly as free ions rather than complexes. Elements in the interior of the

periodic table are generally present at lower concentrations. These elements have higher Z/r ratios, form bonds of a more covalent character, and are strongly hydrolyzed. The latter tendency leads to their rapid removal by adsorption on particle surfaces. A few elements are exceptions to this pattern. These are elements, such as S, Mo, Tl and U, that form highly soluble oxyanion complexes, for example, SO_4^{2-}, MoO_4^{-2}, UO_2^{2+} or soluble simple ions (e.g., Tl^+).

Although solubility provides a guide to elemental concentrations in seawater, the composition of seawater is not controlled by solubility. Rather, the composition of seawater is controlled by a variety of processes, from tectonism on the planetary scale to surface adsorption/desorption reactions at the atomic scale.

Many of the same processes that remove the elements from seawater, and thus play a role in controlling its composition, also impose vertical, and to a lesser degree horizontal, concentration gradients in the ocean. Table 15.1 also assigns each element to one of three categories based on their vertical distribution in the water column: C: conservative, CG: conservative gas, N: biologically controlled, "nutrient-type" distribution), S: scavenged. In the following sections, we will examine the behavior of each of these groups and the processes responsible for these gradients.

SPECIATION IN SEAWATER

The wide variety of elements and the relatively high concentrations of ligands in seawater leads to the formation of a variety of complexes. The fraction of each element present as a given species may be calculated if the stability constants are known (Chapter 6). Calculation of major ion speciation requires an iterative procedure, similar to that in Example 6.7. Calculation of trace element speciation is fairly straightforward, as demonstrated in Example 15.2. Table 15.1 lists the principal

EXAMPLE 15.2. INORGANIC COMPLEXATION OF Ni IN SEAWATER

Using the stability constants (β^0) for Ni complexes and the free ligand concentrations in the adjacent table, calculate the fraction of total dissolved Ni in each form. Assume a temperature of 25°C. Use the following free single ion activity coefficients for the ligands: OH^-: 0.65, Cl^-: 0.63, CO_3: 0.2, SO_4: 0.17. Use the Davies equation (equation 3.88) to obtain the remaining activity coefficients.

Complex	Log β^0	Log [Cation]
$NiOH^+$	6.3	–5.7
$Ni(OH)_2$	12.1	–5.7
$NiCl^+$	2.8	–2.6
$NiCO_3$	13.1	–4.5
$Ni(SO_4)$	2.1	–2.0

Answer: Our first task is to calculate apparent stability constants for seawater, a high ionic strength solution. The ionic strength of seawater is 0.7; using the Davies equation, we calculate a log γ for Ni^{2+} of -0.5, and log γ of -0.125 for singly charged species and a log γ of 0 for neutral species. The apparent stability constants may then be calculated as:

$$\log \beta^* = \log \beta^0 + \log \gamma_{Ni} + \nu \log \gamma_L - \log \gamma_{NiL} \qquad 15.11$$

where L designates the ligand and ν is its stiochiometric coefficient (e.g., 2 for $Ni(OH)_2$, 1 for all others). The concentration of each complex is given by:

$$[NiL_n] = \beta^*[Ni^{2+}][L]^n$$

The conservation equation for Ni is:

$$\Sigma Ni = [Ni^{2+}] + [Ni(OH)^-] + [Ni(OH)_2] + [NiCl^-] + [NiSO_4] + [NiCO_3]$$

We can rewrite this as:

$$\Sigma Ni = [Ni^{2+}](1 + \beta^*[Ni^{2+}][OH^+] + \beta^*[Ni^{2+}][OH^+]^2 + \ldots)$$

PRINCIPAL Ni COMPLEXES IN SEAWATER

	log β^*	Log [NiL]/[Ni]	% form
Ni^{2+}		1	4.4%
$NiOH^+$	3.53	-2.17	0%
$Ni(OH)_2$	8.12	-3.28	0%
$NiCl^-$	0.02	-0.24	2.6%
$NiSO_4$	1.15	–0.85	0.6%
$NiCO_3$	5.82	-1.32	92%

A little rearranging allows us to obtain the fraction of Ni present as each species listed in the table. Ni is present predominately as carbonate, with minor amounts of the free ion and as chloride.

species present for each element. The major ions in seawater, Na^{2+}, K^{+}, Mg^{2+}, Ca^{2+}, Cl^{-}, SO_4^{2-}, and HCO_3^{-} are predominately present (>95%) as free ions. Many of the trace metals, however, are present primarily as complexes.

TABLE 15.1. CONCENTRATIONS OF ELEMENTS DISSOLVED IN SEAWATER AND RIVER WATER

Element	Average Seawater Concentration (μg/liter)	Average Seawater Concentration (μM/l)	Open Ocean Concentration Range	Principal Dissolved Species	Distribution	River Water Concentration (μg/liter)
H	1.1×10^8	55.6×10^6		H_2O	C	1.1×10^8
He	7.2×10^{-3}	0.0018		He	NG	—
Li	185	26.5		Li^+	C	12
Be	0.0023	2.5×10^{-5}	8-50 pM	$BeOH^+$, $Be(OH)_2$	S/N	—
B	4.61×10^3	427		$B(OH)_3$, $B(OH)_4^-$	C	18
C	2.64×10^4	2200		HCO_3^-, CO_3^{2-}, $MgHCO_3^+$	N	—
C(org.)	1×10^2	8.3		various	—	—
N	8540	610		N_2	CG	—
N	430	31		NO_3^-	N	—
O	8.9×10^8	55.6×10^6		H_2O	C	—
O	2870	179	0-200 μM	O_2	inverse N	—
F	1333	70.13		F^-	C	5.3
Ne	0.164	0.0081		Ne	CG	—
Na	1.105×10^7	4.806×10^5		Na^+	C	5,300
Mg	1.322×10^6	5.439×10^4		Mg^{2+}, $MgSO_4^{2-}$	C	3,100
A1	0.30	0.011	1-150 nM	$Al(OH)_3$, $Al(OH)_4^-$	S	50
Si	2800	100	0-250 μM	H_4SiO_4, $H_3SiO_4^-$	N	5,000
P	62	2.0	0-3.5μM	HPO_4^{2-}, $NaHPO_4^-$, $MgHPO_4$, PO_4^{-3}	N	115
S	9.063×10^5	2.826×10^4		SO_4^{2-}, $NaSO_4^-$, $MgSO_4^{2-}$	C	2840
Cl	1.984×10^7	5.596×10^5		Cl^-	C	4700
Ar	636	15.9		Ar	CG	—
K	4.10×10^5	1.046×10^4		K^+	C	1450
Ca	4.22×10^5	1.054×10^4		Ca^{+2}, $CaSO_4^{2-}$	~C	14,500
Sc	*0.0006*	*1.33×10^{-5}*		$Sc(OH)_3$	S/N	0.004
Ti	0.007	1.4×10^{-4}	4-560 pM	$TiO(OH)_4$	S/N	10
V	1.78	0.035	34-38 nM	HVO_4^{2-}, $H_2VO_4^-$	~C	0.8
Cr	0.2	0.004	2.3-5.5 nM	CrO_4^{2-}, $NaCrO_4^-$, $Cr(OH)_2^+$	S/N	1
Mn	0.02	3.7×10^{-4}	<0.3-40 nM	Mn^{+2}, $MnCl^+$	S	8.2
Fe	0.03	5.5×10^{-4}	0.05 – >6nM	Fe^{2+}, $FeCl^+$, $Fe(OH)_3$	S/N	50
Co	0.002	3.4×10^{-5}	7-70pM	Co^{+2}, $CoCl^+$	S	0.2
Ni	0.49	8.4×10^{-3}	3-12 nM	Ni^{+2}, $NiCl^+$, $NiCO_3$	N	0.5
Cu	0.15	2.4×10^{-3}	0.8-4nM	$CuCO_3$, $Cu(CO_3)_2^{2-}$, $CuOH^+$	S/N	1.5
Zn	0.38	0.006	0.5-9 nM	Zn^{+2}, $ZnCl^+$, $ZnSO_4$	N	30
Ga	0.0012	1.8×10^{-5}	2-30 pM	$Ga(OH)_3$	S/N	0.09
Ge	0.05	0.0007	<5-200 pM	H_4GeO_4,$H_3GeO_3^-$	N	0.09
As	1.23	0.016	13-27 nM	$As(OH)_3$, $As(OH)_4^-$	S/N	1.7
Se	0.159	0.002	0.5-2.5 nM	SeO_3^{2-}, SeO_4^{2-}	N	0.003
Br	6.9×10^4	863		Br^-	C	20
Kr	0.32	0.0038		Kr	CG	
Rb	124	1.45		Rb^+	C	1.5
Sr	7930	90.5	89-92 μM	Sr^{+2}	~C	60
Y	0.017	1.96×10^{-4}		YCO_3^+, $Y(CO_3)_2^-$	S/N	0.008
Zr	0.012	1.6×10^{-4}	10-300 pM	$Zr(OH)_5^{1-}$	S/N	0.09
Nb	*0.0046*	*5×10^{-5}*		NbO_6^-, NBO_5	S?	—
Mo	11	0.114		MoO_4^{-2}	C	0.5
Ru	<0.005	$<5 \times 10^{-5}$		—	?	—
Rh	.08	8×10^{-4}		—	N	—

TABLE 15.1 (CONTINUED)

Element	Average Seawater Concentration (μg/liter)	(μM/l)	Open Ocean Concentration Range	Principal Dissolved Species	Distribution	River Water Concentration (μg/liter)
Pd	4.3×10^{-5}	4×10^{-7}	0.2-0.7 pM	$PdCl_4^{2-}$	N	— —
Ag	0.023	2.2×10^{-5}	1-30 pM	AgCl	N	0.3
Cd	0.067	6×10^{-4}	0-1000 pM	$CdCl^+$, $CdCl_2$	N	0.02
In	0.00001	9×10^{-8}	0.02-0.15 pM	$In(OH)_3$	S	—
Sn	4.7×10^{-4}	4×10^{-6}	1.4-40 pM	$SnO(OH)_3^-$	S	—
Sb	0.24	0.002	0.7-2 nM	$Sb(OH)_3$	~C	0.008
Te	0.0001	8×10^{-7}	0.1-1.7 nM	$Te(OH)_6$, TeO_3^{2-}, $HTeO_3^-$	S	—
I	59.5	0.468	0.4-0.6 μM	IO_3^-	~C	0.05
Xe	0.065	5×10^{-4}		Xe	CG	—
Cs	0.3	2.3×10^{-3}		Cs^+	C	0.035
Ba	15	0.11	30-130 pM	Ba^{+2}, $BaCl^+$	N	60
La	5.7×10^{-3}	4.13×10^{-5}	4-50 pM	$LaCO_3^+$, $La(CO_3)_2^-$	S/N	0.019
Ce	7.2×10^{-4}	5.12×10^{-6}	2-8 pM	$CeCO_3^+$, $Ce(CO_3)_2^-$	S/N	0.024
Pr	7.2×10^{-4}	5.09×10^{-6}	1-10 pM	$PrCO_3^+$, $Pr(CO_3)_2^-$	S/N	0.005
Nd	3.4×10^{-3}	2.35×10^{-5}	3-40 pM	$NdCO_3^+$, $Nd(CO_3)_2^-$	S/N	0.018
Sm	5.8×10^{-4}	3.89×10^{-6}	1-8 pM	$SmCO_3^+$, $Sm(CO_3)_2^-$	S/N	0.004
Eu	1.7×10^{-4}	1.15×10^{-6}	0.1-2 pM	$EuCO_3^+$, $Eu(CO_3)_2^-$	S/N	0.001
Gd	9.2×10^{-4}	5.87×10^{-6}	1-10 pM	$GdCO_3^+$, $Gd(CO_3)_2^-$	S/N	0.006
Tb	1.7×10^{-4}	1.1×10^{-6}	0.3-2 pM	$TbCO_3^+$, $Tb(CO_3)_2^-$	S/N	0.001
Dy	1.12×10^{-3}	6.94×10^{-6}	1.5-13 pM	$DyCO_3^+$, $Dy(CO_3)_2^-$	S/N	0.005
Ho	3.7×10^{-4}	2.24×10^{-6}	0.4-3.7 pM	$HoCO_3^+$, $Ho(CO_3)_2^-$	S/N	0.001
Er	1.2×10^{-3}	7.35×10^{-6}	1.5-12 pM	$ErCO_3^+$, $Er(CO_3)_2^-$	S/N	0.004
Tm	2×10^{-4}	1.21×10^{-7}	0.3-2 pM	$TmCO_3^+$, $Tm(CO_3)_2^-$	S/N	0.001
Yb	1.23×10^{-3}	7.11×10^{-6}	1.5-13 pM	$YbCO_3^+$, $Yb(CO_3)_2^-$	S/N	0.005
Lu	2.3×10^{-4}	1.35×10^{-6}	0.3-2.3 pM	$LuCO_3^+$, $Lu(CO_3)_2^-$	S/N	0.001
Hf	1.6×10^{-4}	9×10^{-7}	0.4-2.4 pM	$Hf(OH)_5^-$	S/N	2.5×10^{-3}
Ta	*2.5×10^{-3}*	*1.4×10^{-5}*		$Ta(OH)_5$	S?	—
W	0.010	5.4×10^{-5}		WO_4^{2-}	~C	1.6×10^{-4}
Re	0.0074	3.96×10^{-5}		ReO_4^-	C	0.0004
Os	*1.7×10^{-6}*	*9×10^{-9}*		—	?	—
Ir	*1×10^{-6}*	*6×10^{-9}*		Ir^{3+}	S?	—
Pt	5×10^{-5}	2.6×10^{-7}		$PtCl_4^{2-}$, $PtCl_6^{2-}$	~C	—
Au	2×10^{-5}	1×10^{-7}	0-240 fM	$AuOH(H_2O)$, $AuCl$, $AuCl_2^-$	S?	0.0001
Hg	0.00014	7×10^{-7}	0.2-2 pM	$HgCl_4^{2-}$, $HgCl_3^-$, $HgCl_2$	S/N	0.07
Tl	1.3×10^{-2}	6.5×10^{-5}	58-78 pM	Tl^+, $TlCl$	~C	3.5×10^{-4}
Pb	2.7×10^{-3}	1.3×10^{-5}	3-170 pM	$PbCl^-$,$PbCl_2$, $PbCO_3$	S	0.01
Bi	3×10^{-5}	1.4×10^{-7}	10-500 fM	BiO^+, $Bi(OH)_2^+$	S	—
Po	—	—		—	—	—
At	—	—		—	—	—
Rn	—	—		Rn	—	—
Fr	—	—		Fr^+	—	—
Ra	1.3×10^{-7}	5.8×10^{-10}		Ra^{+2}	N	—
Ac	—	—		—	—	—
Th	2×10^{-5}	8.6×10^{-8}	50-650 fM	$Th(OH)_4$	S	0.1
Pa	—	—		—	—	—
U	3.3	0.0138		$UO_2(CO_3)_3^{-4}$	C	0.19

Concentrations based on single analyses or only pre-1980 data are shown in italics. Category: C Conservative, N: Nutrient/Biologically Controlled, S: Scavenged CG: conservative gas; NG non-conservative gas. Sources: Seawater Concentrations: modified from Martin and Whitfield (1983), Broecker and Peng (1982), and Quinby-Hunt and Turekian (1983), and the electronic supplement to Nozaki (1997); Speciation: Morel and Hering (1995), Turner and Whitfield (1981), Cantrell and Byrne (1987), Bruland (1983), Erel and Morgan (1991); River Concentrations: Table 12.2, and modified from Martin and Whitfield (1983), Broecker and Peng (1982).

Chapter 15: Oceans

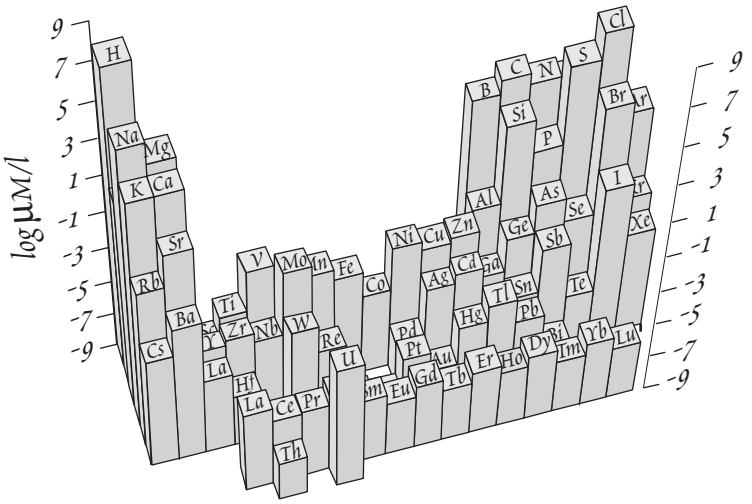

Figure 15.5. The composition of seawater. The most abundant elements are those on the sides of the periodic table. Elements in the interior tend to be less abundant.

Conservative Elements

The conservative elements share the property of being always found in constant proportions to one another and to salinity in the open sea, even though salinity varies. All the major ions in seawater, except for bicarbonate, are included in this group. Their concentrations are listed in Table 15.2. This constancy of the major ion composition of seawater, which is typically expressed as a ratio to Cl, is sometimes called the *Law of Constant Proportions*, and has been known for nearly 2 centuries. For most purposes, we may state that concentrations of these elements vary in the ocean only as a result of dilution or concentration of dissolved salts by addition or loss of pure water. While chemical and biological processes occur within the ocean do change seawater chemistry, they have an insignificant effect on the concentrations of conservative elements.

The major ions do vary in certain unusual situations, namely (1) in estuaries, (2) in anoxic basins (where sulfate is reduced), (3) when freezing occurs (sea ice retains more sulfate than chloride), (4) in isolated basins where evaporation proceeds to the point where salts begin to precipitate, and (5) as a result of hydrothermal inputs to restricted basins (e.g. red sea brines). Ca and Sr are slight exceptions to the rule in that they are inhomogeneously distributed even in the open ocean, though only slightly. The concentrations of these elements, as well as that of HCO_3^-, vary as a result of biological production of organic carbon, calcium carbonate, and strontium sulfate† in the surface water and sinking of the remains of organisms into deep water. Most of these biologically produced particles breakdown in deep water, releasing these species into solution (we explore this in greater detail below). Thus there is a particulate flux of carbon, calcium, and strontium from surface waters to deep waters. As a result, deep water is about 15% enriched in bicarbonate, 1% enriched in Sr, and 0.5% enriched in Ca relative to surface water. As we shall see, these biological processes also create much larger vertical variations in the concentrations of many minor constituents.

Some minor and trace elements are also present in constant proportions; these include Rb, Mo, Cs, Re, Tl, and U. Vanadium is nearly conservative, with a total range of only about ±15%. All these elements share the properties that they are not extensively utilized by the biota and form ions or radicals that are highly soluble and not surface reactive.

Table 15.2. Major Ions in Seawater

Ion	g/kg (ppt) at S = 35‰	Percent of Dissolved solids
Cl^-	19.354	55.05
SO_4^{2-}	2.649	7.68
HCO_3^-	0.140	0.41
$B(OH)_4^-$	0.0323	0.07
Br^-	0.0673	0.19
F^-	0.0013	0.00
Na^+	10.77	30.61
Mg^{2+}	1.290	3.69
Ca^{2+}	0.412	1.16
K^+	0.399	1.10
Sr^{2+}	0.008	0.03

Dissolved Gases

The concentrations of dissolved gases in the oceans are maintained primarily by

† A class of protozoans called Acantharia build shells of $SrSO_4$.

exchange with the atmosphere. These gases may be divided into conservative and non-conservative ones. The noble gases and nitrogen constitute the conservative gases. As their name implies, their concentrations are not affected by internal processes in the ocean. Concentrations of these gases are governed entirely by exchange with the atmosphere. Since they are all minor constituents of seawater, we can use Henry's Law to describe the equilibrium solubility of atmospheric gases in the ocean:

$$C = kp \qquad 15.12$$

where C is the concentration in seawater, k is the Henry's Law constant, or Bunsen absorption coefficient, and p is the partial pressure of the gas in the atmosphere. The equilibrium concentrations of atmospheric gases in seawater at 1 atm (0.1 MPa) are listed in Table 15.3. The conservative gases are not uniformly distributed in the ocean. This is because of the temperature dependence of gas solubility: they are more soluble at lower temperature. Over a temperature range of 0° to 30° C, this produces a variation in dissolved concentration of about a factor of two for several gases. As may be seen in Figure 15.6 and Table 15.3, the temperature dependence is strongest for the heavy noble gases and CO_2, and weakest for the light noble gases. Thus the concentration of conservative gases in seawater depends on the temperature at which atmosphere-ocean equilibration occurred. Another interesting aspect of the solubilities curves in Figure 15.6 is their non-linearity. Because of this non-linearity: mixing between water masses that have equilibrated with the atmosphere at different temperatures will lead to concentrations above the solubility curves. We also notice in Figure 15.6 that solubility for the different gases ranges over nearly 2 orders of magnitude; the light noble gases are the least soluble; the heavy noble gases and CO_2 are the most soluble.

Table 15.3. Dissolved Gases in Seawater

	Atmospheric Partial Pressure	Equilibrium Conc. in Seawater (ml/l) 0°C	24°C
He	5.2	4.1×10^{-5}	3.8×10^{-5}
Ne	1.8	1.8×10^{-4}	1.5×10^{-4}
N_2	0.781	14.3	9.2
O_2	0.209	8.1	5.0
Ar	9.3×10^{-3}	0.39	0.24
Kr	1.1×10^{-6}	9.4×10^{-5}	8.5×10^{-5}
Xe	8.6×10^{-8}	1.7×10^{-5}	8.5×10^{-6}
CO_2	3.6×10^{-4}	0.47	0.24
N_2O	3×10^{-7}	3.2×10^{-4}	1.4×10^{-4}

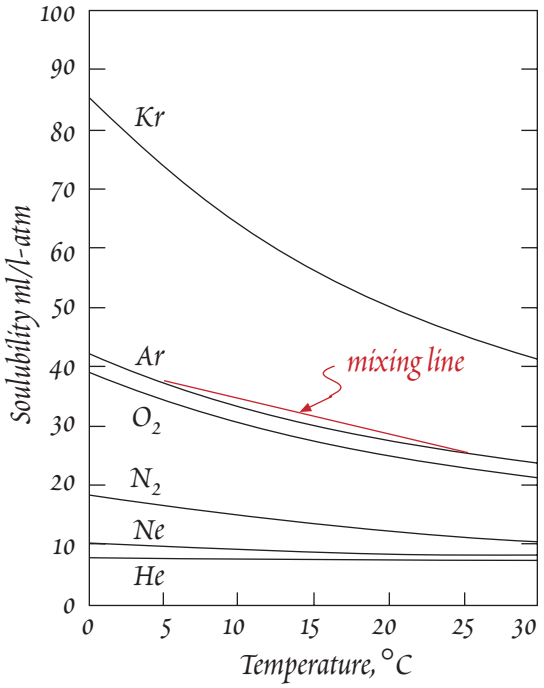

Figure 15.6. Solubility of gases in seawater as a function of temperature. Adapted from Broeker and Peng (1982).

Gas solubility is also strongly dependent on salinity and pressure. For example, at 20 ° C the solubility of oxygen is 20% lower in seawater with a salinity of 35‰ than in pure water. Over the range of salinities typical of open ocean water (34‰ to 38‰) solubility of oxygen varies by about 3%. According to equation 15.11, the equilibrium concentration will increase directly with pressure. Atmospheric pressure at the air-sea interface is effectively constant; however, pressure increases rapidly with depth in the ocean, by 1 atm for every 10 meters depth. When actual concentrations are compared with predicted equilibrium concentrations, the surface ocean is oversaturated by a few percent. This is thought to be due to bubbles, produced by breaking waves, being carried to depth in the ocean. Bubbles need only be carried to depths of a few tens of centimeters to account for the observed oversaturation.

O_2 and CO_2 are the principal non-conservative gases. They vary because of photosynthesis and respiration. Nitrogen is also biologically utilized. However, only a small fraction of the dissolved N_2 is present as "fixed" nitrogen (as NH_4,

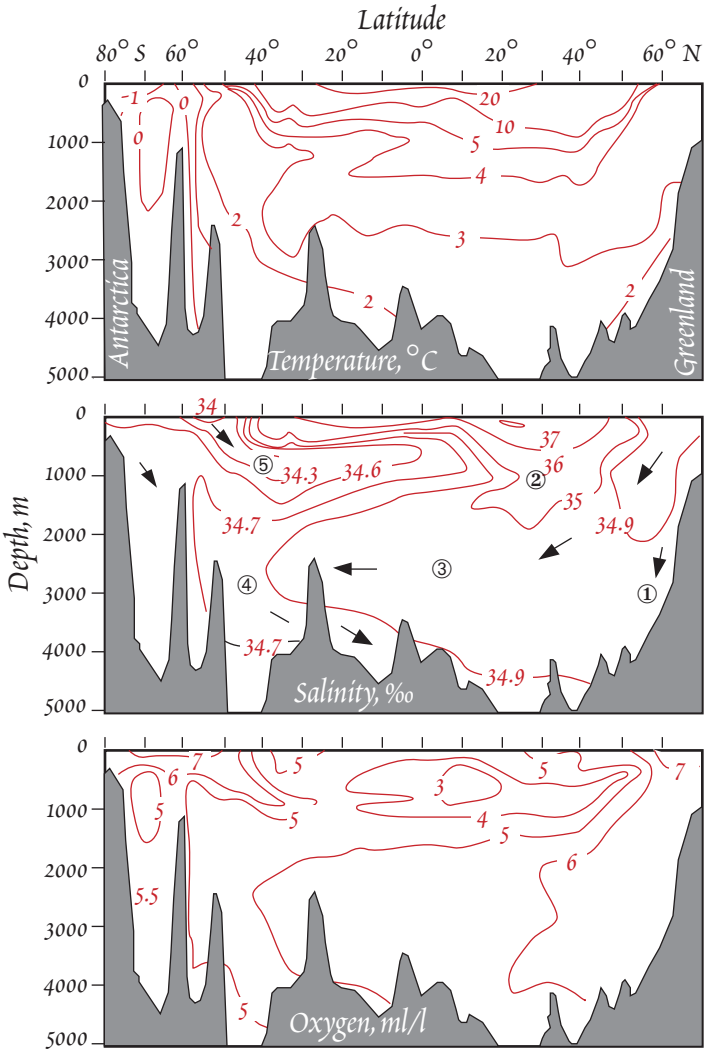

Figure 15.7. Temperature, salinity and oxygen distribution in a north-south cross-section of the Atlantic Ocean. The salinity panel also shows water movements and water masses, indicated by numbers: ① North Atlantic Bottom Water, ② Mediterranean Water, ③ N. Atlantic Deep Water, ④ Antarctic Bottom Water, ⑤ Antarctic Intermediate Water.

NO_3^-, and N_2O), hence N_2 behaves effectively as a conservative element.

Helium is another non-conservative gas because of the input of He to the ocean by hydrothermal activity at mid-ocean ridges. Elevated He concentrations and high $^3He/^4He$ ratios found at mid-depth, particularly in the Pacific, reflecting this injection of mantle He by mid-ocean ridge hydrothermal systems. In the following sections, we examine the variation of O_2 and CO_2 in the ocean in greater detail.

O_2 Variation in the Ocean

Biological activity occurs throughout the oceans, but is concentrated in the surface water because it is only there that there is sufficient light for photosynthesis. This part of the water column is called the *photic zone*. Both respiration and photosynthesis occur in the surface water, but the rate of photosynthesis exceeds that of respiration in the surface ocean, so there is a net O_2 production the surface layer. Most organic matter produced in the surface ocean is also consumed there, by a small fraction sinks into the deep water. This sinking organic matter is consumed by bacteria and scavenging organisms living in the deep water. Respiration in the deep water and the absence of photosynthesis results in a net consumption of oxygen. Within the deep water, two factors govern the distribution of oxygen. The first is the "age" of the water, the time since it last exchanged with the atmosphere. The longer deep water has been away from the surface, the more depleted in oxygen it will be. The second factor is the abundance of organic matter. The abundance of food decreases with depth, so that respiration, and hence oxygen consumption, is highest just below the photic zone and lowest in the deepest water. Thus the vertical distribution of oxygen is characterized by an oxygen minimum that typically occurs within the thermocline. Furthermore, the rate of organic matter production in the surface waters varies geographically (for reasons we will subsequently discuss). Oxygen is more depleted in deep water underlying high biological productivity regions that beneath regions of low productivity.

Figure 15.7 shows the distribution of O_2 in the Atlantic Ocean. Highest O_2 concentrations are found in surface waters at high latitudes, where the water is cold and the solubility of O_2 is highest. The

minimum O_2 concentrations are found in mid-latitudes at depths of 500 to 1000 m. Oxygen minima at these depths characterize most of the world ocean at temperate and tropical latitudes. At greater depth, as well as at higher latitudes, the concentration of O_2 is higher because the water there is generally younger, i.e., it has more recently exchanged at the surface. Because deep water in the Pacific and Indian Oceans is older than deep water in the Atlantic, oxygen concentrations are generally lower. A particularly strong O_2 depletion occurs beneath high productivity regions of the eastern equatorial Pacific and conditions are locally suboxic (i.e., no free O_2). Anoxic conditions develop in deep water in basins where the connection to the open ocean is restricted. The best example is the Black Sea. The Black Sea is a 2000 m deep basin whose only connection with the rest of the world ocean is through the shallow Bosporus Strait. As a result, water becomes anoxic at a depth of about 100 m. Anoxia is also present in the Curaco Trench, off the northern coast of South America. Here anoxia is a result both of restricted circulation and high productivity in the overlying surface water. Anoxic conditions also develop in some deep fjords.

Distribution of CO_2 in the Ocean

As we found in previous chapters, most CO_2 dissolved in water will be present as carbonate or bicarbonate ion. Nevertheless, we will often refer to all species of carbonate and CO_2 simply as CO_2. CO_2 cannot be treated strictly as a dissolved gas, as there are sinks and sources of CO_2 other than the atmosphere. For example, much of the dissolved CO_2 is delivered to the ocean by rivers as bicarbonate ion. These properties make the distribution of CO_2 more complicated than that of other gases.

Like oxygen, CO_2 concentrations are affected by biological activity and its solubility is affected by temperature. These factors result in a significant geographic variation in CO_2 in surface water. Surface water is often supersaturated with respect to the atmosphere in equatorial regions as upwelling brings CO_2-riched deeper water to the surface and warming decreases it solubility. In the subtropical gyres P_{CO_2} is generally maintained below saturation values by photosynthesis. The greatest degree of undersaturation occurs in polar regions, where photosynthesis decreases CO_2 and cooling increases it solubility. The North Pacific is an exception as it appears to be supersaturated both within much of the North Pacific gyre and at high latitudes (Takahashi, 1989). Thus there is a net flux of CO_2 from the ocean to the atmosphere in low latitudes and a net flux from the atmosphere to the ocean in high latitudes.

Biological activity is responsible for vertical variations in CO_2 in the ocean. Photosynthesis converts CO_2 to organic matter in the surface water. Most of this organic matter is remineralized within the photic zone, but some 5% is transported out of this zone into deep water (mainly by falling fecal pellets, etc.; but vertically migrating zooplankton and fish also transport organic carbon from the surface to the deep layer), depleting surface water in CO_2. Respiration converts most of the falling organic matter back into dissolved CO_2 and only a very small fraction of the organic matter produced is buried in the sediment. This aspect of biological activity thus affects CO_2 distributions in exactly opposite way it affects oxygen. However, a few planktonic organisms, most notably foraminifera (protozoans), pteropods (snails), and coccolithophorids (algae), produce carbonate shells, which results in an additional extraction of CO_2 from surface waters. These shells, or tests as they are properly called, also sink into the deep water when the organisms die. The solubility of calcium carbonate increases with depth, for reasons we will discuss shortly, so that much of the car-

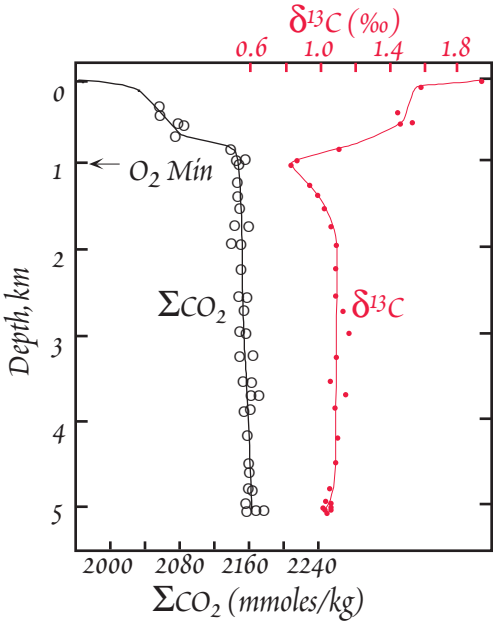

Figure 15.8. Depth profile of total dissolved inorganic carbon (ΣCO_2) and $\delta^{13}C$ of dissolved inorganic carbon in the North Atlantic.

bonate redissolves. The total amount of dissolved CO_2 converted to carbonate is small compared to that converted to organic carbon. However, a much large fraction of biogenic carbonate sinks out of the photic zone, so that the downward flux of carbon in carbonate represents about 20% of the total downward flux of carbon. A larger fraction of carbonate produced is also buried, so that the flux of carbon out the ocean is due primarily to carbonate sedimentation rather than organic matter sedimentation.

The transport of CO_2 from surface to deep water as organic matter and biogenic carbonate is called *the biological pump*. As we might expect, the biological pump produces an enrichment of CO_2 in the deep ocean over the shallow ocean, as is illustrated in Figure 15.8. Many vertical profiles of ΣCO_2 show a maximum at the same depth as the oxygen minimum, although the example in Figure 15.8 does not. It occurs for the same reasons as the oxygen minimum: there is more organic matter at this level and hence higher respiration, and deep water is often "younger". As does oxygen enrichment, the extent of enrichment of CO_2 in deep water depends on the age of the water mass and the downward flux of organic matter (and therefore ultimately on the intensity of photosynthesis in the overlying water). It depends additionally on the rate of calcium carbonate dissolution.

Biological activity also produces a variation in the isotopic composition of carbon is seawater. We found in Chapter 9 that photosynthetic organisms utilize ^{12}C in preference to ^{13}C. Thus photosynthetic activity in the upper layer depletes surface water in ^{12}C, increasing $\delta^{13}C$. When organic matter is remineralized at depth, the opposite occurs: deep water in enriched in ^{12}C. Biological activity therefore imposes a gradient in $\delta^{13}C$ on the water column (Figure 15.8). Comparing the ΣCO_2 with the $\delta^{13}C$ profile, we see that the latter shows a pronounced maximum while the former does not. Why? The answer to this question is left as a problem at the end of the chapter.

The extent of depletion of ^{12}C in surface water will depend on biological activity: $\delta^{13}C$ will be higher in productive waters than in unproductive waters. The extent of enrichment of ^{12}C in deep water, as does CO_2, depends on the age of the deep water. "Old" deep water will have lower $\delta^{13}C$ than "young" deep water.

SEAWATER pH AND ALKALINITY

We found in Chapter 6 that the pH of most natural waters is buffered by the carbonate system and this is certainly true of seawater. Compared to other natural waters, seawater has a relatively constant pH, with a mean of about 8, but the variations in dissolved CO_2 do produce pH variations of about ±0.3. This variation is largely due to biological activity: removal of dissolved CO_2 by photosynthesis increases pH, while release of CO_2 by respiration decreases it. The reason for this is easy to understand. At the pH of seawater, bicarbonate is the predominant carbonate species. Thus we can describe the dissolution of CO_2 as:

$$CO_2 + H_2O \rightleftarrows H^+ + HCO_3^- \qquad 15.13$$

Photosynthesis extracts CO_2 from water, so reaction 15.13 is driven to the left, consuming H^+. Respiration produces CO_2, driving this reaction to the right, producing H^+. For this reason, the pH of the ocean decreases with depth. In the profile shown in Figure 15.9, we see a minimum in pH at the same depth as the O_2 minimum, reflecting the high rate of respiration at this depth.

pH is also affected by precipitation and dissolution of calcium carbonate. Since bicarbonate is the most abundant carbonate species, the precipitation reaction is effectively:

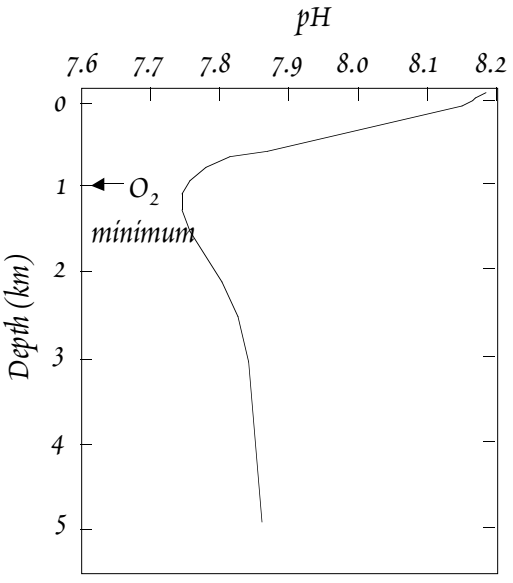

Figure 15.9. pH profile in the North Pacific Ocean. Position of the oxygen minimum is shown.

$$Ca^{2+} + HCO_3^- \rightleftarrows H^+ + CaCO_3 \qquad 15.14$$

Here is it easy to see that precipitation of calcium carbonate decreases pH while dissolution increases it. Thus production of biogenic carbonate in surface water and its dissolution in deep water acts to reduce the vertical pH variations produced by photosynthesis and respiration.

Another important parameter used to describe ocean chemistry, and one closely related to pH is alkalinity. In Chapter 6 we defined alkalinity as the sum of the concentration (in equivalents) of bases that are titratable with strong acid. It is a measure of acid-neutralizing capacity of a solution. An operational definition of total alkalinity for seawater is:

$$Alk = [HCO_3^-] + 2[CO_3^{2-}] + [B(OH)_4^-] + [H_2PO_4^-] + 2[HPO_4^{2-}] + [NO_3^-] + [OH^-] - [H^+] \qquad 15.15$$

Often, particularly in surface water, the phosphate and nitrate terms are negligible (in anoxic environments, we would need to include the HS^- ion). Carbonate alkalinity is:

$$CAlk = [HCO_3^-] + 2[CO_3^{2-}] + [OH^-] - [H^+] \qquad 15.16$$

(which is identical to 6.32). One of the reasons alkalinity is important is that it can be readily determined by titration.

In Chapter 6, we stated that alkalinity is "conservative", meaning that it cannot be changed except by the addition or removal of components. It is important to understand that alkalinity is not conservative in an oceanographic sense, as is, for example, salinity. In an oceanographic sense, we define a "conservative" property to be one that changes only at the surface by concentration or dilution. While addition and removal of components may occur, through precipitation and dissolution, these processes have negligible effects on conservative properties. Concentration and dilution affect alkalinity; indeed, these processes are the principal cause of variation in alkalinity (alkalinity is strongly correlated with salinity). However, precipitation and dissolution in the ocean do significantly affect alkalinity (whereas the affect on salinity is negligible), so alkalinity is not conservative in an oceanographic sense. Indeed, alkalinity typically varies systematically with depth, being greater in deep water than in the surface water.

What causes this depth variation? It might be tempting to guess that photosynthesis and respiration are responsible. However, these processes have no direct effect on alkalinity. When CO_2 dissolves in water, it dissociates to produce a proton and a bicarbonate ion. In the alkalinity equation, these exactly balance, so there is no effect on alkalinity. Production and oxidation of organic matter do affect alkalinity through the uptake and release of phosphate and nitrate, but the concentration of these nutrients is generally small. The main cause of the systematic variation of alkalinity in the water column is carbonate precipitation and dissolution. For every mole of calcium carbonate precipitated, a mole of carbonate is removed and alkalinity increases by 2 equivalents, and visa versa, so the effect is quite significant.

Carbonate Dissolution and Precipitation

From the preceding sections, we can see that precipitation of calcium carbonate in surface waters and its dissolution at depth is an important oceanographic phenomenon. Carbonate sedimentation is also an important geological process in other respects, including its role in the global carbon cycle. Let's examine carbonate precipitation and dissolution in a little more detail. Two forms of calcium carbonate precipitate from seawater. Most carbonate shell-forming organisms, including the planktonic foraminifera and coccolithophorids that account for most carbonate precipitated, precipitate calcite. Pteropods and many corals, however, precipitate aragonite, even though aragonite, the high pressure form of calcium carbonate, is not thermodynamically stable anywhere in the ocean. The surface ocean is everywhere supersaturated with respect to both calcite and aragonite, usually to depths of 1000 m or more[1]. Nevertheless, except in some rather rare and unusual situations, carbonate pre-

[1] You might ask how aragonite can be supersaturated if it is not thermodynamically stable. It is supersaturated because aragonite has a lower Gibbs Freee Energy than seawater, but aragonite has a higher Gibbs Free Energy than calcite, so it is unstable with respect to calcite.

cipitation occurs only when biologically mediated. There are two interesting questions here. First, why does the ocean go from supersaturated at the surface to understaturated at depth, and second, why doesn't calcium carbonate precipitate without biological intervention?

There are three reasons why the oceans become undersaturated with respect to calcium carbonate at depth. First, increasing P_{CO_2} of deep water drives pH to lower levels, increasing solubility. This might seem counter-intuitive, as one might think that that increasing P_{CO_2} should produce an increase the carbonate ion concentration and therefore drive the reaction toward precipitation. However, increases in P_{CO_2} and ΣCO_2 with depth produce a *decrease* in $CO_3^{=}$ concentration. This is most easily understood if we express the carbonate ion concentration as a function of P_{CO_2} using the solubility and dissociation constants for the carbonate system (equations 12.21 through 12.23):

$$[CO_3^{2-}] = \frac{K_2 K_1 K_{Sp-CO_2} P_{CO_2}}{[H^+]^2} \qquad 15.17$$

This equation shows that while carbonate is proportional to P_{CO_2}, it is inversely proportional to the square of $[H^+]$. The pH drop resulting from production of CO_2 by respiration is thus dominant. Carbonate ion concentrations drop by over a factor of three from the surface waters to the waters with the highest dissolved CO_2.

The second reason is that the solubility of calcium carbonate increases with increasing pressure. This results from the positive ΔV of the precipitation reaction. Calcite and aragonite are about twice as soluble at 5000 m (corresponding to a pressure of 500 atms) than at 1 atmosphere. Third, the solubility of $CaCO_3$ changes with temperature, reaching a maximum around 12°C (see Example 15.3). As we might expect, the solubility of calcite is also dependent on salinity (due to the effect of ionic strength on the activity coefficients), but salinity variations are not systematic with depth.

The kinetics of carbonate precipitation are still not fully understood, in spite of several decades of research. Quite a bit is known, however, particularly about the calcite precipitation and dissolution. A number of laboratory studies (e.g., Chou et al., 1989; Zuddas and Mucci, 1994) have concluded that the principal reaction mechanism of calcite precipitation in seawater is:

$$Ca^{2+} + CO_3^{2-} \rightleftarrows CaCO_3 \qquad 15.18$$

Example 15.3. Pressure Dependence of Calcite Solubility

The ΔV_r for calcite precipitation is 37 cc/mol. If the apparent calcite solubility product, K´ is 4.30 $\times 10^{-7}$ mol^2/kg^2 at atmospheric pressure, how will the solubility product vary between the sea surface and a depth of 5000 m? Assume that ΔV_r is independent of pressure, constant salinity, a constant temperature of 2°C, and that pressure increases by 0.1 MPa for every 10 m depth in the ocean.

Answer: The pressure dependence of the equlibrium constant is:

$$\frac{\partial \ln K}{\partial P} = -\frac{\Delta V_r}{RT} \qquad (3.109)$$

Integrating, we have:

$$K_P = K_P \, e^{-\frac{\Delta V_r (P_1 - P_2)}{RT}}$$

Sea level pressure (P_1) is 0.1 MPa, the pressure at 5000 m is 50 MPa. Substutiting values, we can construct the graph shown in Figure 15.10. We see that calcite is somewhat more than twice as soluble at a depth of 5000 m than at the surface.

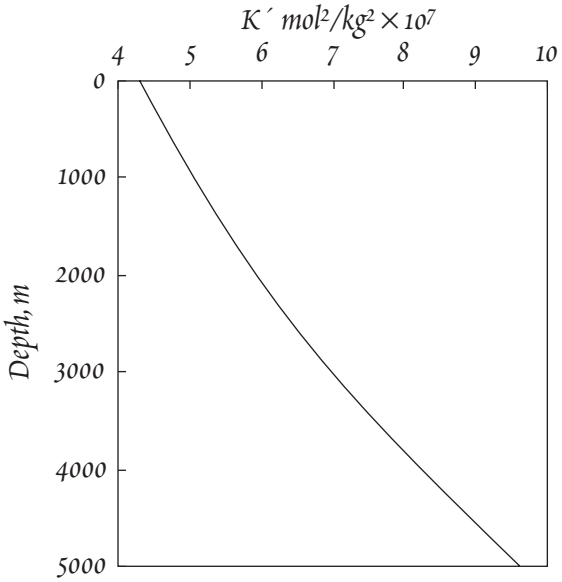

Figure 15.10. Calculated change of the calcit solubility product with depth in the ocean.

EXAMPLE 15.4. TEMPERATURE DEPENDENCE OF CALCITE SOLUBILITY

For sea water of 35‰ salinity, the temperature dependence of the apparent calcite solubility product may be expressed as (in units of moles^2 per kg^2):

$$\log K' = A + BT + C/T + D\log(T) \qquad 15.23$$

where A = -178.34874, B= -0.061176, C= 3894.39267, D=71.595 (Mucci, 1983; Millero, 1995). For seawater of average Ca^{2+} ion concentration (Table 15.2), how does the carbonate ion concentration at which saturation is acheived vary between 0°C and 35°C?

Answer: The equilibrium carbonate ion concentration is given by:

$$[CO_3^{2-}] = \frac{K_{CaCO_3}}{[Ca^{2+}]} \qquad 15.24$$

The concentration of Ca given in Table 15.2 corresponds to a molal concentration of 10.28 mM/kg. Substituting 15.23 into 14.24, we can construct the graph shown in Figure 15.11. Maximum solubility is achieved at about 12°C and decreases at both higher and lower temperatures.

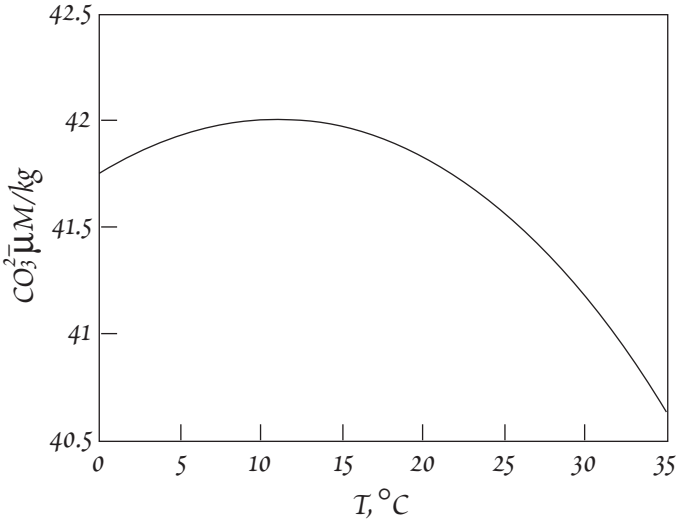

Figure 15.11. Calculated temperature dependence of the concentration of carbonate ion in 35‰ salinity seawater in equilibrium with calcite.

In other words, this simple stoichiometric expression best represents what actually occurs on an molecular level (however, other mechanisms appear to predominate at lower pH). In Chapter 5, we found that the net rate of reaction can be expressed as:

$$\Re_{net} = \Re_+ + \Re_- \qquad (5.73)$$

If reaction 15.18 is the elementary reaction describing precipitation, then:

$$\Re_+ = k_+ [Ca^{2+}][CO_3^{2-}] \qquad 15.19$$

and

$$\Re_- = k_-[CaCO_3] \qquad 15.20$$

where k_+ and k_- are the forward and reverse rate constants respectively. Taking the concentration of $CaCO_3$ in the solid is 1, the net reaction rate should be:

$$\Re_{net} = k_+ [Ca^{2+}][CO_3^{2-}] - k_- \qquad 15.21$$

However, Zhong and Mucci (1993) and Zuddas and Mucci (1994) found that under conditions of constant $[Ca^{2+}]$, the overall rate equation is:

$$\Re_{net} = k_f[CO_3^{2-}]^3 - k_- \qquad 15.22$$

where k_f is an apparent rate constant (incorporating both the rate constant and Ca^{2+} concentration). In other words, the reaction is third order with respect to the carbonate ion, rather than first order as expected. This indicates that other processes must be involved and strongly influence the reaction rate. Exactly what these other processes are is not yet fully understood.

It is known that the presence of Mg^{2+} and SO_4^{2-} ions strongly retard calcite precipitation rates (Berner, 1975; Busenberg and Plummer, 1985). Why is not yet fully understood. One possibility is that the formation of ion pairs, such as $(Mg^{2+})(CO_3^{2-})$ and $(Ca^{2+})(SO_4^{2-})$, reduces the availability of reactants. Another possibility is that Mg and SO_4^{2-} are absorbed on the surface and thus block addition of new Ca^2 and CO_3^{2-} to the surface.

In contrast to the precipitation reaction, dissolution of carbonate appears to begin close to the depth where undersaturation is reached. However, dissolution is not instantaneous. If we could remove the water from the ocean basins, we would find that mountain peaks in the ocean are covered with white carbonate sediment, but that carbonate is absent from the deeper plains and valleys. This picture is very much reminiscent of what we often see in winter: mountains peaks covered with snow while the valleys are bare. Although the snow line, the elevation where we first find snow, depends on temperature, it does not necessarily correspond to the 0° C isotherm. Indeed, it will generally be somewhat lower than this. The snow line is that elevation where the rate at which snow falls just matches the rate at which it melts. In the ocean, the "carbonate snow line" is called the *carbonate compensation depth* (CCD), and it is depth at which the rate at which carbonate accumulates just equals the rate at which it dissolves. This is always lower than the depth where it begins to dissolve, a depth known as the *lysocline*. Like the snow line, the depth of the CCD does ultimately depend on thermodynamic factors, and it varies. It is deepest in the Atlantic, where it as deep as 5500 m, and shallowest in the North Pacific, where it is as shallow as 3500 m. The average depth of the CCD is about 4500 m. Since aragonite is more soluble than calcite, it is restricted to even shallower depths. Pteropod oozes, sediments composed primarily of the aragonitic shells of pteropods, are largely restricted to the mid-ocean ridge crests and tops of seamounts.

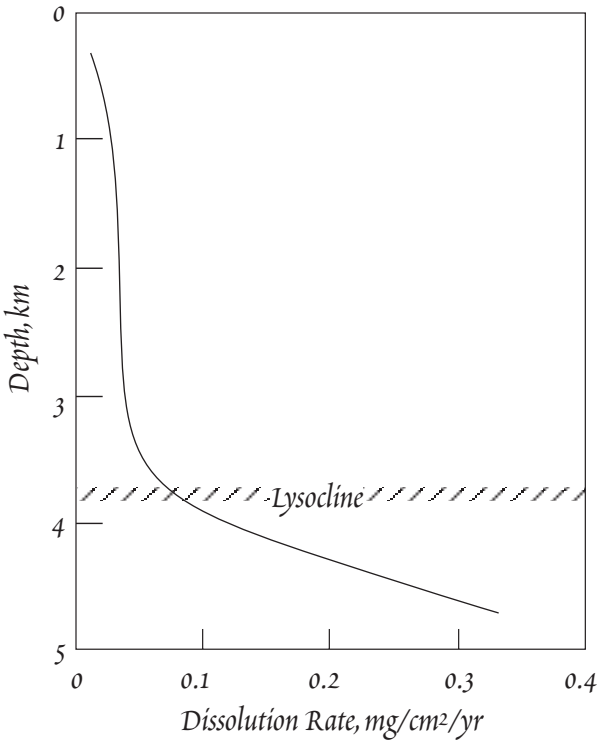

Figure 15.12. Dissolution rate of calcite as a function of depth in the Pacific at 19° N 156° W as determined by the Peterson spheres experiment.

The survival of carbonate in sediment is, then, a question of kinetics as much as of thermodynamics. The kinetics carbonate dissolution in seawater have been addressed with both laboratory and field experiments. Figure 15.12 shows the rate of calcite dissolution determined by an ingenious experiment performed by Peterson (1966) three decades ago. Peterson hung carefully weighed spheres of calcite at various depths in the ocean for 265 days. He then recovered the spheres and reweighed them to determine the rate of dissolution as a function of depth. The results showed a rapid increase in dissolution at a depth of about 3500 m. Since then, this experiment has been duplicated several times with increasing sophistication. The results show that the depth at which rapid dissolution begins, the lysocline, corresponds reasonably closely to the depth at which undersaturation is reached. Below that depth, the rate of dissolution increases rapidly, and correlates with the degree of undersaturation. Laboratory studies have shown that at the pH of seawater, the dominant dissolution mechanism also appears to be the reverse of reaction 15.18 (e.g., Chou et al., 1989). If that is the case, then the net rate of dissolution should be:

$$\Re_{net} = k_{-} - k_{f}[\,CO_3^{2-}]^3 \qquad 15.25$$

The strong dependence of the dissolution rate on carbonate ion concentration is consistent with the rapid increase in dissolution rates below the lysocline. Hence field and laboratory investigations appear to yield consistent results, but more experimental work on dissolution mechanisms and rates under conditions relevant to seawater is still needed.

Chapter 15: Oceans

Nutrient Elements

In addition to CO_2, many other elements are essential to life and are taken up by phytoplankton in the course of organic matter production. Two of the most important nutrient elements in the ocean are phosphorus and nitrogen. As we found in Chapter 14, nitrogen is a component of proteins and nucleic acids, and phosphorus is involved in many energy transfer reactions. Both are essential for all life. For most primary producers, nitrogen must be "fixed" before it can be utilized. Thus NO_3^-, N_2O, and NH_4^+ are nutrients, but N_2 is not (in the following discussion we shall use N to refer only to fixed inorganic nitrogen). Biological uptake of these nutrients typically leads to their severe depletion in surface waters. Indeed, nitrate levels sometimes fall below detection limits. The uptake of nutrients from surface waters and their release into deep water from falling organic particles imposes a vertical gradient on the concentration on nutrients in the ocean (Figure 15.13). Redfield (1958) found that C, N, and P were present in living tissue in nearly constant proportions of 106:16:1. These are called the *Redfield ratios* (more recent work suggests that marine organic matter is actually richer in carbon and just slightly poorer in nitrogen, with the best current estimate of the Redfield ratios being about 126:16:1). Thus we would expect the concentration of phosphate and nitrate to be highly correlated in seawater, and this is indeed the case.

Several planktonic organisms, most notably diatoms, which are among the most important photosynthesizers in the ocean, build tests of SiO_2. For such organisms, Si is as important a nutrient as N and P and it is also strongly depleted in surface water (Figure 15.14a). It appears that in many regions of the oceans, the availability of one or all of these three nutrients limits biological productivity. For this reason, these elements are known as *biolimiting*.

Maxima in nutrient profiles sometimes occur in the depth range of 500-1500 m, reflecting relatively high rates of respiration at these depths. Since nutrients accumulate in deep water, we would expect that the oldest waters would have the highest nutrient concentrations. This is indeed the case. Atlantic deep water shows considerably less enrichment in nutrients than the Pacific because it is

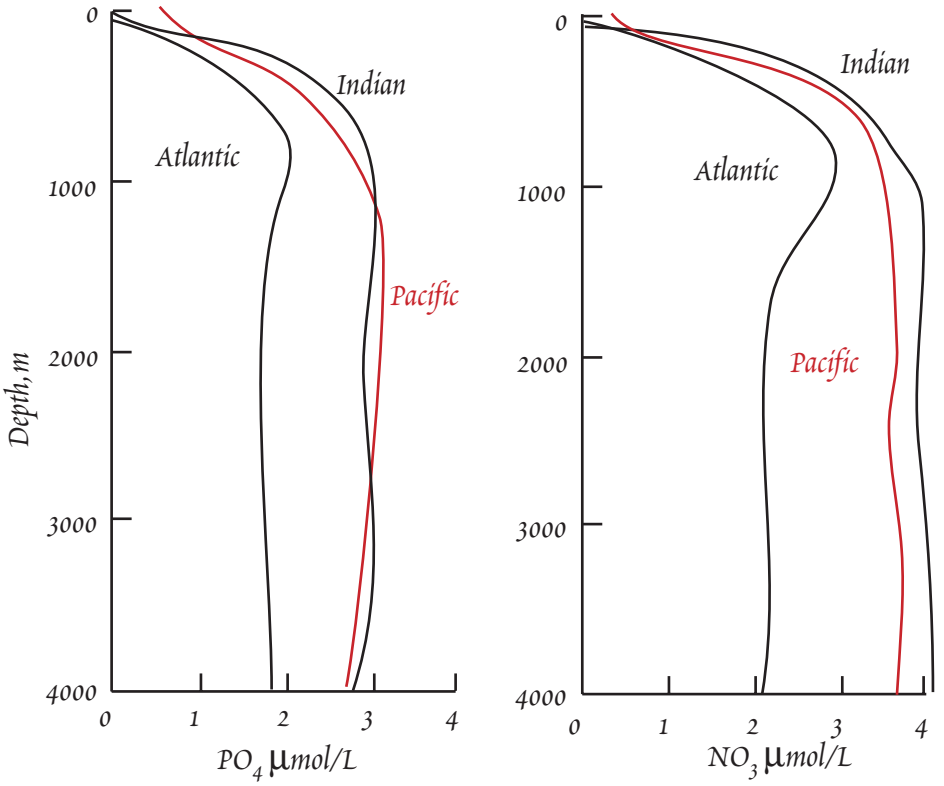

Figure 15.13. Depth profiles of two important nutrients, nitrate and phosphate, in the oceans.

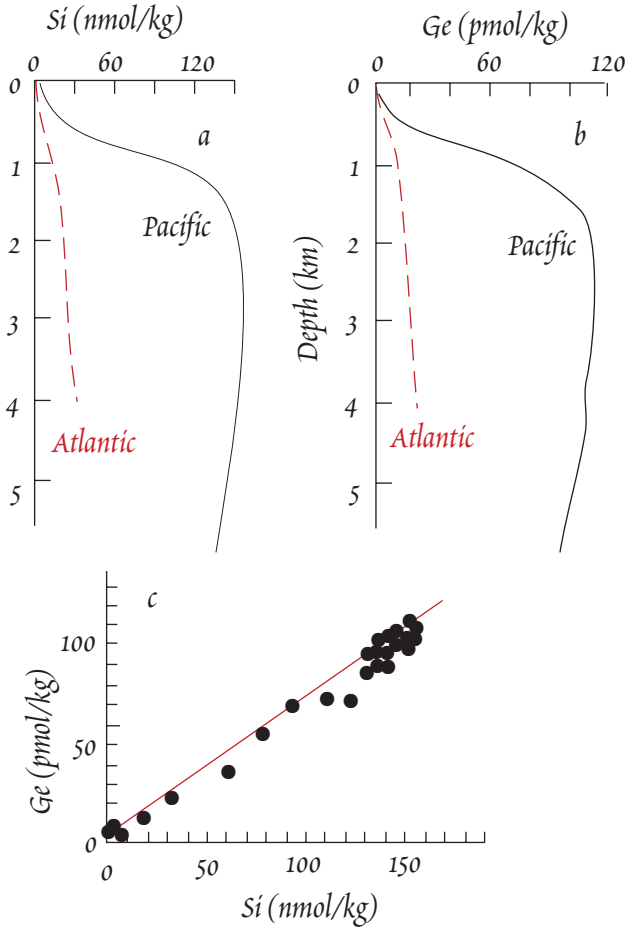

Figure 15.14. Depth profiles of Si (a) and (b) Ge in the Pacific (solid lines) and the Atlantic (dashed red lines). (c) shows the correlation between Si and Ge in the Pacific profile. Modified from Froelich et al. (1985).

younger. The flux of deep water from the Atlantic to the Pacific results in a flux of nutrient elements from the Atlantic to the Pacific and an enrichment the Pacific in nutrient elements compared to the Atlantic.

Upwelling of deep water returns nutrients to surface water. Rivers and wind blown dust deliver nutrients to surface waters from the continents. Thus coastal regions and regions of upwelling, such as in polar regions and along the equator, characteristically have high biological productivity due to this addition of nutrients. External nutrient sources are very limited in the great central gyres, so that these regions have low biological productivity.

Many other elements are also essential for life. B, Na, Mg, S, Cl, K, Ca, and Mo are widely or universally required and F, Br and Sr are required by some species. However, these elements are sufficiently abundant in seawater that biological activity produces no, or very little, variation in their concentration in the ocean. For this reason, these elements are sometimes referred to as *biounlimited*. In addition to these elements, Mn, Fe, Cu, and Zn are widely or universally required and the elements V, Cr, Ni, Se, and I are required by some species. These elements are in sufficiently low concentrations that biological activity imposes vertical and horizontal gradients in their concentration in the ocean. Some of these elements, such as Fe and Zn, also show severe depletion in the surface water and are also classed as biolimiting elements. Indeed, Martin and Gordon (1988) argued that the availability of Fe limits phytoplankton growth in high productivity regions such as the Subarctic, Antarctic, and equatorial Pacific, where major nutrients are not severely depleted. In these areas, Fe concentrations are as low as 0.1 nmol/l. That Fe can indeed limit phytoplankton productivity was confirmed in an experiment carried out in the eastern equatorial Pacific in 1993. Fe (as $FeSO_4$) was added to a 100 km^2 patch of ocean where Fe concentrations were very low. Within days of adding Fe, phytoplankton productivity increased significantly (Martin et al., 1994).

For other elements, such as V, Cr, and Se, only slight surface water depletion occurs. Elements such as these are known as *biointermediate*. An example of one of these biointermediate elements, Se, is shown in Figure 15.15.

The distributions of several of these biolimiting and biointermediate elements are also significantly affected by non-biological processes in the ocean and as a result, they can have vertical concentration profiles that differ from the classic nutrient profile see in Figures 15.13 and 15.14. This can occur as a result of oxidation and reduction, adsorption onto particle surfaces, a process called scavenging, and by other inputs, such as input from hydrothermal vents and sediments of the ocean bottom. We will consider the vertical distribution of these elements, and the processes creating them, in more detail in the next section.

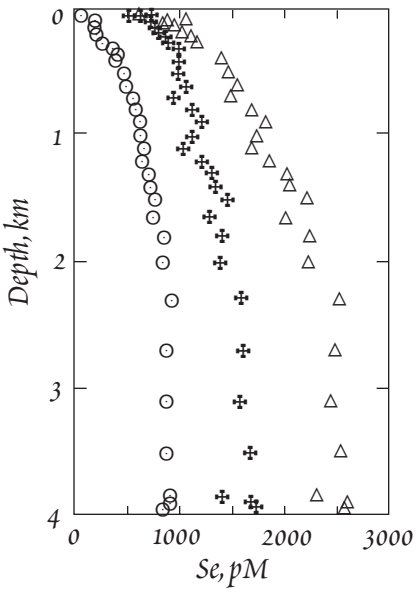

Figure 15.15. Selenium profiles in the Panama Basin. Circles: Se^{IV}, crosses: Se^{VI}, triangles: total Se. From Measures et al. (1984).

ated decomposition of soft tissues of organisms. Si is incorporated only in the inorganic tests, which undergo dissolution without biological mediation (however, passage of these tests through the gut of higher organisms undoubtedly speeds dissolution). This abiologic dissolution is slower. Elements that are rapidly released are referred to as *labile* elements; those released more slowly, such as Si, are referred to as *refractory*. Labile nutrients include nitrate, Mn, Cd, and Ni. Since Ge concentrations correlated with those of Si, we include it with the refractory elements. It was once thought that all refractory elements were incorporated in hard tissues, such as tests. However, Collier and Edmond (1984) demonstrated that several refractory elements are present only in soft tissues of plankton, but nevertheless undergo only slow release. These elements include

A number of other elements show nutrient type distribution patterns, that is depleted in surface water and enriched in deep water, even though they have no known biological function. These include As (which shows only slight surface depletion), Sc, Ge, Pd, Ag, Cd, Ba, the rare earths, Pt, and Ra. Ba appears to be precipitated by biological mediated reactions (as $BaSO_4$), but the details are not yet understood. Other elements are inadvertently taken up; that is, organisms appear not to be able to discriminate between them and needed elements. Ge provides a well-documented example. It is chemically similar to Si and apparently is taken up by diatoms in place of Si. Like Si, its concentration approaches 0 in surface water and increases with depth (Figure 15.14). Overall, its concentration is strongly correlated with that of Si. Clearly, biological activity controls the distribution of Ge in the oceans.

Comparing the phosphate and silicate profiles in Figure 15.16, we see that concentrations of phosphate increase more rapidly that that of SiO_2. Essentially all release of phosphate occurs with in the upper 1000 m, and most within the upper 500 m. Maximum Si concentrations are only reached at depths of 1500 to 2000 m. The reason for these different distributions is straightforward. P is released by biological medi-

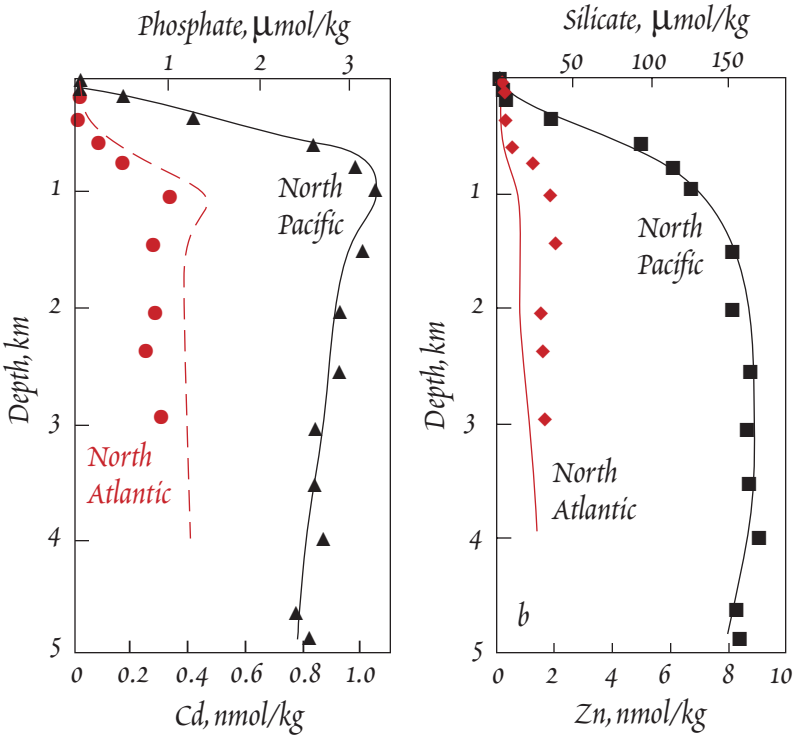

Figure 15.16. Comparison of labile and refractory nutrients. a. Concentration profiles of two labile nutrients (Cd: points and phosphate: curves) in the North Atlantic and North Pacific. b. Concentration profiles of two refractory nutrients (Zn: points and silicate: curves) in the North Atlantic and North Pacific. Modified from Bruland (1983).

Cu, Zn, and Fe. Thus whether an element is labile or refractory apparently depends on how readily its organic host molecule is decomposed, as well as whether it is incorporated in hard or soft tissue.

It is interesting to compare the distribution of Si and Ca, both utilized by organisms to build tests. In both cases, the tests have some tendency to dissolve after the organism dies, and thus there is some recycling of these elements back to seawater. But because the flux of Si to the oceans is low, the concentration is relatively low everywhere and the plankton utilizes essentially all of it in surface waters. Plenty of Ca is supplied to the oceans and its concentration is high; organisms utilizing only a portion of that available. The relative variation in Ca concentration is only about 0.5%. Both Si and Ca provide good demonstrations of the lack of control of equilibrium thermodynamics on ocean chemistry, at least on a large scale. Calcium carbonate is oversaturated in surface water, yet precipitates only in biologically mediated reactions. In contrast, the ocean is everywhere undersaturated with respect to opal (though is locally oversaturated with respect to quartz), yet it is biologically precipitated and redissolved only slowly upon death of the organism. The oceans are certainly an example of a kinetically controlled, rather than thermodynamically controlled, system.

PARTICLE-REACTIVE ELEMENTS

The vertical and horizontal distributions of a number of trace elements in seawater, including Al, Ga, Sn, Te, Hg, Pb, Bi, and Th are controlled by abiologic reactions with particles. These reactions include surface adsorption and desorption, and oxidative and reductive dissolution and precipitation. (Even here, however, the biota plays some role, in the production of particles, production of organic molecules that coat particles and affect their surface properties, and in catalyzing oxidation and reduction reactions.) The distribution of Be, Cu, Ti, Cr, Mn, Fe, Zr, the REE, Hf, and Pt are controlled by both biological processes and abiologic reactions with particles. A common characteristic of these all these elements is that they are strongly hydrolyzed in seawater, i.e., at seawater pH they react with water to form hydroxo complexes (e.g., $Al(OH)_3$, $Al(OH)_4^-$). Most particles in the ocean have large numbers of O-donor surface groups. Cations that form hydroxo complexes in solution are readily adsorbed to these surfaces. Hence these elements are highly "particle reactive", meaning they readily absorb to particle surfaces.

Erel and Morgan (1991) proposed that the seawater concentrations of these particle-reactive elements are controlled by two opposing processes: adsorption to and transport on inorganic and organic particle surfaces and desorption driven by complexing with dissolved ligands in seawater. Surface adsorption constants provide a measure of the extent of adsorption; complexation constants a measure of the extent of complexation. The data on surface adsorption constants for marine particles is sparse, but Erel and Morgan point out that constants of adsorption of trace metals to O-donor surface groups of oxide, hydrous oxide, and organic surfaces are linearly related to hydrolysis constants (Dzombak and Morel, 1990). In other words, the adsorption constants can be approximated by:

$$\log K_{ads} = a \times \log(\beta^0_{MOH}) + b \qquad 15.26$$

where $$\beta^0_{MOH} = \frac{[M(OH)^{(n-1)+}]}{[M^{n+}][OH^-]}$$

For hydrous ferric oxide, *a* has a value of 1.2 and *b* a

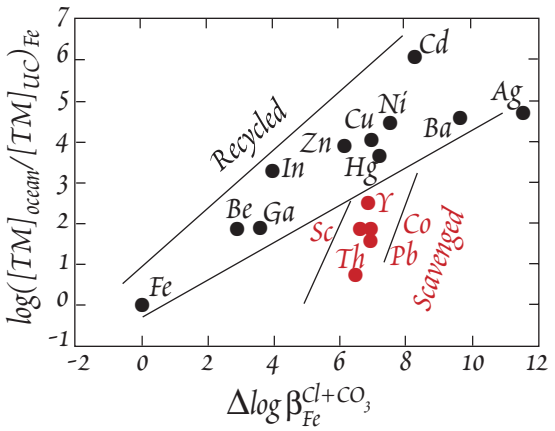

Figure 15.17. Log of the ratio of concentration in the ocean to the concentration in the upper crust plotted against the log difference between hydroxo and chloride plus carbonate stability constant for 16 trace metals. Both parameters are normalized to the same parameter for Fe. The nutrient (or "recycled") and particle reactive (or "scavenged") elements define separate correlations. These correlations illustrate the strong control exerted by surface and aqueous complexing on elemental concentrations in the ocean. From Erel and Morgan (1991).

value of –4.4 (Dzombak and Morel, 1990). In this case, then, the ratio of the dissolved to adsorbed concentration of an element should depend on the ratio of the stability constants of dissolved complexes to the first hydrolysis constant. Chloro- and carbonato- complexes are the dominate complexed species in seawater. Hence dissolved to adsorbed ratio can be approximated by:

$$\frac{[TM]_{diss}}{[TM]_{ads}} = \frac{\beta^0_{MCl}[Cl^-] + \beta^0_{MCO_3}[CO_3^{2-}]}{\beta^0_{MOH}10^b[\text{surface sites}]/[H^+]} = \Delta\beta^{Cl+CO_3} \qquad 15.27$$

Figure 15.17 is a plot of this ratio (normalized to the same ratio for Fe) against the ratio of the seawater concentration of the element to its upper crustal ratio (again normalized to the same ratio for Fe). It shows a linear correlation for the "nutrient elements", indicating adsorption/complexation are indeed strong controls on elemental concentrations in seawater. The plot distinguished the "nutrient" elements from the scavenged, "or "particle-reactive" ones. The latter fall below the correlation because they are adsorbed by carbonate surface groups in addition to OH^- surface groups.

Particle-reactive elements show a variety of vertical concentration profiles. Al, Ga, Te, Hg, Pb, Bi, and Th are typically enriched in surface water and depleted at depth. Lead provides an example (Figure 15.17). In the case of Al, Ga, Sn, Te, and Pb, the surface enrichment in results input wind-born particulates to the surface water followed by partial dissolution; in the case of Th, it results from riverine input (Whitfield and Turner, 1987). These elements are then progressively scavenged by particles. In the case of Sn, Te, Hg, and Pb, a significant part of the aeolian flux may be anthropogenic, hence the surface maxima may not be permanent features of the ocean.

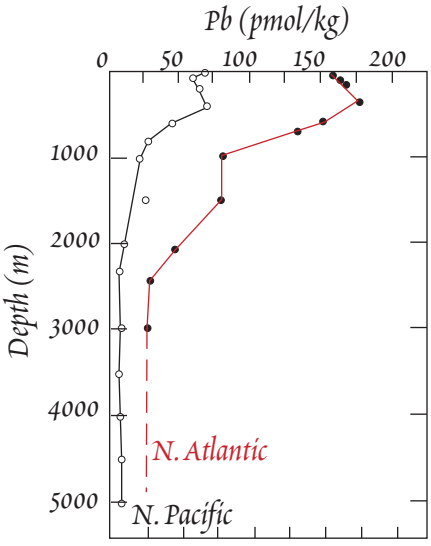

Figure 15.18. Depth profiles of Pb in the Pacific and Atlantic Oceans. From Schaule and Patterson (1983).

In another commonly seen profile, concentrations increase with depth after first decreasing to a mid-depth minimum (e.g., Al in Figure 15.19). Again, high concentrations in surface waters result from riverine or aeolian inputs while decreasing concentrations with depth result from particle scavenging. Higher concentrations in deep water reflect diffusion out of sediment pore waters. Pore water enrichment occurs as ions are desorbed from surfaces as a result of a decrease in pH in sediment pore water. This in turn is a consequence of respiration and production of CO_2.

A continuous increase in concentration with depth is seen in some profiles of Be, Cu, Ti, Zr, and Hf. Such profiles result from a combination of aeolian and/or riverine surface input, biological uptake in surface waters, scavenging, and input from sediment pore water to bottom water (e.g., Bruland, 1980). The profile of Ti in Figure 15.20 provides and example.

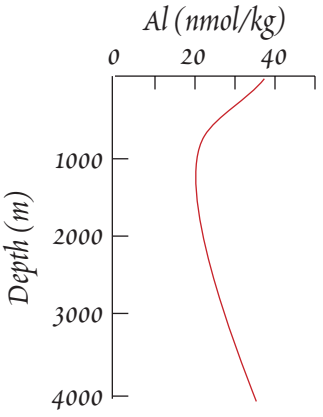

Figure 15.19. Typical vertical concentration profile for Al. After Bruland (1983).

Mid-depth maxima may occur for several reasons. The first is hydrothermal input. Most hydrothermal activity in the oceans occurs on mid-oceans ridges, who depth is typically in the range of 2500-3500 m. Hydrothermal fluids mix with surrounding water and form slightly warm, and therefore slightly buoyant, plumes, which rise hundreds of meters above the ridge crest and are then transported laterally by ocean currents. Elements strongly enriched in hydrothermal fluids will be enriched in these plumes, creating mid-depth maxima for these elements. He is one such element, Mn is another.

Profiles of Mn, and to a lesser degree Fe, can also show maxima associated with the O minimum. These maxima occur because particle-bound Mn and Fe are reduced in O-poor water and the reduced species, Fe^{2+} and Mn^{2+}, are much more soluble than the oxidized species. In reducing con-

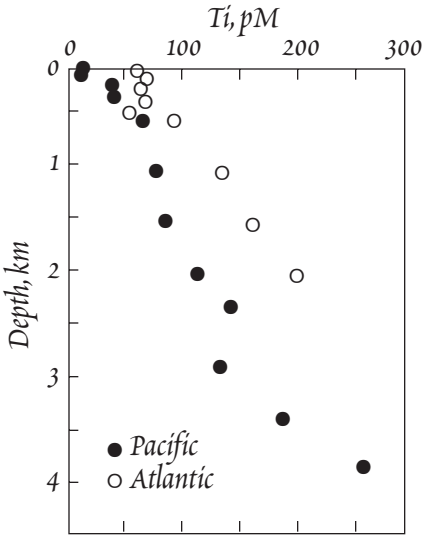

Figure 15.20. Profiles of dissolved Ti in the Atlantic and Pacific Oceans. From Orians et al. (1990).

ditions then, Fe and Mn can be released from particulates rather than scavenged. Both these can have higher concentrations in basins where deep circulation is so limited that deep waters become anoxic, e.g., the Cariaco trench, some Norwegian fjords, and the Black Sea. Two vertical Mn profiles are shown in Figure 15.21. The maximum at 1000-1500m in the left profile is associated with the O_2 minimum. This profile also shows surface enrichment due to riverine input. River water is less dense than seawater, hence it tends to mix horizontally rather than vertically. The right profile is located over the Galapagos Spreading Center and shows the effect of hydrothermal input on Mn concentrations.

The One-Dimensional Advection-Diffusion Model

Let's examine these concentration-depth profiles in a bit more detail. Concentration profiles such as these can be readily modeled using a *one dimensional advection-diffusion model* (Craig, 1974). The essential assumption of such a model is that the profile observed is a steady-state feature; that is that the variation with depth is the same today as it was, say, 1000 years ago. Let's begin by considering the simple case of the vertical variation of conservative property of ocean water, such as salinity, between fixed values of salinity at the top and bottom of the water column. Salinity will vary only because of transport of water (by our definition of "conservative", chemical and biological processes have no effect). Two kinds of transport are of interest: turbulent transport and vertical velocity of the water. Turbulent transport is also known as "eddy diffusion". Its is exactly analogous to chemical diffusion

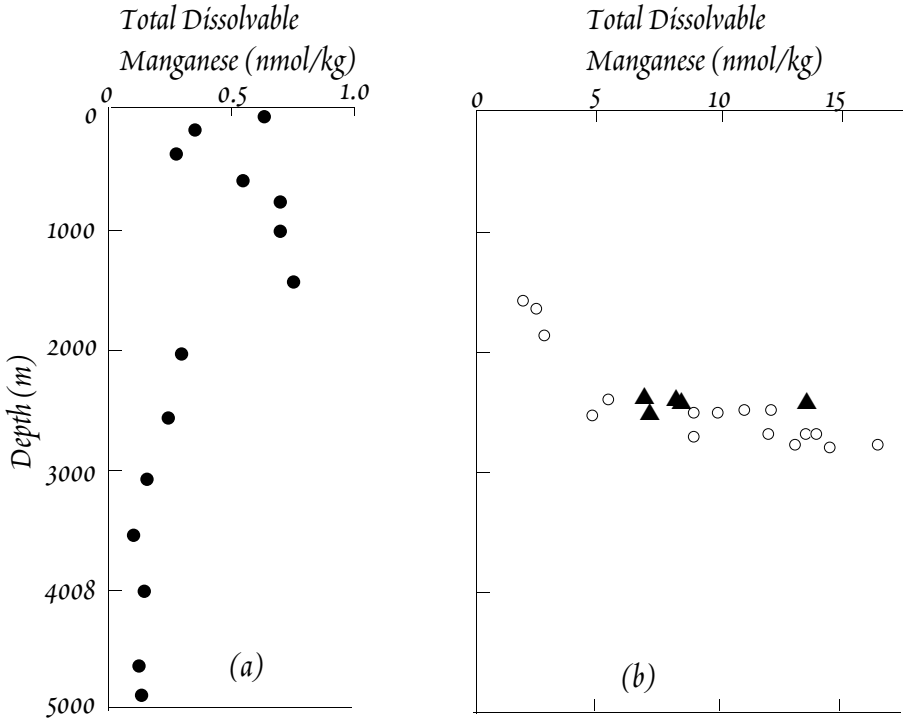

Figure 15.21. Profiles of Mn in the North Central Pacific (left) and over the Galapagos vent areas (right).

and may be described by the equation:

$$\frac{\partial c}{\partial t} = K\frac{\partial^2 c}{\partial z^2} \qquad 15.28$$

where c is a concentration (such as salinity), K is the eddy diffusion coefficient and has units of m^2/yr, and z is depth. Notice that equation 15.28 is identical to Fick's Second Law (equation 5.91) except that we have replaced the chemical diffusion coefficient, D, with K (and x with z; we define z as being positive upward). Adding a term for vertical velocity, we have:

$$\frac{\partial c}{\partial t} = K\frac{\partial^2 c}{\partial z^2} - \omega\frac{\partial c}{\partial z} \qquad 15.29$$

Notice that the velocity term in equation 15.29 is exactly analogous to the one in equation 5.159, which we derived from sediment diagenesis. At steady-state $\partial c/\partial t = 0$, so:

$$K\frac{\partial^2 c}{\partial z^2} = \omega\frac{\partial c}{\partial z} \qquad 15.30$$

This is a second-order differential equation with respect to c, the solution depends on the boundary conditions. These are that c is fixed at $c = c_0$ at the bottom ($z = 0$) and $c = c_Z$ at the surface ($z=Z$). The solution to this equation is:

$$c(z) = (c_Z - c_0)f(z) - c_0 \qquad 15.31$$

where

$$f(z) = \frac{\exp(\frac{z\omega}{K}) - 1}{\exp(\frac{Z\omega}{K}) - 1} \qquad 15.32$$

Since c(z) is a linear function of $f(z)$, equation 15.31 can be used to test the appropriateness of the one dimensional model. If a truly conservative parameter, such temperature of salinity, is plotted against $f(z)$, a straight line should result. Any deviation from linearity would indicate there is significant horizontal advection and that the one dimensional model is not appropriate. Provided horizontal advection is not occurring, we can use equation 15.31 to determine whether a particular species is conservative or not: any deviation from linearity on a plot of c versus $f(z)$ would indicate non-conservative behavior.

Now let's consider a non-conservative species that is actively scavenged from seawater through surface adsorption on particles. We assume that the adsorption rate is proportional to the concentration, i.e., first order kinetics. The change of concentration with time can then be described as:

$$\frac{\partial c}{\partial t} = K\frac{\partial^2 c}{\partial z^2} - \omega\frac{\partial c}{\partial z} - \psi c \qquad 15.33$$

where ψ is the scavenging rate constant, which we assume is constant with depth. The sign of ψ is such that positive ψ corresponds to removal from seawater, i.e., adsorption, negative to desorption. ψ has units of inverse time; the inverse of ψ is known as the *scavenging residence time* and is denoted τ_ψ.

At steady-state:

$$K\frac{\partial^2 c}{\partial z^2} = \omega\frac{\partial c}{\partial z} + \psi c \qquad 15.34$$

The solution to this equation, which again depends on the boundary conditions, is:

$$c(z) = c_Z F(\psi,z) + c_0 G(\psi,z) \qquad 15.35$$

where:

$$F(\psi,z) = \frac{\exp(-[Z-z]\omega/2K)\sinh(Az\omega/2K)}{\sinh(AZ\omega/2K)}$$

$$G(\psi,z) = \frac{\exp(z\omega/2K)\sinh(A[Z-z]\omega/2K)}{\sinh(AZ\omega/2K)}$$

and $$A = (1 + 4K\psi/\omega^2)^{1/2}$$

Finally, suppose that in addition to these processes, there is a steady production of the dissolved species through biological decomposition of organic matter. The production in that case would be independent of concentration. The rate of change of concentration is then:

$$\frac{\partial c}{\partial t} = K\frac{\partial^2 c}{\partial z^2} - \omega\frac{\partial c}{\partial z} - \psi c + J \qquad 15.36$$

where J is the rate of production. For simplicity, we assume that it is independent of depth. At steady state:

$$K\frac{\partial^2 c}{\partial z^2} - J = \omega\frac{\partial c}{\partial z} + \psi c \qquad 15.37$$

J can also be used to represent "zero-order" removal; zero-order implying that the rate of removal is independent of concentration. The solution to equation 15.37 is given by replacing all concentration terms in 15.35 by $(c - J/\psi)$. For $\psi = 0$, i.e., for no scavenging, this solution is clearly undefined. The solution in that case is:

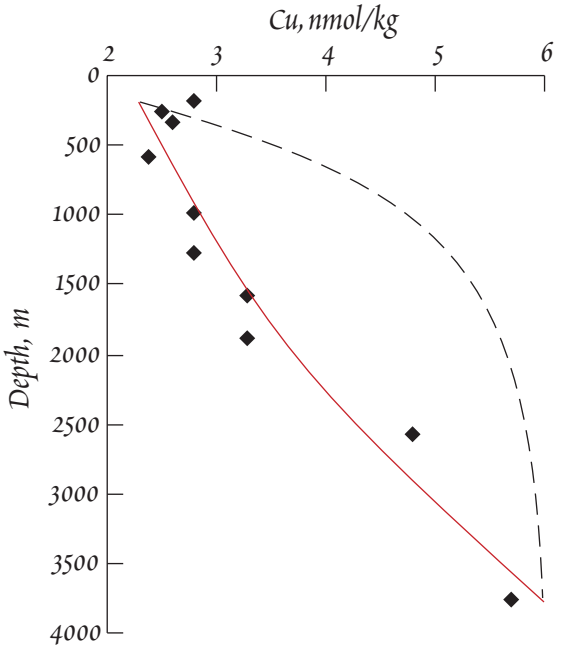

Figure 15.22. Cu data from GEOSECS station 345 in the eastern Pacific (Boyle et al., 1977). Dashed line shows the expected distribution for a one dimensional advection-diffusion model if Cu is behaving conservatively (K = 2886 m^2/yr; ω = 3.7 m/yr). Solid red line shows the fit for $\psi = 0.0012$ yr^{-1}.

$$c(z) = (c_z - c_0)f(z) - c_0 + J/\omega[z - Zf(z)] \qquad 15.38$$

The value of the vertical velocity, ω, can be determined from ^{14}C analyses. Typical values are in the range of –3 to –4 m/yr. Once this is known, equation 15.32 can be fit to a conservative parameter (typically temperature or salinity) to determine K. K is typically in the range of 2000 to 3000 m^2/yr. With values for K and ω, the values of J and ψ may be determined by finding the best fit of equation 15.38 to the data. Figure 15.22 shows an example of the one dimensional advection-diffusion model applied to copper concentrations from GEOSECS station 345 in the eastern Pacific (22°31' N, 122° 12' W) between 200 m and 3800 m. ω was determined from ^{14}C distributions and K then determined by fitting potential temperature to the model. The black dashed line shows the expected Cu distribution if Cu were behaving conservatively. Clearly, Cu concentrations are lower than expected in that case. The red line shows the fit of the model for $\psi = -0.0012$ and J = 0. The ψ implies a scavenging residence time for Cu of about 830 years.

Sources and Sinks of Dissolved Matter in Seawater

Most elements are present in seawater at concentrations far below their equilibrium solubility. Ca is present in surface water at concentrations above solubility. Clearly then, the composition of seawater is not controlled by thermodynamic solubility (only the concentrations of the inert gases are controlled by equilibrium solubility). Rather, the composition of seawater is kinetically controlled; specifically, it is controlled by the rates at which dissolved matter is added to and removed from seawater. Rivers represent the principal "source" of dissolved solids in seawater and sediments represent the principal "sink". There are, however, a variety of other sources and sinks. These are shown in Figure 15.23, which illustrates the marine geochemical cycle of Mn. For any given element,

one of these sources or sinks might dominant, and some or most of the sources might be negligible. In the following sections, we will discuss each of these sources and sinks. Before we do, however, we introduce a useful concept in marine geochemistry, that of residence time.

RESIDENCE TIME

An important concept in the chemistry of seawater is that of *residence time* (Barth, 1952; Goldberg and Arrhenius, 1958). Residence time, τ, is defined as the ratio of the mass of an element in the ocean divided by the flux to the ocean, i.e.:

$$\boxed{\tau = \frac{A}{dA/dt}} \qquad 15.39$$

where A is the mass of the element of interest, and dA/dt is the flux to seawater. Implicit in the residence time concept is the assumption that *the oceans are in steady state*, that is, the composition does not change with time, so that the flux of an element into seawater must equal the flux out of seawater. Thus it does not matter whether we use the flux into or the flux out of the oceans in equation 15.39.

If river water is the principal source of the element, equation 15.39 can be re-expressed as:

$$\tau = \frac{C_{sw}}{C_{RW}} \times \frac{\text{mass of seawater}}{\text{flux of river water}} = \frac{C_{SW}}{C_{RW}} 3.7 \times 10^4 \text{yr} \qquad 15.40$$

where C_{SW} and C_{RW} are the concentrations in seawater and river water respectively. (For water, these two terms are essentially both equal to one, so equation 15.40 that on average a water molecule goes through the hydrologic cycle once every 37,000 years.) For example, rivers are the principal source of Na in seawater. The concentration of sodium is 3.9 mg/kg in river water and 10.77 k/kg in seawater, so we calculate a residence time of 103 Ma for Na. About half the sodium in river water is derived from cyclic salts; i.e., it has simply been cycled through the hydrologic system. If we don't count this cycling in the residence time, then sodium has an ocean residence time of about 200 Ma. Many elements have several sources and the fluxes from these are poorly known; thus their residence times are

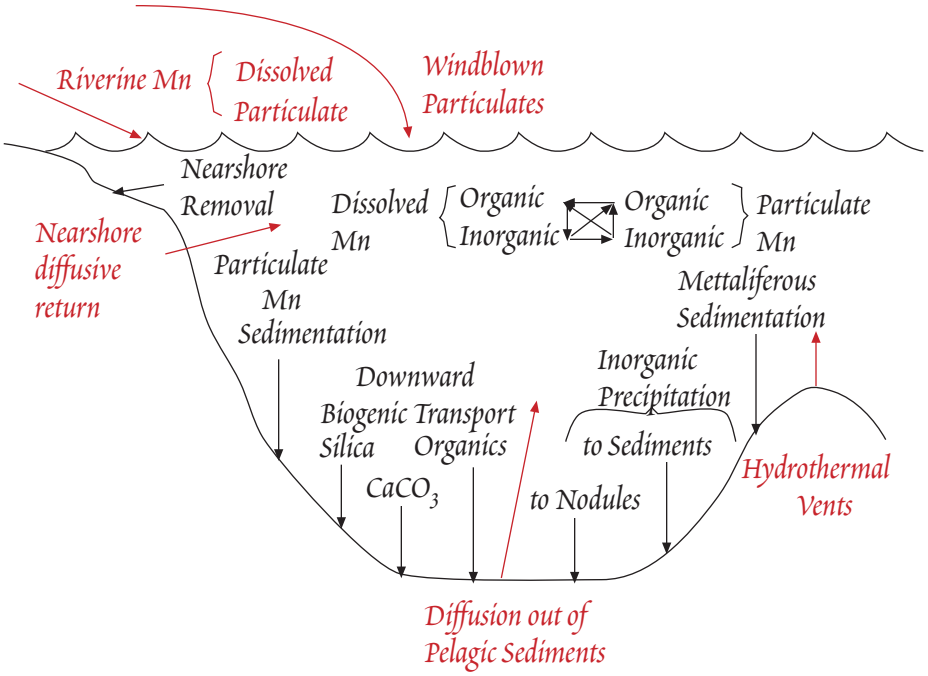

Figure 15.23. Marine geochemistry of Mn, illustrating the range of possible sources and sinks, as well as internal processing, of dissolved material in seawater.

not well known for all elements. Nevertheless, residence times of elements in seawater clearly vary greatly: from 150 Ma for Cl (300 is cyclic salts are not included) to a few tens of years for Fe.

Figure 15.23 shows ocean residence time of the elements plotted against the ratio of their concentration in seawater to the upper crustal concentration, the principal source of most elements in seawater. The two are strongly correlated. Thus residence time is a good indicator of the enrichment (or depletion) of an element in seawater relative to its upper crustal concentration.

Over the last 2 decades, remarkable progress has been main in defining the composition of seawater. However, the fluxes of many elements to (and from) the ocean remain poorly known. As a result, the residence times of most elements are poorly constrained and may be significantly revised in the future.

The Riverine Source

Overall, rivers are the main source of dissolved salts in the ocean, though they are not the main source for all elements. Current estimates of average concentrations in river water are given in Table 15.1. We discussed the factors that controlled river water composition in Chapter 13. These were the chemical composition of the source rock, climate, topography, and the intensity of weathering in the catchment basin.

As we found in Chapter 13, rivers vary widely in composition. Since there are many rivers and each is in some respect unique, the task of estimating the average composition of rivers and their combined flux to the ocean is not an easy one. The largest 20-25 rivers carry only 15% of the flux to the oceans. Relatively few rivers have been subjected to thorough geochemical investigations; for some trace elements there are few data for any rivers. Furthermore, the composition of many rivers has been disturbed by mining, agricultural, industrial, and other activities, so that their modern compositions may not be representative of the composition in the past. Finally, the composition of most rivers varies with river flow. Thus characterizing the composition of a river requires many measurements made over the course of a year or more. For all these reasons, there is considerable uncertainty in the concentrations listed in Table 15.1.

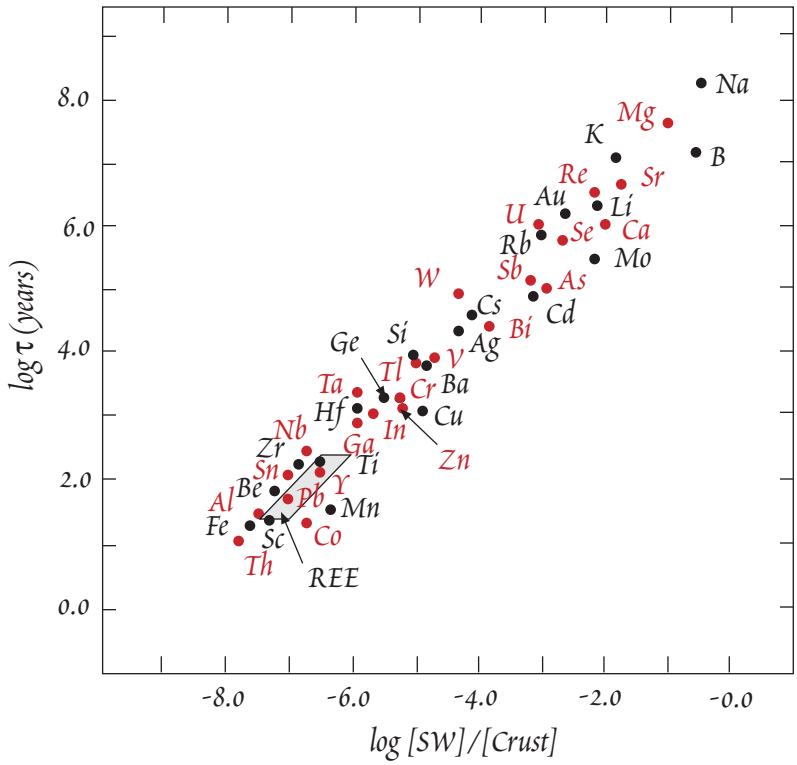

Figure 15.24. Log of seawater residence time plotted against the ratio of seawater to upper crustal concentration. Modified from Taylor and McLennan (1985).

Estuaries

Even if the compositions of rivers were well known, the task of determining the riverine flux to the sea would still be a very difficult one. The reason for this is that estuaries act as flow-through chemical reactors, in which dissolved components are added and removed, and what flows out is not the same as what flows in. This is a consequence of changes in solution chemistry that occur when river and sea water mix.

An estuary is that portion of a river into which coastal seawater is carried by tidal forces; estuaries are thus zones of mixing

of fresh and sea water. They may be lagoons behind barrier islands (e.g., Pamlico Sound, North Carolina), river deltas (e.g., the Rhine Delta), drowned river valleys (e.g., the Gironde Estuary, France), tectonic depressions (e.g., San Francisco Bay), or fjords (Sannich Inlet, British Columbia). In the typical estuary, there is a downstream flow of fresh water at the surface and an upstream flow of seawater at depth; the fresh water overlies the salt water because of its lower density. Depending on the geometry of the estuary, the strength of the tides, and the strength of the river flow, these two layers will mix to varying degrees. Low river flow and strong tides produce a "well mixed" estuary in which there is little vertical gradient in salinity; strong river flow and weak tides lead to a "salt wedge" estuary in which a strong pycnocline develops at the interface between the layers.

The principal chemical changes that can occur in estuaries are as follows.

- changes in ionic strength,
- changes in the concentrations of major cations, which affects speciation of minor components,
- changes in pH,
- changes in the concentration and nature of suspended matter, and
- changes in the redox state within the water and sediment.

In the following paragraphs, we consider these changes in greater detail.

As seawater mixes with river water, the resulting increase in ionic strength and change in pH and solute composition induces the flocculation of riverine colloids which dramatically affects trace metal chemistry. As a practical matter, aquatic and marine chemists often consider "particulates" to be the material retained on 0.4 μm filters and anything passing through such a filter to be "dissolved". Unfortunately, nature is not so neat: in reality there is a continuum between truly dissolved substances and readily recognizable particles. Materials between these are termed *colloids*. Colloids are often defined as having sizes in the range of 10^{-9} to 10^{-6} m and may be separated by special techniques such as ultrafiltration and membrane filtration. Entities at the small end of this range would consist of ~10^3 or fewer atoms and approach the size of larger humic acids, while particles at the large end of the range would be retained on filter paper. Colloids are a surprisingly important component of natural waters. Most of the Fe^{III}, as well as several other readily hydrolyzed metals such as the rare earths, are present as colloids of hydrous ferric oxide and metal humates rather than true dissolved species (e.g., Boyle et al., 1977). A significant fraction of humic acids is probably also colloidal (Sholkovitz, et al., 1978).

The stability of colloids depends strongly on their surface charge. Because they are small, colloids have high surface area to volume ratios. As a result, individual colloids settle very slowly and may remain in suspension indefinitely, behaving essentially as dissolved species. When colloids coagulate, however, the surface area to volume ratio decreases, allowing them to settle out of suspension. Whether or not they coagulate depends on the balance of forces acting between individual particles. As is the case for larger particles, colloids typically have a surface charge, which is balanced by the ions adjacent the surface, the electric double layer (Chapter 6). The double layer produces a repulsive force between particles. The thickness of the double layer is inversely related to the square root of the ionic strength of the solution (equation 6.116). Countering this repulsion is an attraction due to van der Waals interactions. The strength of the van der Waals interactions decrease with the inverse square of distance and are independent of ionic strength. When ionic strength increases, as it does when sea water mixes with river water, the diffuse outer layer, or Gouy layer, is compressed, allowing individual particles to approach each other more closely. Once they approach within a critical distance, the van der Waals attraction binds them together. The process eventually produces particles large enough to settle out, a process called *flocculation*.

Surface charge is affected by adsorption of ions to surface sites; it therefore depends on solution chemistry. Surface charge is also pH dependent (e.g., Figure 12.35). Thus changes in pH and solute chemistry during estuarine mixing may also promote coagulation. Eckart and Sholkovitz (1976) and Boyle et al. (1977) found that flocculation of humic acids occurs when Ca and Mg bind to carboxylic acid groups, neutralizing their negative surface charge. This allows them to coagulate and precipitate.

In a series of experiments, Sholkovitz (1976, 1978) demonstrated that mixing of sea and water from the River Luce of Scotland results in removal of 95% of Fe and lesser amounts of humic acids, Cu, Ni, Mn, Al, Co, and Cu by colloid flocculation. Boyle et al. (1977) demonstrated that this is a general phenomenon occurring in many estuaries and estimated that 90% of the riverine flux of Fe is removed in this way. The exact nature of colloidal iron in rivers and its precipitation in estuaries is only partly understood. Boyle et al. (1977) point out that the iron-carbon ratio of flocculated material is too high for all Fe to be organically complexed. They suggested instead that the hydrous ferric oxide forms a stable colloidal dispersion with humic acids in rivers.

Subsequent studies revealed that other elements, such as the rare earths, are also removed by this process. For example, Hoyle et al. (1984) found that 95% of the heavy rare earths and 65% of the light rare earths dissolved in river water were removed by flocculating colloids in the estuary of the River Luce, a river particularly rich in organic matter. Loss of rare earths as a function of salinity was similar to that of iron, as shown in Figure 15.25, so that Hoyle et al. concluded that the rare earths were adsorbed or coprecipitated with Fe-organic colloids. Organic matter colloids appear to be the carriers of rare earths as no REE removal was observed in laboratory experiments in which seawater was mixed with organic-poor river water. Hoyle et al. (1984) found that heavy rare earths were preferentially removed. Subsequent work showed that in most cases, it is the light rare earths that are preferentially associated with colloidal phases and removed by flocculation (Elderfield, et al., 1990; Sholkovitz, 1992).

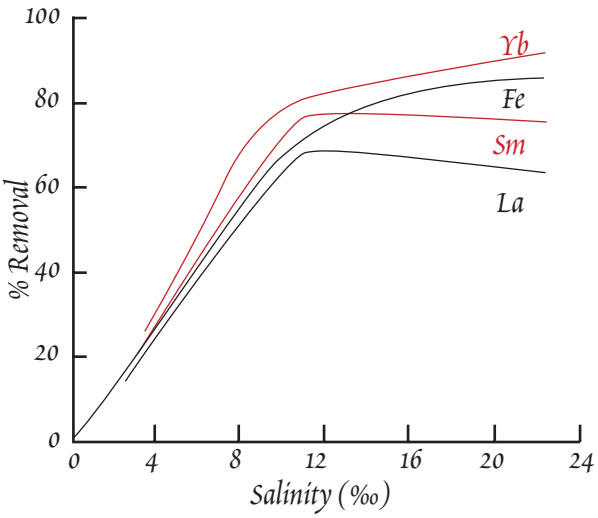

Figure 15.25. Removal of Fe and REE during mixing of seawater and organic-rich water from the River Luce in Scotland. Removal apparently occurs by coagulation and precipitation of Fe-organic colloids. Modified from Hoyle et al. (1984).

Flocculation is not restricted to colloids. The electric double layer surrounding larger particles is also condensed as river water mixes with seawater, causing them to flocculate as well. As a result of this process, estuary act as sediment traps. As much as 90% of the suspended load of rivers never reaches the open sea, being deposited in the estuarine or near-shore environment instead (Chester, 1991).

Increasing ionic strength also results in a decrease in activity coefficients, as would be predicted, for example, by the Debye-Hückel equation (equation 3.84). This decreases the *effective* concentration of dissolved species and thus drives precipitation-dissolution and adsorption-desorption reactions toward dissolution and desorption. Mixing of river and seawater also results in changing concentration of major ions. This af-

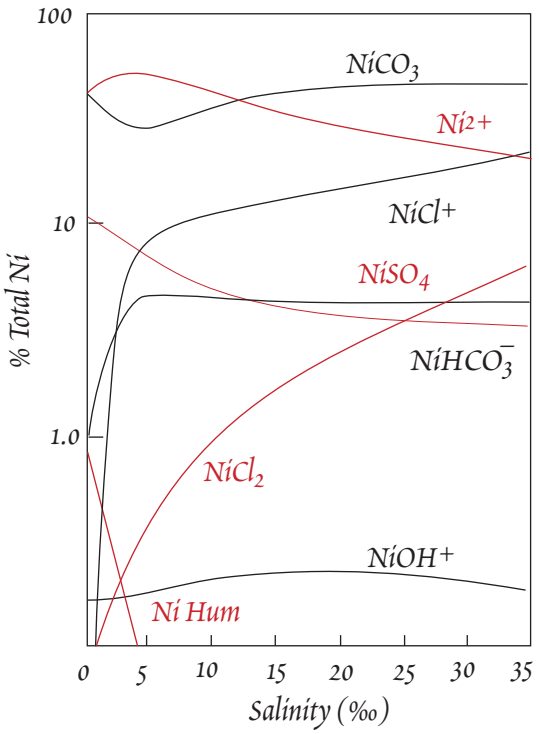

Figure 15.26. Ni speciation as a function of salinity in estuaries. From Montoura et al. (1978).

fects speciation of trace ions in several ways. First, as the proportion of seawater increases, trace metals are replaced on cation binding sites of organic molecules such as humic and fulvic acids by Mg and Ca. Second, as the concentrations of inorganic ligands increase, metals ions are increasingly complexed by them. These changes are illustrated for nickel in Figure 15.26. The result is a decrease in the free ion concentration of many metals, which in turn results in desorption of surface-bound species. Thus as a result of changing speciation, as well as the increase in ionic strength, the total dissolved concentration of some ions may increase in an estuary. Changes in pH, of course, will also affect speciation.

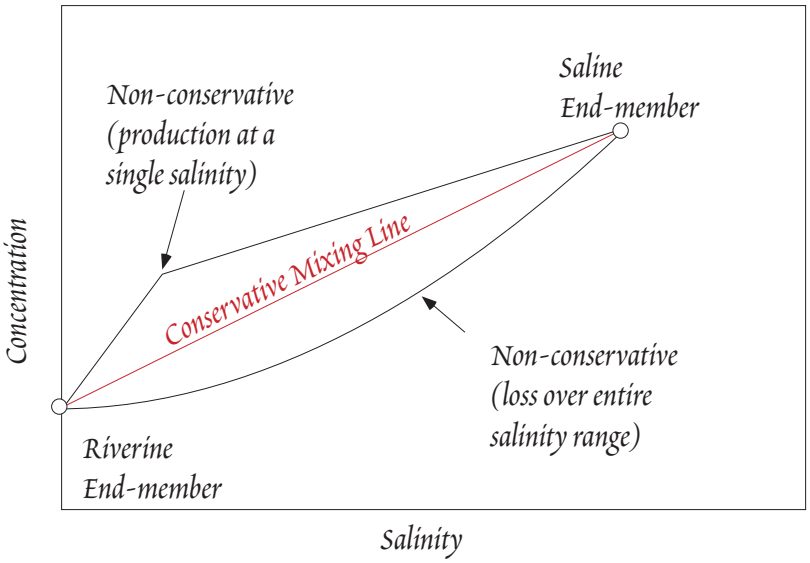

Figure 15.27. Cartoon illustrating the use of concentration-salinity diagrams in estuaries.

Whether a dissolved component is added to or removed from solution in an estuary can be readily determined by plotting its concentration against salinity. The concentration of any *conservative* species in an estuary will be a function only of the proportions in which sea and river water are mixed. Salinity is always conservative in estuaries because addition or removal of major species does not occur to a significant extent. The concentration of any other conservative species should therefore be a simple linear function of salinity. As illustrated in Figure 15.27, any deviation from linearity indicates removal or addition of that species.

The behavior of barium in the Yangtze estuary provides an example of addition demonstrated by a concentration-salinity diagram (Figure 15.28). The addition of Ba probably results from replacement of adsorbed Ba on surfaces by major cations as we described above (Edmond et al., 1985). Figure 15.29 shows concentration-salinity diagrams for metal ions in the Gironde estuary, France. Fe concentrations plot along a curve below the conservative mixing line, consistent with its removal by colloid flocculation. Ni plots along a curve above the mixing line, indicating addition. Kraepiel et al. (1997) concluded this results from desorption of Ni from sediment particle surfaces, which in turn is due to a decrease in the free Ni ion concentration due to complexation by inorganic ligands. Essentially all of the Ni addition occurs at salinities lower than 10‰, at high salinities Ni behave nearly conservatively. Pb appears to be nearly conservative. Pb is strongly particle-reactive, so truly conservative behavior would be surprising. Its apparent conservative behavior could be due to a combination

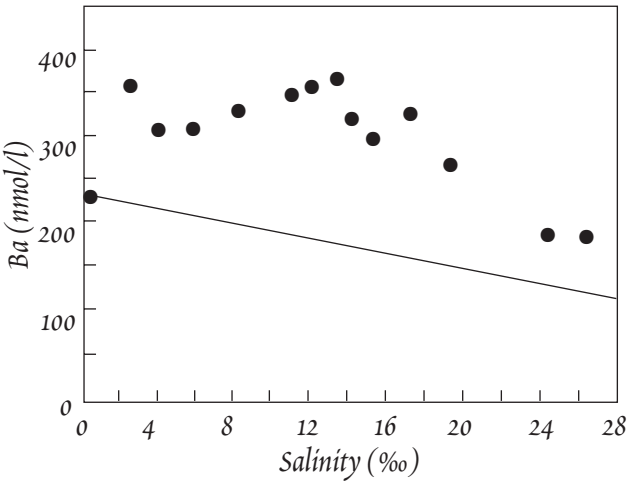

Figure 4.28. Ba concentrations as a function of salinity in the estuary of the Yangtze River compared with a conservative river-seawater mixing line. Ba is being added to solution at salinities of about 2 and 14. After Edmond et al. (1985).

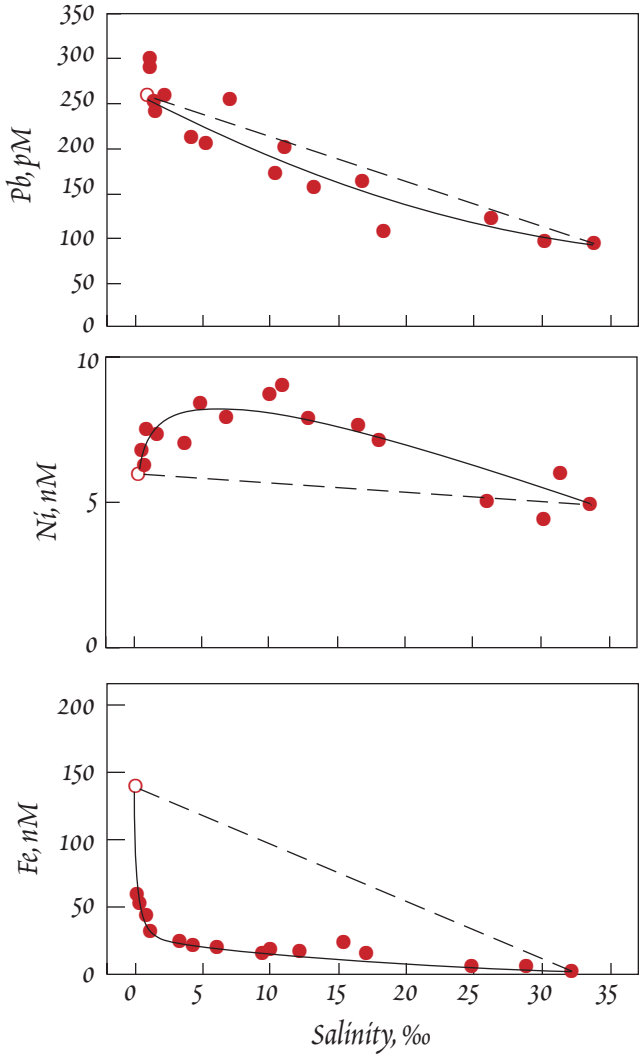

Figure 15.29. Concentrations of dissolved Pb, Ni, and Fe measured in the Gironde estuary, Bordeaux, France. Open symbol is the average concentration of river water. Dashed line is the conservative mixing line, solid line is visual best fit to the data. The curves indicate removal of Fe and Pb and addition of Ni. Modified from Kraepiel et al. (1997).

of addition by desorption from solid surfaces and removal by coprecipitation with colloidal Fe hydroxides and humates.

Redox reactions in estuaries also affect solution chemistry. Increasing pH speeds the oxidation of ferrous to ferric iron, while the presence of suspended matter, increases the rate of oxidation of Mn^{2+}, which may be present metastably in rivers. In some estuaries, the development of a strong pycnocline inhibits exchange of gas between the deeper saline layer and the atmosphere. Many estuaries are surrounded by wetlands (salt marshes or wetlands), which export both dissolved and particulate organic matter. Bacterial respiration of this organic matter can lead to anoxic conditions in the deep layer. Anoxia may also develop when algal growth is stimulated by anthropogenic additions of nitrate and phosphate and bacterial decomposition of the algal remains occurs. Chesapeake Bay is a good example of this situation; the bottom waters of which become anoxic in the summer. In such circumstances, species whose solubility depends on their redox state, most notably Fe and Mn, may redissolve in the anoxic water.

Where anoxia does not develop in the water column, it may still develop within the sediment because of high organic sedimentation rates. Fe and Mn may be reduced in the sediment and diffuse back into the overlying water column. Hence reduced sediments may serve as a source of metals ions. A study of Narragansett Bay, Rhode Island by Elderfield et al. (1981) provides an example. Although the bay water is oxygenated, oxygen is rapidly depleted within the uppermost sediment due to the high organic content. As a result, Mn^{4+} in the sediment is reduced to soluble Mn^{2+}, the concentration of which increases to 2 to 7 μM within the top cm of sediment, well above the 0.5 μM concentrations found in Bay water. Remobilized Mn then diffuses out of the sediment into Bay water. The resulting benthic flux of Mn into the Bay is 40% of the riverine flux. In contrast, the reducing conditions within the sediment lead to precipitation of Ni, Cd, and Cu sulfides, so that there is a net diffusive flux of these elements from Bay water to the sediment. The Ni and Cu fluxes into the sediment were 60% and 30% of the riverine fluxes respectively.

Reductive dissolution can also remobilize particle-reactive elements scavenged by Mn and Fe oxides and hydroxides. This apparently occurs in Buzzards Bay, Massachusetts, where the sediment becomes reducing at depth. Elderfield and Sholkovitz (1987) found rare earth concentrations in sediment pore waters that were 10 to 50 times local seawater values. Much of the remobilized REE are

readsorbed or reprecipitated by Mn and Fe oxides in the upper sediment, but Elderfield and Sholkovitz (1987) nevertheless concluded that benthic flux of REE to the bay was of a magnitude similar to the riverine flux.

In summary, chemical processes in estuaries significantly modify the riverine flux to the oceans. This modification occurs primarily through solution-particle reactions that occur as a result of mixing of sea and river water. The results of these processes differ between estuaries because of differences in physical regime, biological productivity, residence time of the water in the estuary, and the nature and concentration of suspended matter. Some generalizations may nevertheless be made. A significant fraction of Fe and other particle-reactive elements such as Al and the REE are removed by colloidal flocculation in estuaries. Though biological productivity removes nutrients (SiO_2, NO_3, PO_4) from solution, these are largely recycled within the estuary so that the net modification to the flux of these elements is probably small (Chester, 1991). The flux of major cations is similarly largely unaffected. Estuaries may act as a source for a number of other elements, such as Ba, Mn, Ni, and Cd through desorption and remobilization in the sediment.

Mid-Ocean Ridge Hydrothermal Systems

One of the most exciting developments in geochemistry in the past 25 years has been the discovery of hydrothermal vents at mid-ocean ridges. Simply the sight of 350° C water, black with precipitate, jetting out of the ocean bottom, surrounded by a vibrant if bizarre community of organisms living in total darkness at depths of 2500 m or more was exciting. But these phenomena were exciting for other reasons as well. Hydrothermal systems are sites of active ore deposition, so scientists were able to directly analyze the kinds of fluids that produce volcanogenic massive sulfide ores. Hydrothermal activity is also an important source for some elements in the oceans, and an important sink for others and has a profound effect on the composition of the oceanic crust. Thus the discovery of hydrothermal vents has provided geochemists with the opportunity to put into place a major piece of the great geochemical puzzle.

The fluids emanating at hydrothermal vents are seawater that has undergone extensive reaction at a variety of temperatures with the oceanic crust. They are reduced (sulfide-bearing), acidic, and rich in dissolved metals. Three kinds of venting has been observed: low temperature diffuse venting, in which hydrothermal solutions that have mixed extensively with seawater solutions in the subsurface diffuse slowly out of the seafloor; "black smokers", in which high temperature (usually >300° C) fluid jets from sulfide "chimneys" and precipitate sulfide and Fe-Mn oxyhydroxide "smoke"; and "white smokers", in which high temperature fluids (200-300°C) jet from anhydrite chimneys and precipitate white anhydrite "smoke".

The Composition of Hydrothermal Fluids

Samples of pure vent fluids have proven difficult to obtain, as vent fluids quickly mix with ambient seawater. The pure vent fluid end-member of the sampled mixture must therefore be calculated. This is straightforward provided the concentration of at least one property of the vent fluid is known. Since the temperature of the vent fluid can be determined, this provides the key to calculating the vent fluid end-member composition. The first vents discovered, on the Galapagos Spreading Center, were diffuse, low temperature vents (<13 ° C). A strong inverse correlation between Mg and temperature was observed, and Edmond, et al. (1979), concluded that the pure hydrothermal fluid had a temperature of 350° C and a Mg concentration of 0. The data from the first high temperature vents discovered, at 21 °N on the East Pacific Rise, extrapolated to a similar temperature and an Mg concentration of 0 (Figure 15.30a; the scatter in the data in this figure is due to the temperature probe flopping about: temperatures were high enough to melt the adhesive holding it in place). Thus Mg appears to be quantitatively extracted from seawater in hydrothermal systems. This was subsequently shown to be true of all other high temperature hydrothermal systems. Having determined that the Mg concentration of the vent fluid is 0, the concentrations of all other species in the vent fluid were easily obtained from the intercept of a plot of the concentration of the species of interest. For example, a plot of sulfate versus Mg extrapolates to 0 sulfate at 0 Mg (Figure15.30b). Thus these vent fluids also have

0 sulfate. The same procedure shows the vent waters are also rich in silica and Li relative to seawater (Figure 15.31).

The pure hydrothermal fluid in the first few vents discovered all had relatively homogeneous compositions and similar temperatures. Subsequently discovered vents were more variable. Temperatures of fluids from vents at 19 sites ranges from 220 to 403°C (this range excludes "diffuse flow"). The lowest temperatures occur where vent fluids exist through sediment overlying the basalt (e.g., the Guaymas Basin in the Gulf of California, Escanaba Trough on the Gorda Ridge, and Middle Valley on the Juan de Fuca Ridge). The highest temperatures were found in vents at the site of a recent volcanic eruption (at 9-10° N on the East Pacific Rise). The majority of vents have temperatures in the range of 300°C to 380°C, a surprisingly narrow range. This narrow range of temperatures probably reflects the large density decrease that occurs when seawater is heated beyond these temperatures. Alternatively, it may reflect a sharp decrease in rock porosity beyond these temperatures (L. Cathles, pers. comm.).

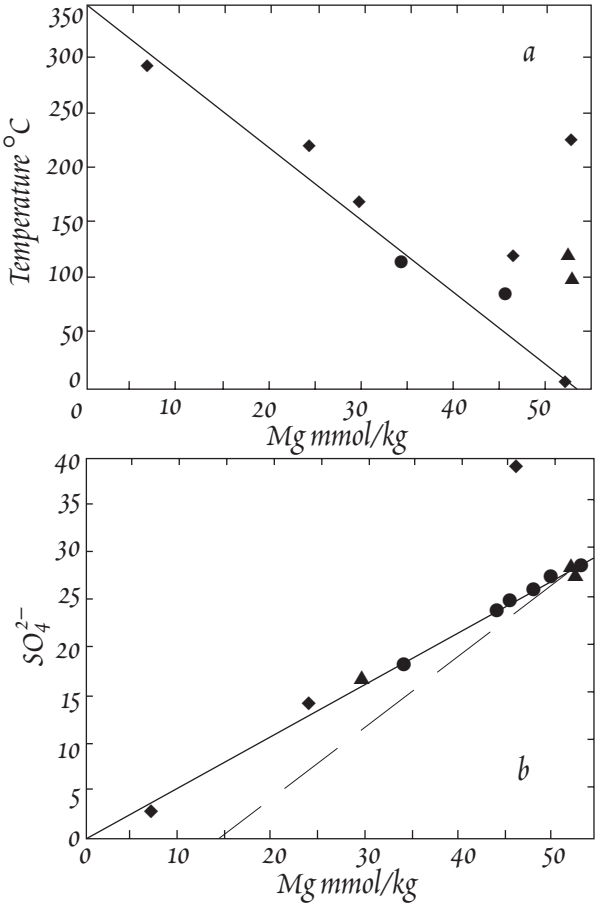

Figure 15.30. (a) Temperature vs. Mg concentration for several vents in the 21°N region of the EPR. (b) Mg-sulfate plot for 21°N vents. From Van Damm et al. (1985).

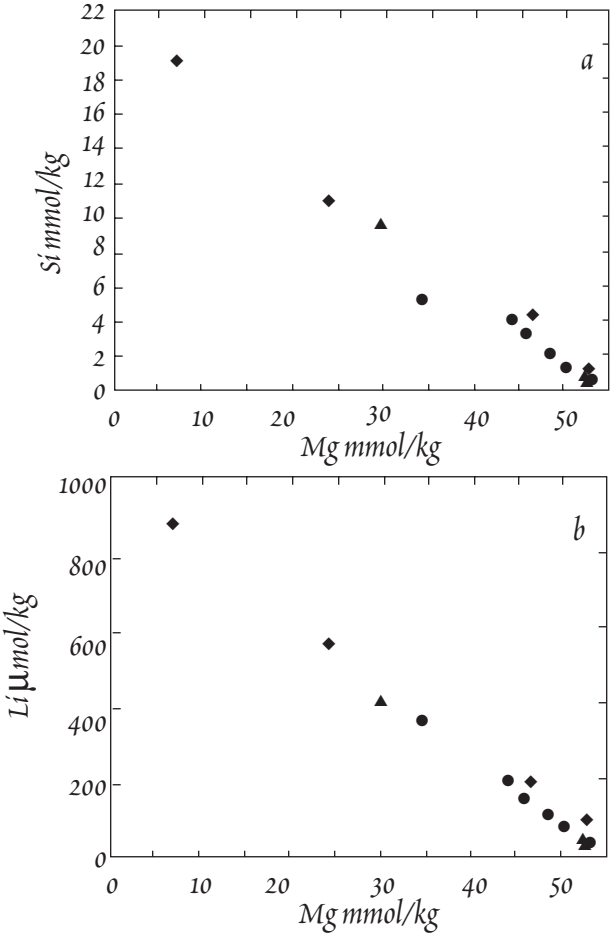

Figure 15.31. (a) SiO_2 vs. Mg for hydrothermal fluids from the 21°N vents. (b) Mg-Li plot for 21°N vents. From Van Damm et al. (1985).

TABLE 15.4. COMPOSITION OF REPRESENTATIVE HYDROTHERMAL VENT FLUIDS

	21°N (EPR)	Escanaba (Gorda)	South Cleft Plume	Axial Volcano Virgin Mound	TAG MAR	Seawater
T °C	273-355	108-217	224	299	335-350	—
pH	3.3-3.8	5.4	3.2	4.4	3.7-3.9	8.2
Li μmol/kg	891-1322	1286	1718	184	845	25.6
δ^6Li	-6.6 to -10				-6.3 to -8.5	-32.3
Be nmol/kg	10-13		95		38.3	0.025
B μmol/kg	500-548	1.71-2.16	496	450	518-530	406
δ^{11}B	30.0-32.7	10.1-11.5	34.2		25.6-26.8	+39.5
CO_2 mmol/kg	5.7		3.7-4.5	285		
CH_4 mmol/kg	0.06-0.09		.082-.09			—
NH_4 mmol/kg	<.01	5.6				—
Na mmol/kg	432-513	560	796	148	510	468
Al μmol/kg	4.0-5.2				5.0-5.3	0-0.15
Si mmol/kg	15.6-19.5	5.6-6.9	23.3	13.5	18.3	0-0.25
H_2S mmol/kg	6.6-8.4	1.1-1.5	3.5	18	5.9	26.9*
δ^{34}S	+1.4-3.4	+7.8	+5.7	+7.3		+21
Cl mmol/kg	489-579	668	1087	176	559	532
K mmol/kg	32.5-49.2	34-40.4	51.6	6.98	23.8	9.96
Ca mmol/kg	11.7-20.8	33.4	96.4	10.2	9.9-10.5	10.3
Mn mmol/kg	.67-1.0	0.01-0.21	3.59	142	659	<0.04
Fe mmol/kg	.75-2.43	0-0.1	18.7	12	1	<0.006
Co nmol/kg			200			<0.07
Cu μmol/kg			1.5	0.4	1.64	<0.004
Zn μmol/kg			780	2.2		<0.009
Ge nmol/kg	130-170		150-260			0-0.2
As nmol/kg	30-452					13-27
Se nmol/kg	<0.6-72		<1			0.5-1.5
Br μmol/kg	802-929	1179	1832	250	847	839
Rb μmol/kg	27-33	80-105	37		10.7	1.45
Sr μmol/kg	65-97	209	312	46	51	87
$^{87}Sr/^{86}Sr$	.7030-.7033	0.7099			0.7028	0.70918
Mo nmol/kg			6			115
Ag nmol/kg			120			<0.03
Cd nmol/kg			910			0-1.0
Sb nmol/kg			18			0.7-1.3
I μmol/kg		99				0.2-0.5
Cs nmol/kg	202	6.0-7.7			179	2.25
Ba μmol/kg	8-16					0.085
Tl nmol/kg			110			<0.08
Pb nmol/kg			1630			<0.002

From compilations of van Damm (1995) and Shanks et al. (1995). EPR: East Pacific Rise, Mar: Mid-Atlantic Ridge. South Cleft and Axial Volcano sites are on the Juan de Fuca Ridge.

* Concentration of *sulfate* in seawater.

Table 15.4 lists compositions of several representative hydrothermal vent fluids (all compositions are calculated on the assumption that the pure vent fluid has an Mg concentration of 0 as described above). The fluids are acidic and reducing (sulfide has replaced sulfate). Most of the vent fluids

have Cl, Na, and B concentrations that are close (within about 20%) to seawater concentrations. In these cases, these elements appear to behave almost conservatively in the hydrothermal system. The Virgin Mound vent on Axial volcano, a "white smoker", has substantially less Cl than seawater, while the South Cleft fluid has substantially more. In general, the vent fluids have substantially less sulfide than seawater has sulfate, thus there has been a net loss of sulfur from solution. All the fluids have much greater concentrations of Li, Be, Al, C, Si, Ge, Rb, Cs, and transition metals (except for Mo) than seawater. All except the Virgin Mound vent higher concentrations of K than seawater.

The composition of hydrothermal fluids depends on a number of factors (Von Damm, 1990): temperature, pressure, the ratio in which water and rock react (the water/rock ratio), whether the rock is fresh or has previously reacted, whether equilibrium is achieved, or compositions are instead controlled by kinetics, whether fluids have undergone phase separation, and whether mixing between different fluids has occurred. We now examine the processes that occur within hydrothermal systems.

Evolution of Hydrothermal Fluids

In a simplistic fashion, hydrothermal systems can be divided into 3 zones (Alt, 1995). The principal processes and reactions involved are shown schematically in Figure 15.32. The first is the *recharge zone*, where seawater enters the oceanic crust and is heated as it penetrates downward. In this zone, which may be several kilometers or more off the axis of the ridge, flow is diffuse, so water rock ratios are low, and temperature of reaction is relatively low (<200° C). The second is the *reaction zone*, which is located near the base of the sheeted dikes and in the upper gabbros (see Chapter 11). In this zone, water reacts with hot rock at high temperature (≥350° C), and the primary chemical characteristics of the fluid are determined. Because of reduced permeability of the crust, water/rock ratios are lower here than in the overlying recharge zone. Phase separation, in which the fluid separates into a high density brine and lower density fluid, may occur in this zone. The third zone, in which the final composition of the fluid is achieved, is the *upflow zone*. Here water rises rapidly and cools somewhat as it does so. Precipitation of some sulfides may occur. Boiling may also occur if pressure is sufficiently low and temperature sufficiently high. Since upflow appears to be quite focused, water/rock ratios are low. Mixing with low temperature seawater may also occur, which leads to extensive sulfide and anhydrite precipitation.

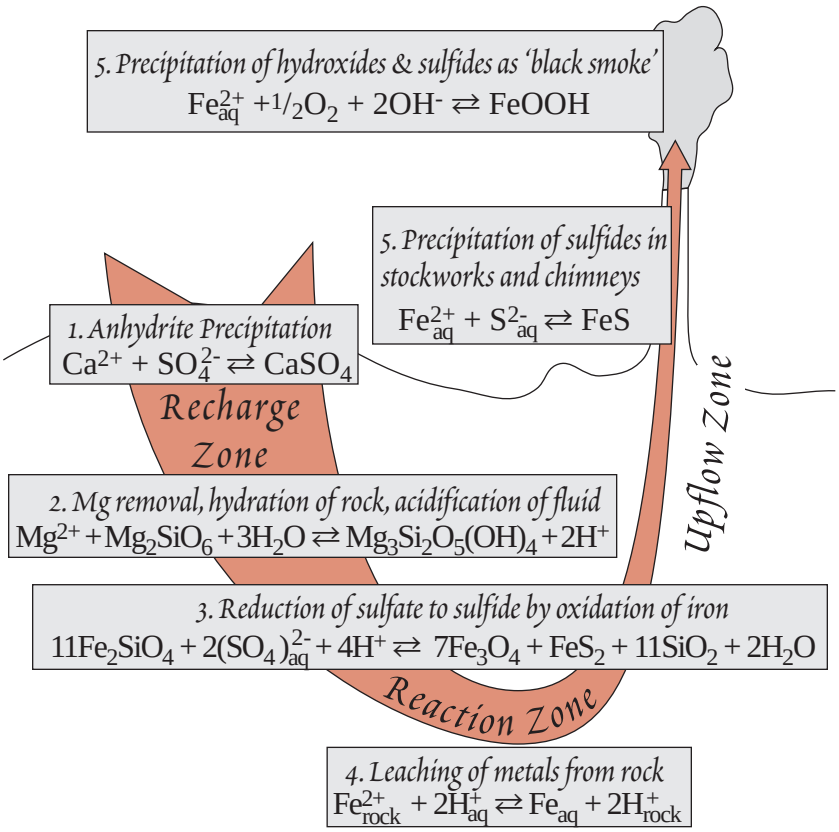

Figure 15.32. Cartoon illustrating some of the important reactions occurring in mid-ocean ridge hydrothermal systems.

- Recharge Zone

As water enters the oceanic crust, low temperature reactions occur in which volcanic

glass and minerals are transformed to clays such as celadonite, nontronite, ferric micas, and smectite, and oxyhydroxides. In this process, the rock takes up alkalis Li, K, Rb, Cs, B, and U from seawater. Calcite may precipitate in veins. Isotopic exchange also occurs, leading to higher Sr and O and lower B and Li isotope ratios in the basalt.

As seawater warms to temperatures around 150° C, anhydrite ($CaSO_4$) precipitates. By 200° C, essentially all the Ca^{2+} and two-thirds of the SO_4^{2-} (as well as a significant fraction of the Sr) are lost in this way. Addition of Ca^{2+} to the fluid by reaction with basalt will result in further removal of sulfate. Thus the fluid entering the reaction zone is severely depleted in calcium and sulfate. Although anhydrite is found in altered oceanic crust, it is rare. Thus it is likely that much of the anhydrite precipitated in this way later dissolves when the crust cools.

The third major reaction in the recharge zone is loss of Mg^{2+} from seawater to the oceanic crust. This occurs through replacement of primary igneous minerals and glass by clay minerals such as sapolite and smectites, for example, by replacing plagioclase:

$$2Mg^{2+} + 4H_2O + 2SiO_2 + 2CaAl_2Si_2O_8 \rightleftarrows Mg_2Ca_2Al_4Si_6O_{20}(OH)_4 + 4H^+$$

At higher temperatures, chlorite forms, for example, by replacing pyroxene:

$$2Mg^{2+} + 6H_2O + 2MgFeSi_2O_6 \rightleftarrows Mg_4Fe_2Si_4O_{10}(OH)_8 + 4H^+$$

The significance of these reactions in not only loss of Mg from the solution, but also the production of H^+ (or, equivalently, the consumption of OH^-). *It is these reactions that account, in part, for the low pH of hydrothermal vent solutions.* This greatly increases the fluid's capacity to leach and transport metals.

- Reaction Zone

Seismic studies of the East Pacific Rise reveal the existence of a "melt lens" at shallow depth (2 km or so) beneath the rise axis. The depth of this magma lens is an upper limit to the depth to which hydrothermal solutions may circulate. This implies pressures in the reaction zone are less than 50 MPa. Geochemical observations are consistent with these geophysical constraints. For instance, Von Damm and Bischoff (1987) used measured SiO_2 concentrations in Juan de Fuca vent fluids together with thermodynamic data to estimate that the fluids equilibrated with quartz at pressures of 46-48 MPa and temperatures of 390-410° C. Geothermometry performed on minerals in altered oceanic crust indicate temperatures as high as 400-500° C. By comparing a thermodynamic model of hydrothermal interactions and assuming fluids are in equilibrium with the assemblage anhydrite-plagioclase-epidote-pyrite-magnetite, Seyfried and Ding (1995) estimated temperatures of 370° to 385° C and 30 to 40 MPa for equilibration of fluids from the 21° N on the EPR and the MARK area of the Mid-Atlantic Ridge.

Under these conditions, reactions would include the formation of amphiboles, talc, actinolite, and other hydrous silicates from reactions involving ferromagnesian silicates (olivines and pyroxenes), the formation of epidote from plagioclase:

$$Ca^{2+} + 2H_2O + 3CaAl_2Si_2O_8 \rightleftarrows 2Ca_2Al_3Si_3O_{12}(OH) + 2H^+$$

as well as the exchange of Na^+ for Ca^{2+} in plagioclase, a process termed *albitization*, and precipitation of quartz:

$$2Na^+ + 2CaAl_2Si_2O_8 \rightleftarrows 2NaAlSi_3O_8 + SiO_2 + 2Ca^{2+}$$

The evidence for albitization comes not only from the identification of albitized plagioclase in hydrothermally altered rocks, but also the inverse correlation between Na/Cl and Ca/Cl in hydrothermal fluids (Figure 15.33). In addition, the fluid will be reduced by oxidation of ferrous iron in the rock, e.g.:

$$2SO_4^{2-} + 4H^+ + 11Fe_2SiO_4 \rightleftarrows FeS_2 + 7Fe_3O_4 + 11SiO_2 + 2H_2O$$

The solubility of transition metals and S increase substantially at temperatures above 350°C, so sulfides in the rock are dissolved, e.g.:

$$Cl^{2-} + 2H^+ + FeS \rightleftarrows H_2S_{aq} + FeCl^0_{aq}$$

The metals released will be essentially completely complexed by chloride, which is by far the dominant anion in the solution, as most sulfate has been removed or reduced and sulfide and CO_2 will be

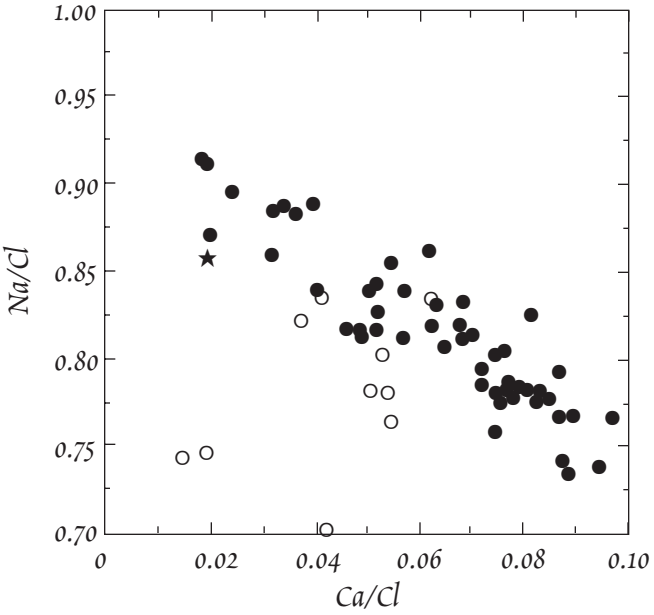

Figure 15.33. Na/Cl vs Ca/Cl in hydrothermal vent fluids. Most fluids define an inverse correlation that results from albitization of plagioclase. Only the fluids from vents in the 9-10°N region of the EPR that developed after the 1991 eruption (open symbols) deviate from this trend. Composition of seawater indicated by the star. After Von Damm (1995).

largely protonated at the prevailing pH. Isotopic compositions of H_2S in vent fluids indicates most is derived from dissolution of sulfides in the rock, with a smaller contribution from reduction of seawater sulfate.

Whereas the alkalis Li, K, Rb, Cs, B, and U are taken up by the rock at low temperature, they are released at high temperature. Loss of K, Rb, and Cs begins around 150° C, but loss of Li probably does not begin until higher temperatures are reached (Na, though, is actively taken up, even at high temperatures, by albitization).

Fluids make their closest approach to the magma chamber in the reaction zone, and magmatic volatiles may be added to fluids within this zone. Hydrothermal vent fluids with seawater chlorinities have CO_2 concentrations as high as 18 mmol/kg, which is substantially more than seawater (~2 mmol/kg). The isotopic composition of this carbon ($\delta^{13}C \approx -4‰$ to -10‰) is similar to that of mantle carbon (see Chapter 9) and distinct from that of seawater bicarbonate ($\delta^{13}C \approx 0$). Thus the excess CO_2 is probably of magmatic origin. Other magmatic volatiles present in the fluid may include He, CH_4, H_2, and even H_2O. In most cases, any contribution of magmatic H_2O will be insignificant compared to seawater-derived H_2O. However, fluids from vents at 9-10°N on the EPR have negative δD values (Figure 15.34), which suggest a small but significant contribution of magmatic water. These vents developed and were sampled shortly after an eruption in 1991. Shanks et al. (1995) calculated that the observed δD values could be explained by addition of 3% magmatic water and that this water could be supplied by degassing of a dike 20 km long, 1.5 km deep and 1 m wide. The magmatic water would be exhausted in about 3 years.

The reaction zone is also the region where phase separation is most likely to occur. Unlike pure water, which cannot boil at pressures above its critical point (see Chapter 2), seawater will undergo phase separation above its critical point, but the two phases produced are different from those produced below the critical point. Below its critical point, at 29.8 MPa and 407° C, seawater boils to produce a low salinity vapor phase and a liquid whose salinity initially approximates that of the original liquid. In the case of hydrothermal fluids, the vapor produced would be strongly enriched in H_2S and CO_2 as well as other volatiles. As boiling continues, the liquid becomes increasingly saline. Above its critical point, seawater separates into a dense brine and a fluid whose salinity initially approximates that of the original liquid. As phase separation continues, the fluid becomes increasingly dilute while the brine becomes more concentrated. The phase diagram (P-X) for the system H_2O-NaCl shown in Figure 15.35 illustrates this. Seawater behaves approximately as 3.5% NaCl solution. At a pressure of 36.4 MPa and 400° C, a 3.5% NaCl solution would be above the two-phase curve, so only one phase exists. At the same pressure and 430° C, it lies just on the two-phase curve, and a brine containing ~10% NaCl begins to separate. If temperature is increased to 450°, NaCl in the brine increases to ~20%, and decreases in the other phase to 0.4%.

Cl behaves nearly conservatively in hydrothermal solutions. Phase separation, and mixing between the fluids produced by it, provides the best explanation for the large variations in Cl content

observed in hydrothermal fluids. Brines produced by phase separation may be too dense to rise to the seafloor. Instead, they may reside at depth for prolonged periods of time, slowly mixing with less saline fluids. The high chlorinity of the North Cleft fluid results from mixing of a fluid with seawater chlorinity and a high salinity brine (Von Damm, 1988). Indeed, most hydrothermal vent fluids appear to be mixtures of 3 components: hydrothermally altered seawater, a high chlorinity brine produced by supercritical phase separation, and a low chlorinity, H_2S-rich vapor produced by subcritical phase separation (Edmonds and Edmond, 1995). The chlorinity of fluids also influences other compositional factors. The solubility of H_2S decreases with increasing chlorinity. However, concentrations of metals such as Fe and Cu increase with increasing chlorinity because of the formation of metal chloride complexes. Thus a fluid produced by mixing will likely be out of equilibrium with the rock and thus undergo further reaction after mixing (Seyfried and Ding, 1995).

Two other important controls on solution chemistry are pH and f_{O_2}. The Fe/Cu ratio of the fluid is sensitive to both of these, high f_{O_2} and low pH favoring a high Fe/Cu ratio. Fe/Cu ratios of hydrothermal fluids indicate pH values in the reaction zones of 4.8 to 5.2 and f_{O_2} buffered by the assemblage anhydrite-magnetite-pyrite (Seyfried and Ding, 1995).

- Upflow Zone

The density decrease caused by heating eventually forces the hydrothermal fluid to rise to the seafloor. The concentrated flow out of vents indicates that the upwelling zone is narrow and flow is strongly focused through fractures. Upflow zones in exposed sections of oceanic crust (ophiolites) are altered to the assemblage epidote-quartz-titanite or actinolite-albite-titanite-chlorite assemblages. This is consistent with thermodynamic calculations, which show hydrothermal fluids in equilibrium with similar assemblages (e.g., Bowers et al., 1988). The fluid experiences decompression as it rises, and may experience phase separation at this point. The low chlorinity Virgin Mound fluid (Table 15.5) is an example of a fluid whose chlorinity has been reduced by mixing with a low salinity vapor phase produced by boiling. The fluid is also very strongly enriched in CO_2, as CO_2 partitions into the vapor during boiling, and this accounts for the high CO_2 of this fluid. The shallow depth of this vent would mean that hydrothermal fluids would reach the critical point nearly 1500 m beneath the seafloor, providing ample opportunity for subcritical phase separation during ascent.

Most fluids appear to have undergone some conductive cooling during ascent, as calculated equilibrium temperatures generally somewhat exceed measured vent temperatures. Cooling of fluids will induce precipitation of sulfides and quartz. In ophiolites, upflow zones are marked by mineralized alteration pipes, or stockworks. The solubility of Cu shows the strongest temperature dependence, followed by Fe, thus the concentrations of these two elements may drop significantly during upflow. The solubility of Mn and Zn are temperature dependent.

In the Guaymas Basin of the Gulf of California and the Escanaba Trough of the southern Gorda Ridge, vent fluids exit through sediment cover. Hydrothermal fluids must traverse up to 500 m of sediment before exiting to seawater. Vent temperatures are somewhat cooler, 100-315°C. The compositions of these fluids is distinct. The fluid alkaline because of the presence of ammonia produced by break-

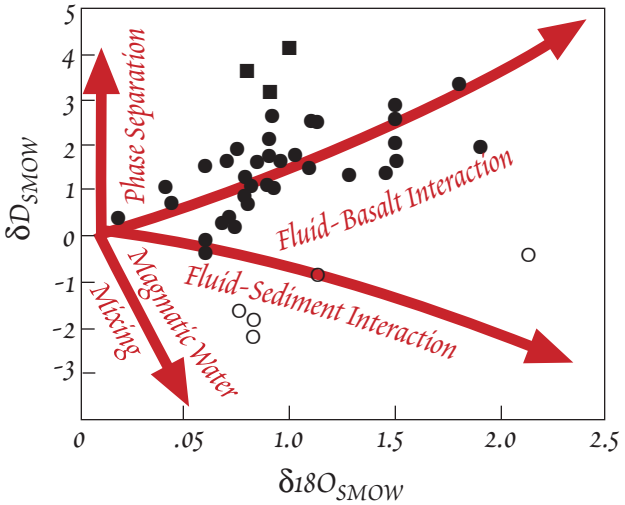

Figure 15.34. Oxygen and hydrogen isotope ratios in hydrothermal vent fluids. Red arrows show predicted paths for various subseafloor processes (phase separation refers to the vapor path during adiabatic phase separation). Only the fluids from the 9-10° N vents (open circles) and Guaymas Basin fluids do not conform to the predicted path for fluid-basalt interaction. Negative values in the 0-10° N fluids indicate mixing with magmatic water. Modified from Shanks et al. (1995).

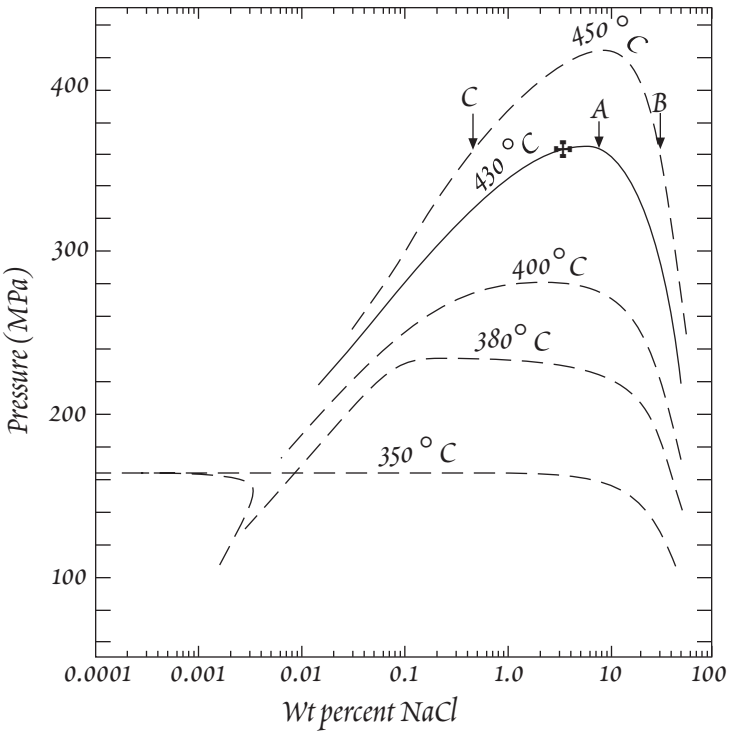

Figure 15.35. Pressure-composition phase diagram for the system H_2O—NaCl. A seawater-like 3.5% NaCl solution at 36.4 MPa (cross) will lie above the 2 phase region at 400° C, and will thus consist of a single phase. At 430° C, it lies just on the two-phase curve and a brine of composition A begins to separate. At 450°, it lies within the 2-phase field and has separated into a fluid of composition C and a brine of composition B. Adapted from Bischoff and Pitzer (1989).

down of organic matter in the sediment. Guaymas Basin fluids are somewhat richer in some alkalis and alkaline earths, due to dissolution of carbonate and leaching of sediment. Both the Guaymas and Escanaba fluids are transition metal-poor, as a result of sulfide precipitation in the sediment. The Guaymas fluid is also rich in hydrocarbons, which are produced by thermal degradation of organic matter in the sediment.

Finally, hydrothermal fluids eventually mix with seawater, either in the shallow subsurface or as they exit the seafloor. This induces additional cooling and precipitation. Along with sulfide precipitation, mixing causes the seawater-derived sulfate to precipitate as anhydrite. Precipitation of anhydrite accounts for the white "smoke" of white smokers (of which the Virgin Mound vent is an example). Precipitation at the sea surface quickly builds chimneys, which can reach more than 10 meters above the seafloor. Chimneys consist primarily of Fe and Cu sulfides such as pyrite (FeS_2), marcasite (FeS_2), pyrrhotite (FeS), chalcopyrite ($CuFeS_2$), bornite (Cu_5FeS_4), cubanite ($CuFe_2S_3$) with lesser amounts of sphalerite (ZnS), wurtzite (ZnS), galena (PbS), silica, silicates, anhydrite, and barite ($BaSO_4$). For the most part, they are rather fragile structures subject to weathering in which anhydrite redissolves and sulfides oxidize to oxyhydroxides once venting terminates.

- Hydrothermal Plumes

As vent fluid is diluted with seawater, a hydrothermal "plume" is created, which can rise hundreds of meters above the vent site because of its slightly warmer temperature and therefore lower density than surrounding water. Precipitation of sulfide "smoke" immediately above the vent removes up to half the dissolved Fe. The remained is oxidized to Fe^{III} and precipitated as oxyhydroxides in the plume. The half life for Fe^{II} oxidation in seawater is anywhere from a few minutes to a day or more, depending on O_2 concentrations and pH. During Fe precipitation, a number of elements may be coprecipitated, including Mn, P, V, Cr, and As. The kinetics of Mn oxidation are considerably slower, and Mn precipitation is generally delayed until the plume reaches neutral buoyancy and begins to spread out horizontally. Mn oxidation appears to be bacterially mediated. The Fe-Mn particles produced within the plume strongly scavenge particle-reactive elements, such as Th, Be, and the rare earths, from seawater.

Hydrothermal Fluxes

The importance of mid-ocean ridge hydrothermal systems in controlling the composition of seawater was immediately realized upon the discovery of the first hydrothermal vents. Initially, it ap-

peared that estimating the flux of elements into and out of the oceanic crust was straightforward (e.g., Edmond et al., 1989; Von Damm et al., 1985). Unfortunately, the problem has proven to be not so simple. A particularly important problem is the differences between high temperature vents and diffuse vents. In diffuse vents, mixing between vent fluids and seawater leads to extensive precipitation of the dissolved metals in the subseafloor; for such elements, the global flux depends strongly on the ratio of diffuse to high temperature venting (Kadko, et al., 1995; Elderfield and Schultz, 1996). Despite the uncertainties, several approaches converge on estimates of heat flux and water flux of ridge crest hydrothermal activity of 2-4 $\times 10^{12}$ W and 2-4 $\times 10^{13}$ kg/yr respectively (Elderfield and Schultz, 1996). Based on these values, it is possible to make rough estimates of the global ridge crest hydrothermal flux to the oceans. The most recent estimates of these fluxes are given in Table 15.6. Estimates of the riverine flux are shown for comparison. These fluxes are lower than those estimated by Edmond et al. (1979) and Von Damm et al. (1985), in many cases by an order of magnitude. Even these recent estimates of fluxes remain substantially uncertain and should be used with caution. Nevertheless, it appears reasonably well established that hydrothermal activity appears to represent a substantial flux for many elements, including the alkalis (Li, K, Rb, Cs), Be, Mn, Fe, and Cu, and an important sink for others (e.g., Mg, U).

Table 15.6. Global Fluxes to Seawater from Ridge Crest Hydrothermal Activity

	Hydrothermal Flux	Low-T Alteration Flux	Riverine Flux
H_2	$0.3 \rightarrow 1.5 \times 10^{10}$		
H_2O		-1.3×10^{10}	2.1×10^{15}
Li	$1.2 \rightarrow 3.9 \times 10^{10}$	$0.2 \rightarrow 1.1 \times 10^{10}$	1.4×10^{10}
Na		-0.3×10^{12}	7.3×10^{12}
K	$2.3 \rightarrow 6.9 \times 10^{11}$	$-1 \rightarrow -7 \times 10^{12}$	1.9×10^{12}
Rb	$2.6 \rightarrow 9.5 \times 10^{8}$	$-1.9 \rightarrow -3.7 \times 10^{8}$	3.7×10^{8}
Cs	$2.6 \rightarrow 6.0 \times 10^{6}$	$-2.0 \rightarrow -3.8 \times 10^{6}$	4.8×10^{6}
Be	$3.0 \rightarrow 12 \times 10^{5}$		3.7×10^{6}
Mg	-1.6×10^{12}	0.2×10^{12}	5.3×10^{12}
Ca	$9 \rightarrow 1300 \times 10^{9}$	-1.3×10^{12}	1.2×10^{13}
Sr	0	9×10^{8}	2.2×10^{10}
Ba	$2.4 \rightarrow 13 \times 10^{8}$		1×10^{10}
CH_4	$0.67 \rightarrow 2.4 \times 10^{10}$		
CO_2	$1.0 \rightarrow 12 \times 10^{11}$	-2.3×10^{12}	
SiO_2	$4.3 \rightarrow 6.6 \times 10^{11}$	-7×10^{11}	6.4×10^{12}
Al	$1.2 \rightarrow 6.0 \times 10^{8}$		6×10^{10}
SO_4	-8.4×10^{11}		3.7×10^{12}
H_2S	$0.85 \rightarrow 9.6 \times 10^{11}$		
Mn	$1.1 \rightarrow 3.4 \times 10^{10}$	2.8×10^{6}	4.9×10^{9}
Fe	$2.3 \rightarrow 19 \times 10^{10}$	3.9×10^{9}	2.3×10^{10}
Co	$6.6 \rightarrow 68 \times 10^{5}$		1.1×10^{8}
Cu	$3 \rightarrow 13 \times 10^{9}$		5.0×10^{9}
Zn	$1.2 \rightarrow 3.2 \times 10^{9}$		1.4×10^{10}
As	$0.9 \rightarrow 140 \times 10^{5}$		7.2×10^{8}
Se	$3 \rightarrow 220 \times 10^{4}$		7.9×10^{7}
Ag	$7.8 \rightarrow 11 \times 10^{6}$		8.8×10^{7}
La	4.1×10^{5}		11.9×10^{6}
Ce	9.1×10^{5}		18.8×10^{6}
Nd	5.3×10^{5}		9.2×10^{6}
Sm	1.0×10^{5}		1.8×10^{6}
Eu	3.4×10^{5}		2.2×10^{5}
Gd	9.0×10^{4}		1.7×10^{6}
Dy	6.4×10^{4}		
Er	2.6×10^{4}		7.9×10^{5}
Yb	1.7×10^{4}		7.6×10^{5}
Lu	2.1×10^{3}		1.9×10^{5}
Pb	$2.7 \rightarrow 110 \times 10^{5}$		1.5×10^{8}
U	$-0.18 \rightarrow -1.6 \times 10^{7}$	-3.8×10^{6}	$3 \rightarrow 6 \times 10^{7}$

All numbers are in moles/year. From Chen et al. (1986), Rudnicki and Elderfield (1993), Kadko et al. (1994), Lilley et al. (1995), Elderfield and Schultz (1996), and Staudigel et al. (1996).

Low temperature basalt-seawater interaction, i.e., weathering, must also be considered in assessing global fluxes. Estimates of these fluxes are included in Table 15.6. For CO_2 Si and Ca, the low temperature flux into the crust may exceed the high temperature flux out of it. The oceanic crust is a sink for U at both high and low temperature. For transition metals, the low temperature flux appears to be insignificant. For K, Rb, and Cs, the high-temperature loss from the oceanic crust appears to slightly exceed the low temperature gain; for Li, the high temperature loss significantly exceeds the low temperature gain (Elderfield and Schultz, 1996). Sr is also interesting. As Table 15.6 shows, there is no net flux of Sr to seawater from hydrothermal vents. Studies of basalt similarly show the concentration of Sr in basalt

TABLE 15.7. RIDGE FLANK HYDROTHERMAL FLUXES

	Flank Flux	Rivers
B	$-0.19 \rightarrow -1.9 \times 10^{10}$	5.4×10^{10}
CO_2	$2.2 \rightarrow 2.9 \times 10^{12}$	
Mg	$-0.7 \rightarrow -1.1 \times 10^{11}$	5.3×10^{12}
SiO_2	$1.3 \rightarrow 1.8 \times 10^{12}$	6.4×10^{12}
P	-3.2×10^{9}	3.3×10^{10}
S	8×10^{12}	3.7×10^{12}
Ca	$2.0 \rightarrow 5.5 \times 10^{11}$	1.2×10^{13}
Ba	2×10^{8}	1×10^{10}
U	-9.7×10^{6}	$3 \rightarrow 6 \times 10^{7}$

All numbers are in moles/year. From Kadko et al. (1994) quoted in Elderfield and Schultz (1996).

TABLE 15.8. HYDROTHERMAL PLUME REMOVAL FLUXES

	Plume Removal Flux	Hydrothermal Flux	Rivers
Be	1.8×10^{6}	$3.0 \rightarrow 12 \times 10^{5}$	3.7×10^{6}
P	1.1×10^{10}		3.3×10^{10}
V	4.3×10^{8}		5.9×10^{8}
Cr	4.8×10^{7}		6.3×10^{8}
Mo	1.9×10^{6}		2×10^{8}
As	1.8×10^{8}	$0.9 \rightarrow 140 \times 10^{5}$	7.2×10^{8}
Y	2.1×10^{7}		
La	7.5×10^{6}	4.1×10^{5}	11.9×10^{6}
Ce	0.9×10^{6}	9.1×10^{5}	18.8×10^{6}
Nd	8.8×10^{6}	5.3×10^{5}	9.2×10^{6}
Sm	2.1×10^{6}	1.0×10^{5}	1.8×10^{6}
Eu	5.0×10^{5}	3.4×10^{5}	2.2×10^{5}
Gd	1.9×10^{6}	9.0×10^{4}	1.7×10^{6}
Dy	1.7×10^{6}	6.4×10^{4}	
Er	1.0×10^{6}	2.6×10^{4}	7.9×10^{5}
Yb	8.1×10^{5}	1.7×10^{4}	7.6×10^{5}
Lu	1.0×10^{5}	2.1×10^{3}	1.9×10^{5}
U	4.3×10^{4}	-8.1×10^{-6}	$3 \rightarrow 6 \times 10^{7}$

All numbers are in moles/year. From compilation by Lilley et al. (1995).

does not change significantly during alteration. However, vent waters have $^{87}Sr/^{86}Sr$ ratios between 0.703 and 0.706, generally more similar to basalt (0.7025) than seawater. Also studies of basalts show their $^{87}Sr/^{86}Sr$ ratios are increased by interaction with seawater. Thus hydrothermal activity serves to buffer the Sr isotopic composition of seawater: the average $^{87}Sr/^{86}Sr$ of river water is 0.7119 (Palmer and Edmond, 1989), that of seawater is 0.71018. This difference reflects the effect of hydrothermal activity. We could say that the oceanic crust is a sink for ^{87}Sr in seawater, but not for the other isotopes of Sr.

Most of the heat lost by the oceanic crust occurs not through high temperature hydrothermal systems at the ridge flanks, but through lower temperature, more diffuse hydrothermal systems operating on ridge flanks. Because the flow is diffuse and of low temperature, these fluids have been more difficult to characterize and these systems are not well understood. Nevertheless, they are undoubtedly important in global fluxes to and from seawater. Elderfield and Schultz (1996) estimate the water flux through ridge flank systems at 3.7-11 $\times 10^{15}$ kg/yr, more than 2 orders of magnitude greater than the ridge crest flow. The most recent estimates of these fluxes are listed in Table 15.7. Some of these fluxes are substantial. The amount of Mg and U removed from seawater in this way is comparable to that removed by ridge crest hydrothermal systems; the Si flux to seawater exceeds that or ridge crest systems, the S flux exceeds the riverine flux.

As we noted earlier, a large fraction of the transition metals dissolved in hydrothermal fluids quickly precipitate or are scavenged by precipitation of Fe sulfides and oxyhydroxides. Additional scavenging of particle-reactive elements occurs through later precipitation of Mn oxides. Estimates of the removal flux in hydrothermal plumes are listed in Table 15.8. For Be, As and the rare earths, the plume removal flux exceeds the primary hydrothermal flux, in most cases by an order of magnitude. Thus hydrothermal plumes are a net sink such elements, even though they are enriched in vent fluids.

Effect on the Oceanic Crust

Though basalt gains Mg, loses silica, etc., such changes in major element concentrations have an insignificant effect on the oceanic crust because of the high concentrations of these elements in the basalt. Minor elements may be more seriously affected. Since the basalt is subducted, these changes will ultimately affect the composition of the mantle. Quite likely, most of the water and CO_2 gained by the oceanic crust during low temperature alteration are lost during subduction. However, there

may be important effects are on those elements involved in radioactive decay schemes. We have noted the Sr isotope ratio of basalt changes as a result of reaction with hydrothermal fluids. The Rb/Sr ratio also changes and there appears to be a net decrease in Rb/Sr. REE are enriched in fluids relative to seawater, but the absolute levels are nevertheless low and the effect on the basalt is small. Thus the Sm-Nd system is little affected. The U-Th-Pb system may be profoundly affected since U, like Mg, seems to be quantitatively removed from seawater in high temperature hydrothermal reactions. Pb, on the other hand, is leached from the basalt. The net effect is an increase in the U/Pb ratio of the oceanic crust. The magnitude of the effect is, however, unclear.

Oxygen Isotope Ratios

Oxygen isotopes also behave differently at high and low temperature. At low temperature, there is a true fractionation, with the heavy isotope, ^{18}O, partitioning preferentially into the solid phase. This tends to increase the $\delta^{18}O$ of the basalt (which starts at +6) and decrease that of seawater (which starts at 0). However, because isotopic fractionation depends inversely on the square of temperature, there is a much smaller fractionation at high temperature, and the principal effect is simple isotopic exchange (mixing). As a result, the $\delta^{18}O$ of the basalt decreases and the $\delta^{18}O$ of the water increases. Muehlenbachs and Clayton (1976) suggested that these opposing reactions actually buffer the isotopic composition of seawater, maintaining a $\delta^{18}O$ of about 0. According to them, the net of low and high temperature fractionations was about +6, just the observed difference between the oceanic crust and the oceans. Thus, the oceanic crust ends up with an average $\delta^{18}O$ value about the same as it started with, and the net effect on seawater must also be close to zero.

Studies of ophiolites have confirmed that the O isotope change at high temperature just about offsets the O isotope change at low temperature, in accordance with the theory of Muehlenbachs and Clayton (1976). Based on their study of the Samail ophiolite, Gregory and Taylor (1981) estimated that the net $\delta^{18}O$ fractionation between oceanic crust and seawater is about $\Delta = 6.1$. Thus, the oceanic crust and seawater end up with a average $\delta^{18}O$ values about the same as they start with, just as Muehlenbachs and Clayton (1976) predicted. The O isotopic composition of the Samail ophiolite is shown in Figure 15.36, illustrating how the $\delta^{18}O$ ratio of the upper crust increases while that of the lower crust decreases. Ocean Drilling Project (ODP) results show much the same pattern as the Samail ophiolite, though no complete section of the oceanic crust has yet been drilled.

Let's consider this in somewhat more detail. What are the controls on the O isotope composition of seawater? Suppose seawater had a much lower $\delta^{18}O$, say -5. In this case, since the Δ for net seawater—oceanic crust interaction is 6.1, but the initial difference between oceanic crust and seawater would be 11.7, seawater—oceanic crust interaction would lower the $\delta^{18}O$ of the oceanic crust by 2.6 and increase the $\delta^{18}O$ of the water with which it reacted by 2.6 (assuming a molar water-rock ratio of 1). Over time, the $\delta^{18}O$ of seawater would gradually increase as seawater is cycled through the crust until it reached a steady-state value equal to that which results from seawater-oceanic crust interaction.

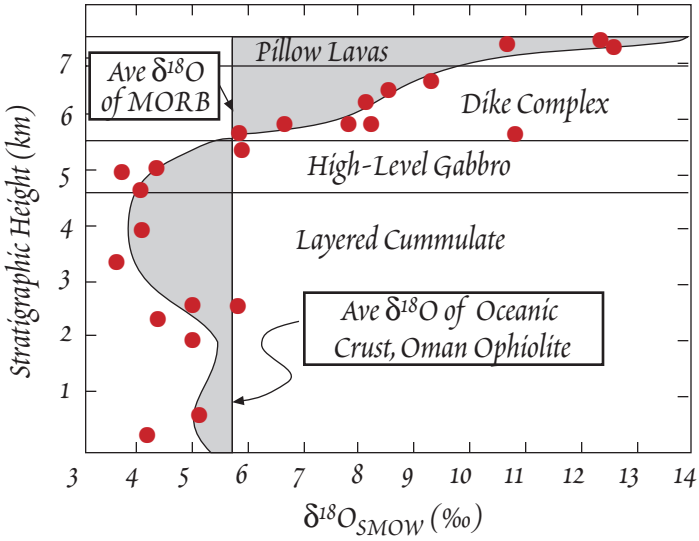

Figure 15.36. $\delta^{18}O$ variations through a cross section of the Samail ophiolite. From Gregory and Taylor (1981).

Since the average $\delta^{18}O$ of MORB is about +5.7 and that of seawater 0, whereas the Δ for the entire process is 6.1, the equilibrium seawater value,

according to Gregory and Taylor (1981), should be -0.4 per mil. This disequilibrium reflects the effect of the Antarctic and Greenland ice sheets. Ice has $\delta^{18}O$ of about -33. Storage of continental ice would tend to increase the $\delta^{18}O$ of seawater (though equilibrium crystallization of ice from seawater would result in the ice having a higher $\delta^{18}O$, this is not the process that stores ice on continents; ice is produced by evaporation and subsequent precipitation after 'Rayleigh distillation'; see Chapter 9).

The "half-time" for this process, has been estimated to be about 46 Ma. The half-time is defined as the time required for the disequilibrium to decrease by half. For example, if the equilibrium value of the ocean is 0 ‰ and the actual value is -2 ‰, the $\delta^{18}O$ of the ocean should increase to –1 ‰ in 46 Ma. It would then require another 46 Ma to bring the oceans to a $\delta^{18}O$ of –0.5‰, etc.

The Atmospheric Source

The atmosphere is, of course, the principal source and sink of dissolved gases in the ocean, but it is also a surprisingly important source of other dissolved constituents, as well as particulate matter, in the oceans. These other constituents are derived from particles in the atmosphere called *aerosols*. Aerosols have several sources: sea spray, mineral dust derived from soils and desert sands, volcanic eruptions, condensation reactions in the atmosphere, the biosphere (including fires), and anthropogenic activity such as combustion of fossil fuels, mining and mineral processing, agriculture, and the production and consumption of various chemicals. Of these sources, sea spray is the most important; natural gas-to-particle conversions, mineral dust, and anthropogenic sources are roughly equal in magnitude; biogenic sources are least important. However, sea spray does not represent a true flux to the oceans as it is derived directly from them.

Interestingly, sea spray does not have the same composition as seawater. Sea spray is enriched in trace metals and other substances. This reflects the enrichment of these elements found in the surface microlayer at the ocean-atmosphere interface. Within the microlayer, metals are adsorbed or complexed by organic substances that form a thin film on the sea surface.

The material flux from the atmosphere to the ocean may occur through *dry deposition*, which includes both settling of particles from the atmosphere and gas adsorption, and *wet deposition*. Wet deposition includes all matter, both particulate and gaseous, first scavenged from the atmosphere by precipitation (i.e., rain and snow) before being delivered to the oceans.

Though marine chemists generally now agree that the atmosphere is an important source for a variety of species in the ocean, quantifying the atmosphere-to-ocean flux is difficult. There are few actual measurements of dry deposition rates, and while there is a fair body of data on wet deposition, both dry and wet deposition rates are very heterogeneous in both space and time, due to variations in climate, wind patterns, and aerosol

Table 15.9. Atmospheric Flux to the Oceans

Element	Atmospheric Dissolved Flux	Riverine Flux	Atmosphere/ River
N	2.14×10^{12}	2.50×10^{12}	0.86
Al	2.49×10^{11}	6.94×10^{10}	3.59
Si	9.98×10^{11}	6.67×10^{12}	0.15
P	9.69×10^{09}	1.39×10^{11}	0.07
Mn	5.94×10^{08}	5.58×10^{09}	0.11
Fe	3.44×10^{10}	1.97×10^{10}	1.75
Ni	1.62×10^{08}	1.90×10^{08}	0.85
Cu	1.78×10^{08}	1.60×10^{08}	1.11
Zn	1.55×10^{09}	9.18×10^{07}	16.92
As	4.45×10^{07}	1.33×10^{08}	0.33
Cd	4.89×10^{06}	2.70×10^{06}	1.81
La	4.10×10^{06}	5.00×10^{06}	0.82
Ce	6.50×10^{06}	6.30×10^{06}	1.03
Nd	4.40×10^{06}	4.60×10^{06}	0.96
Sm	9.10×10^{05}	1.10×10^{06}	0.83
Eu	2.00×10^{05}	3.00×10^{05}	0.67
Gd	8.50×10^{05}	1.40×10^{06}	0.61
Dy	7.20×10^{05}	1.20×10^{06}	0.60
Er	4.50×10^{05}	8.00×10^{05}	0.56
Yb	3.20×10^{05}	1.10×10^{06}	0.29
Lu	5.80×10^{04}	2.00×10^{05}	0.29
Pb	2.27×10^{08}	1.00×10^{07}	22.74

All fluxes are in moles/yr. Data from Duce et al. (1991) and Greaves et al. (1993). Fluxes for Cu, Pb, Al, and Fe modified based on revised solubilities given by Chester et al. (1993). Mn flux estimated from the crustal Mn/Fe ratio, the Fe atmospheric flux of Duce, and solubilities given in Chester et al. (1993).

source distribution. Particle concentrations can be extremely high, up to 700 μg per cubic meter of air, over the Atlantic between 30° and 5° N, where the Northeast trades carry mineral dust from Saharan dust storms. There is also a significant flux of dust from the Asian deserts to the North Pacific, though it is smaller than the Saharan dust plume. In contrast, particle concentrations re less than 0.01 $\mu g/m^3$ over remote areas of the South Pacific. Aerosol composition also varies widely, due both to difference in sources and fractionation that occurs as the aerosol is transported from the source area. This variability, together with the vastness of the ocean, makes it difficult to derive global fluxes.

There is considerably more data on the composition of aerosols than on actual deposition rates. Thus most estimates of the atmosphere-to-ocean flux are calculated by multiplying the mean atmospheric concentration times a deposition velocity (e.g., Chester, 1990; Duce et al., 1991):

$$F = CV \qquad 15.41$$

Estimates of deposition velocity are based on models that incorporate such factors as meteorology and the nature of the sea-air interface. The reader is referred to Duce et al. (1991) for a fuller discussion.

The next question we must ask is what fraction of the particulate matter deposited on the ocean surface dissolves? This depends both on the element and the nature of the particle. Whereas the sea spray aerosol dissolves entirely, only a fraction of the mineral aerosol dissolves. Anthropogenic particles have intermediate solubilities. For example, Chester et al. (1993) found that 8% and <1% of the Al is leached by seawater from an anthropogenic aerosol collected over the U.K and a mineral dust aerosol from the Arabian Sea respectively. From these same two aerosols, 29% and 35%, respectively, of the Mn was leached.

Table 15.9 gives estimates of the atmospheric flux of dissolved matter from the oceans. The estimates were derived from the product of atmospheric concentrations, depositional velocities, and solubilities. These data suggest that the atmosphere is the principal source of dissolved Al, Fe, Cu, Zn, Cd, Ce, and Pb in the ocean. However, the fluxes of Cu, Zn, Cd, and Pb are primarily anthropogenic, as are the fluxes of Ni and As. Hence these fluxes do not necessarily represent the steady state for these elements. The fluxes of Al, Fe, and Ce are, however, primarily due to mineral dust, so that even in the absence of anthropogenic activity, the atmosphere may be the principal source of these elements.

Sedimentary Sinks and Sources

Sediments are, in one way or another, the major sink for dissolved matter in the oceans. There are several ways in which elements find their way into sediments: (1) biologic uptake, (2) scavenging by organic particles, (3) scavenging or adsorption by or reaction with clay and other particles, (4) precipitation of, coprecipitation with, or adsorption by hydroxides and oxides, and (5) precipitation as evaporite salts. In addition, diffusion of dissolved species into or out of sediments may occur. In the latter case, sediments may serve as a source, rather than a sink, for a particular element.

Biogenic Sediments and Evaporites

As we have seen, biological activity controls the distribution of not only the major nutrients but also the micronutrients. Biogenic particles incorporated in sediment are an important sink for such elements. About 60% of the ocean floor is covered with biogenic siliceous and calcareous oozes. However, the cycle of biologically utilized elements is not simple. For example, it is estimated that the residence time of SiO_2 in seawater before biological utilization is some 200-300 years. But the overall residence time is about 18,000 yrs. In other words, a Si atom will cycle between seawater and biogenic SiO_2 an average of 60 to 90 times before leaving the oceans for good. Recalling that Si is a refractory nutrient, we can expect that labile nutrients, such as P, Ni, and Cd, are recycled many more times before finally leaving the system. Biogenic opal and carbonate particles also scavenge other dissolved components from seawater as they fall through the water column, hence biogenic sediments serve as a sink even for elements not biologically utilized.

Bathymetric and oceanographic factors control the distribution of biogenic sediments. As we found earlier, calcareous oozes are found only above the carbonate compensation depth because of the increasing solubility of carbonate with depth. The distribution of siliceous oozes, on the other hand, is

largely independent of depth and reflects the biological productivity in overlying surface water. Siliceous oozes are found beneath the Pacific equatorial high productivity belt and beneath the productive waters at high latitudes, particularly in the Southern Ocean.

Burial of significant fractions (>0.5%) of organic matter in sediments is unusual and restricted to highly productive upwelling areas. In such circumstances, the downward flux of organic matter is greater than what can be consumed by scavenging organisms. Organic carbon that survives early diagenesis may eventually be converted to petroleum, as we found in Chapter 14. The coast of Southern California in one example of an area of petroleum generation. Beneath other upwelling areas, phosphorite actively precipitates from P-rich sediment pore waters. The P has been redissolved from sediment originally enriched in P because of the high flux of organic matter to the bottom.

Evaporites are an important sink for several of the major species in seawater, such as Na, Cl, K, and SO_4. As their name implies, they form when seawater is evaporatively concentrated. When this occurs, salts precipitate in the order calcium carbonate, $CaSO_4 \bullet H_2O$ (gypsum), NaCl (halite), $MgSO_4$, NaBr, and KCl. However, evaporites rarely form in a closed system. Open system evaporation, where seawater is supplied and removed from a basin, but at rates such that saturation in the least soluble salts is maintained, but saturation of the more soluble salts not achieved. Such a system can produce extensive gypsum, or gypsum and halite, layers without precipitation of subsequent salts. Significant evaporite formation is episodic; there are only a few places where evaporites are currently form, and in all cases the volume of salt precipitating is inconsequential for the marine budget. Nevertheless, there are many examples of ancient massive evaporites in the sedimentary record. For example, much of the Mediterranean Sea is underlain by evaporites that formed some 5 million years ago when that Sea's connection to the rest of the ocean was cut by tectonic processes. Hence over geologic time, evaporites do represent a major sink for major ions. It is estimated that evaporite deposits contain about as much Cl as do the oceans.

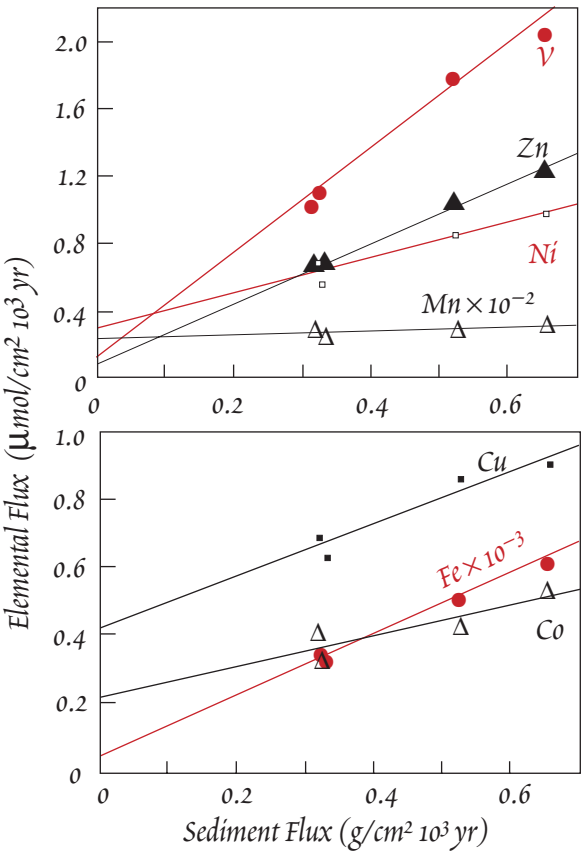

Figure 15.37. Elemental accumulation rate plotted against sedimentation rate for Nares Plain sediments. (After Thomson et al., 1984).

Red Clays, Metalliferous Sediments, and Mn Nodules

Lithogenous particles also scavenge dissolved components from seawater. The predominant sediment in the deep, remote areas of the world ocean is *red clay*. Red clays consist of lithogenous particles, derived from the continents and delivered by winds or rivers, that are strongly enriched in transition metals and other particle-reactive elements. Indeed, their brownish red appearance and name reflect their iron-rich nature.

Why red clays are so much more enriched in these elements than rapidly accumulating sediments is best illustrated by a study of Atlantic sediments by Thomson et al. (1984). In the Nares Abyssal Plain (northeast of Puerto Rico), both 'red' and 'gray' clays occur. The gray clays are fine-grained distal ends of turbidity currents originating on the North American shelf. Red clays are restricted to areas of low sedimentation rate and have a lower $^{87}Sr/^{86}Sr$ ratio than gray clays (0.722 vs. 0.728). However, after leaching the $^{87}Sr/^{86}Sr$ of the two were identical.

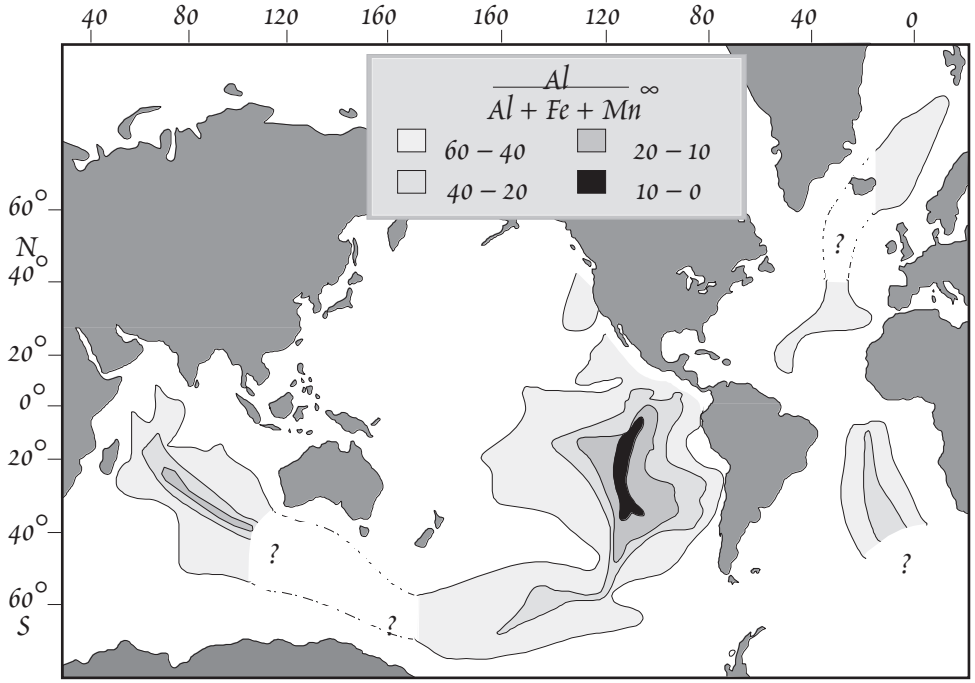

Figure 15.38. Distribution of metalliferous sediments in the oceans. From Edmond et al. (1982).

Thomson et al. (1984) also found that when the sedimentation flux of a specific element was plotted against overall sedimentation rate, a straight line resulted whose intercept was greater than zero (Figure 15.37), implying there was a flux of the metals even when there was no sediment flux! How can this be?

The interpretation is as follows. The red and gray clay both had the same origin on the North American continent, but the red clay, which accumulates slowly, contained an adsorbed component of seawater Sr ($^{87}Sr/^{86}Sr$=0.709), which could be removed by leaching. Metals were also adsorbed on the gray clays, but less so because they had spent a shorter had spent a shorter period exposed to seawater than the red clay particles. The non-zero intercept indicates authigenic flux of elements such as Fe and Mn, the value of the authigenic flux being independent of the flux of sediment to the bottom. When sedimentation rates are high, the authigenic component is simply highly diluted. Lack of this dilution at low sedimentation rates results in high Fe and Mn concentrations.

Another means of removal of elements from seawater is precipitation of oxides and hydroxides, principally of Mn and Fe, and coprecipitation or adsorption of particle-reactive elements by them. This occurs in two principle ways. The first is in hydrothermal plumes. As we found in above, hydrothermal fluids are enriched in Fe^{2+} and Mn^{2+}. Fe quickly oxidizes and precipitates. Oxidation of Mn is somewhat slower, so that most precipitation is delayed until the plume becomes neutrally buoyant and begins to spread laterally. As they settle out of the water column, precipitated particles then scavenge other particle-reactive elements from seawater. When these hydrothermal particles are abundant, they produce so-called "metalliferous sediment". Al is not enriched in hydrothermal fluids and Al in marine sediments is derived entirely from continental sources. Thus sediments enriched in hydrothermally derived particles will have low ratios of Al/(Al+Fe+Mn). Figure 15.38 shows the distribution of these metal-rich sediments. Highest concentrations of metalliferous sediments are found near the mid-ocean ridges, particularly adjacent fast spreading regions of the EPR, but the influence of hydrothermal plumes can still be seen thousands of kilometers from the ridge crest.

Mn and Fe oxides and hydroxides may also precipitate directly on the seafloor, with a previously existing surface acting as a nucleation site. In sediment-covered areas, shards of volcanic glass, shark's teeth and other such particles may serve as a nucleation site, with the Mn-Fe precipitates eventually forming a coating of up to 10 or more centimeter diameter. Typically, the form flattened spheres with botryoidal, smooth, or rough surfaces. These are known as *manganese nodules*. Solid surfaces, such as the surface of a lava flow, may also provide a nucleation site. In this case, the Mn-Fe precipitates will form a coating on the surface up to several cm thick. Such coatings are known as *manganese crusts*. These nodules and crusts grow extremely slowly and occur only in areas of low sedimentation rate. They are most common in the deep basins of the Central Pacific, as low sedimentation rates are most common there, but they also occur in the other oceans. Nodules and crusts also occur on seamounts, mid-ocean ridges, and some areas of continental margins.

Mn nodules and crusts consist principally of mixtures of δMnO_2, birnessite (also called 7Å manganite), toderokite (also called 10Å manganite), and amorphous iron hydroxide ($FeOOH \bullet nH_2O$). δMnO_2, birnessite, and manganite all consist of primarily of sheets of MnO_2, but differ in their structure and the amount of water and other metals they contain. Their average composition is given in Table 15.10. As Mn and Fe particles of hydrothermal plumes, nodules and crusts scavenge other particle-reactive elements from solution so that they are usually strongly enriched in several transition metals as well as other particle reactive elements such as the rare earths, as may be seen from Table 15.10. This enrichment has generated interest in the possibility of mining nodules for Ni, Cu, and Co, but while mining companies have invested in exploration and research on Mn nodules, no large scale mining operations have been undertaken yet.

Nodules may grow by precipitation* from seawater or by precipitation from sediment pore waters. Nodules growing from seawater are called "hydrogenous"; those growing from sediment pore waters

Table 15.10. Average Composition of Manganese Nodules and Crusts

Element	Average Conc. wt. percent	Enrichment Factor	Element	Average Conc. ppm	Enrichment Factor
Na	1.94	0.82	B	277	27.7
Mg	1.82	0.78	Sr	830	2.2
Al	3.06	0.34	Y	310	9.39
Si	8.62	0.31	Zr	648	3.92
P	0.22	2.13	Mo	412	274.7
K	0.64	0.31	Pd	0.0055	0.83
Ca	2.47	0.56	Ag	6	85.7
Sc	0.00097	0.44	Cd	7.9	39.5
Ti	0.65	1.14	Sn	2.7	13.5
V	0.056	4.13	Te	50	
Cr	0.0035	0.35	La	160	5.33
Mn	16.02	168.6	Yb	31	10.33
Fe	15.55	2.76	W	60	40
Co	0.28	113.6	Ir	0.00935	70.83
Ni	0.48	64.0	Au	0.00248	0.62
Cu	0.26	47.0	Hg	0.50	6.25
Zn	0.078	11.2	Tl	129	286.66
Ga	0.001	0.67	Pb	900	72.72
Ba	0.20	4.73	Bi	8	47.05

From Cronan, 1980. Enrichment Factor is the enrichment over average continental crust.

* Hydrogenous nodules and crusts may grow primarily from colloidal, rather than dissolved, Mn and Fe in seawater. Strictly speaking, then, the process is not one of precipitation and accumulation may better term.

and are called "diagenetic". Hydrogenous nodules tend to be dominantly composed of δMnO_2, while toderokite is more common in diagenetic nodules. Dymond et al. (1984) distinguished two kinds of diagenetic growth: oxic and suboxic. Suboxic diagenetic nodules occur beneath high productivity regions where sufficient organic matter reaches the sediment that they become reducing at depth, thereby mobilizing Mn as Mn^{2+}. Most nodules are of mixed diagenetic and hydrogenetic origin, growing both upward by precipitation from seawater and downward, by precipitation from porewater. This produces a compositional difference between the tops and bottoms of nodules. In contrast to nodules, crusts, which form on impermeable surfaces, grow by accretion from seawater and are thus strictly "hydrogenous". Near mid-ocean ridges and other submarine volcanos, crusts may grow primarily from metals provided by hydrothermal vents. Such crusts are termed "hydrothermal".

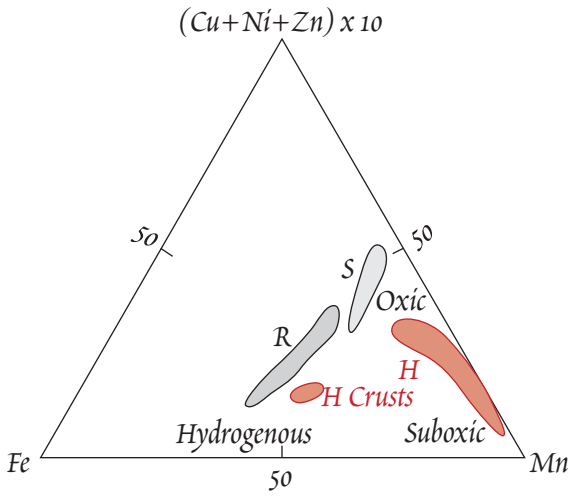

Figure 15.39. Fe, Mn, and Cu, Ni, and Zn concentrations of nodules and crusts from three sites in the eastern equatorial Pacific analyzed by Dymond et al. (1984). Nodules from the red clay site (Site R) have combined hydrogenous and oxic diagenetic growth mechanisms. Nodules from the siliceous ooze site (Site S) grow predominantly through oxic diagenesis. Nodules from the hemipelagic site (Site H) grow primarily by suboxic diagenesis, which results from high organic matter content of the sediment. Crusts from site H, which are hydrogenous, are compositionally similar to site R nodules. From Dymond et al. (1984).

As mentioned, most Mn nodules grow extremely slowly, rates of 3-5 mm/Ma are typical. Growth rates of suboxic diagenetic nodules may be substantially higher, up to 200 mm/Ma. The slow growth explains why nodules are found only in areas of low sedimentation rate: in other areas, the nuclei are buried before having a chance to grow. Nevertheless, many nodules appear to grow are rates lower than the local sedimentation rate. Even more puzzling, they are concentrated at the sediment surface: there are typically twice as many nodules at the sediment surface as buried in the upper meter of sediment. This appears to be due to the action of burrowing organisms that keep the nodules at the sediment surface. Nodules vary greatly in abundance, both regionally and locally. This variation is largely related to sedimentation rate. On a local scale, nodules are more abundance on topographic highs, apparently because currents can keep such areas relatively sediment-free.

There are significant variations in the composition of nodules and crusts, as is shown in Table 15.11. These variations are related to the growth mode and variations in the supply of metals (Figure 15.39). Hydrogenous crusts and nodules tend to be richest in Fe and Co. Nodules growing principally through oxic diagenesis are richest in Cu, Ni, and Zn, while suboxic diagenetic nodules are rich in Mn and depleted in Co. Hydrothermal crusts are generally poor in Fe as well as Co, Ni, and Cu. Even within a single genetic type, however, significant compositional variations occur. In a study of Mn crusts from the Line Islands in the central equatorial Pacific, Aplin and Cronan (1984) found that the concentrations of most trace metals, including Co, Ni, Cd, Mo, Zn, and Pb were highest in crusts from depths of less than 2000 m. These crusts also had the highest Mn concentrations. Concentrations of Fe, Cu, and Be were highest in those crusts from >2000 m depth. Aplin and Cronan (1984) suggested these variations reflected higher concentrations of dissolved and colloidal Mn at depths of 1000 to 2000 m in the Pacific. This Mn enrichment results from both reductive dissolution of particulate Mn in the oxygen minimum and horizontal advective transport of Mn diffusing out of sediments of the continental margins. They argued that variation in concentrations of other metals primarily reflects the differing affinities of these metals for Fe and Mn oxide surfaces, with elements such as Co, Ni, Cd, and Mo being particularly strongly scavenged by Mn oxides compared to Fe oxides.

TABLE 15.11. COMPARISON OF COMPOSITION OF DIFFERENT MARINE FE-MN DEPOSITS.

	Hydrogenous Crust	Oxic Diagenetic Nodule	Suboxic Diagenetic Nodule	Hydrothermal Crust	Hydrothermal Crust
Mn (wt %)	22.2	31.65	48.0	41.0	55.0
Fe (wt %)	19.0	4.45	0.49	0.8	0.2
Co ppm	1300	280	35	33	39
Ni ppm	5500	10100	4400	310	180
Cu ppm	1480	4400	2000	120	50
Zn ppm	750	2500	2200	400	2020
Mn/Fe	1.2	7.1	98	51	275

From Chester (1990).

Diffusion Into and Out of Sediments

Sediments can serve as a sink for dissolved matter in yet another way: through diffusion of dissolved components into sediments. Dissolved components may also diffuse out of sediment poor waters into seawater, or pore water may be expelled by compaction. In these latter cases, sediments serve as a source of dissolved matter in seawater. As we found in Chapter 5, diffusion occurs only when a compositional gradient exists. Sediment pore water originates simply as seawater trapped between sedimentary particles. Its composition is thus initially identical to seawater. Reactions occurring within the sediment, however, produce changes in pore water composition, establishing chemical gradients that drive diffusion into or out of the sedimentary column. Furthermore, as sediment is buried beneath subsequently accumulating material, it is compacted, driving pore water back into the overlying seawater, producing a flux of porewater-enriched components to seawater. In this section we consider the examples of two elements: U and Li. Diffusion into sediments is an important sink for dissolved U, while diffusion and porewater expulsion is an important source of dissolved Li in the oceans.

U is present in seawater in the VI state, generally as the soluble uranyl tricarbonate species ($UO_2(CO_3)_3^{-4}$). The reduced species, however, U (IV) is relatively insoluble. While seawater only rarely becomes reducing (examples are the deep or bottom waters of the Black Sea, some fjords, and the Cariaco Trench), suboxic or anoxic conditions are more frequently achieved at depth in marine sediments. This occurs in regions where there is a flux of high organic carbon to the seafloor as a result of high biological productivity in the overlying surface water. Such areas occur most often on or near continental margins and cover roughly 8% of the total area of the sea floor.

Figure 15.40a shows an example of the U profiles determined by Klinkhammer and Palmer (1991) in cores taken from the California continental shelf just south of the Monterey Fan. Between 1 and 2 cm depth, U pore water concentrations slightly exceed the seawater concentration (13.4 nmol/l). This results from release of U from labile organic phases in the upper part of the core. At great depths, however, U pore water concentrations to concentrations around 5 nmol/l above seawater values occur. U concentrations in the coexisting solid phase increase sharply from 2.7 ppm to 5.7 ppm at depths of 6 to 9 cm. Consumption of the 2.5% organic carbon in this core lead to suboxic conditions and reduction of U^{6+} to U^{4+}, as well as reduction of Mn and Fe. Judging from the sharp increase in U concentrations in the solid phase, it appears that pe values appropriate for reduction of U first occur at depths of around 6 cm. Increases in pore water concentrations of Mn and Fe from these cores (Figure 15.40b) suggests that Mn and Fe reduction begin within the top 2 or 3 cm of the core (this order, Mn, Fe, U, is consistent with thermodynamic prediction), because both Mn and Fe are highly insoluble in their oxidized states. Once reduced, U is immobilized in the solid phase, reducing it concentration in the pore waters. This produces a concentration gradient that causes U to diffuse downward from seawater into the sediment.

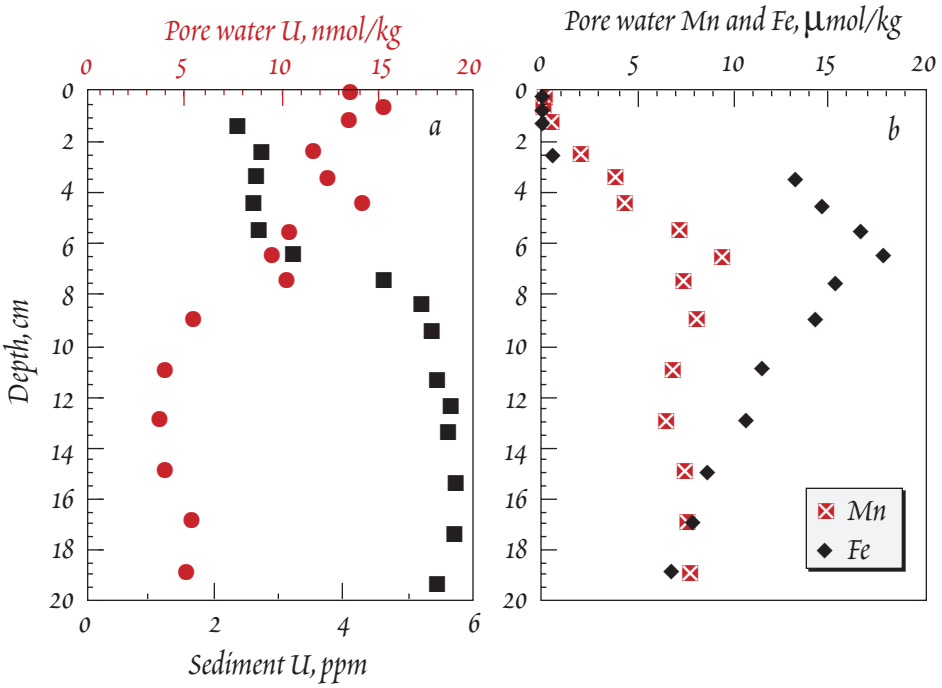

Figure 15.40. a. U concentration in sediment (black squares, in ppm) and pore waters (red circles, in nmol/kg), from the California Shelf sediments. b. Mn (red squares) and Fe (black diamonds) in the same pore waters as in (a). Data from Klinkhammer and Palmer (1991).

Organic-rich sediments tend to be rich in U generally. Whether this reflects biological uptake of U or adsorption of U on dead organic particles falling through the water column remains unclear. This U may be released when the organic matter is remineralized in the sediment, producing high concentrations of U in sediment pore water and, consequently, diffusion of U from sediments to seawater. This appears to be occurring, for example, in sediments on the Brazilian continental shelf near the Amazon River.

On the whole, diffusion into sediments appears to be dominant. Table 15.12 shows the marine U budget according to Barnes and Cochran (1990). They estimate diffusion into suboxic sediments, as exemplified by the Figure 15.39, removes 0.25 to 0.32 $\times 10^{10}$ g/yr. Klinkhammer and Palmer (1991) estimate a higher flux of 0.67 $\times 10^{10}$ g/yr for suboxic diagenesis. Both sets of authors find that this is the single largest sink for dissolved U in the oceans.

Diffusion out of sediments appears to be an important source of dissolved Li in the oceans. Li is readily incorporated into interlayer sites of clays at low temperature, with some clays mineral containing as much as 500 ppm Li. Because of it high hydration energy, however, Li is easily removed from these sites. Thus as sediments are subjected to increasing temperatures during burial, Li is lost from the sediment solid phases and its concentration in pore waters increases. This sets up a concentration gradient that drives diffusion of Li out of the sediment. Perhaps more importantly, Li-rich pore waters are expelled from the sediment as it compacts, producing a flux of dis-

Table 15.12. The Marine U Budget

Sources (10^{10} g U/yr)	
Riverine Input	1
Amazon Shelf Sediments	0.14
Total	1.14
Sinks (10^{10} g U/yr)	
Sediments	
Oxic, deep sea	0.08
Metalliferous	0.14
Underlying anoxic water	0.13
Suboxic	0.25-0.32
Corals and Molluscs	0.08
Oceanic Crust	
Low temperature	0.23
High temperature	0.04
Total	0.95-1.02

From Barnes and Cochran (1990).

solved Li to seawater. Li concentrations in pore waters and coexisting sediments from ODP Site 688 on the Peru margin analyzed by Martin et al. (1991) shown in Figure 15.41 provide an example. Concentrations increase from near seawater values (25.6 μM) at the top of the core to over 500 μM at a depth of 450 m. At the same time, Li concentrations in the sediment decrease. This decrease in Li concentration in sediments does not seem sufficient to account for the increase in pore water Li concentrations and Martin et al. (1991) speculated that additional Li was being released from underlying basement rocks.

Martin et al. (1991) estimated that expulsion of pore waters of continental margin sediments supplied 1 to 3×10^{10} moles/yr to the ocean. The high end of this estimate exceeds both the riverine flux ($1.1–1.7 \times 10^{10}$ moles/yr) and the hydrothermal flux ($0.4 – 1.3 \times 10^{10}$ moles/yr). Thus sediment pore water may be the dominant source of dissolved Li in the oceans. Even the minimum value represents a substantial flux, supplying 20-25% of the marine Li.

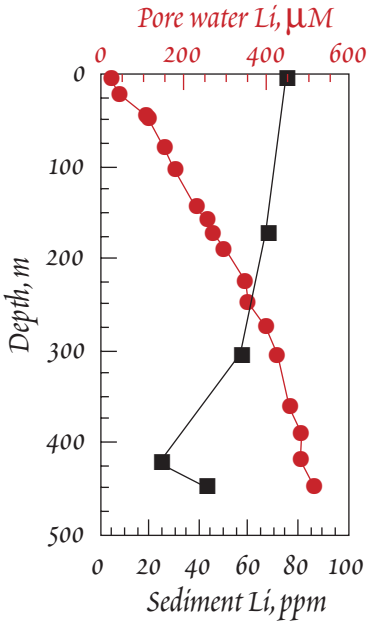

Figure 15.41. Li concentrations in pore waters (red circles, μM) and sediments (black squares) from ODP Site 688 on the Peru continental shelf. Data from Martin et al. (1991).

REFERENCES AND SUGGESTIONS FOR FURTHER READING

Alt, J. C. 1995. Subseafloor processes in mid-ocean ridge hydrothermal systems. **In** *Seafloor Hydrothermal Systems: Physical, Chemical, Biological and Geological Interactions, Geophysical Monograph Vol. 91*, S. E. Humphris, R. A. Zierenberg, L. S. Mullineaux and R. E. Thomson. ed., pp. 85-114. Washington: AGU.

Aplin, A. C. and D. S. Cronan. 1985. Ferromanganese oxide deposits from the Central Pacific Ocean, I. Encrustations from the Line Islands Archipelago. *Geochim. Cosmochim. Acta*. 49: 427-436.

Barnes, C. E. and J. K. Cochran, 1990. Uranium removal in oceanic sediments and the oceanic U balance. *Earth. Planet. Sci. Lett.*, 97: 94-101.

Barth, T. W. 1952. *Theoretical Petrology*. New York: John Wiley.

Berner, R. A. 1975. The role of magnesium in the crystal growth of aclite and aragonite from seawater. *Geochim. Cosmochim. Acta*. 39: 489-504.

Bischoff, J. L. and K. S. Pitzer. 1989. Liquid-vapor relations for the system NaCl-H2O: summary of the P-T-x surface from 300° to 500°C. *Am. J. Sci.* 289: 217-248.

Boyle, E. A., J. M. Edmond and E. R. Sholkovitz. 1977. The mechanism of iron removal in estuaries. *Geochim. Cosmochim. Acta*. 41: 1313-1324.

Boyle, E. A., F. R. Sclater and J. M. Edmond. 1977. The distribution of dissolved copper in the Pacific. *Earth Planet. Sci. Lett.* 37: 38-54.

Bowers, T. S., A. C. Campbell, C. I. Measures, A. J. Spivack and J. M. Edmond. 1988. Chemical controls on the composition of vent fluids at 13°-11°N and 21°N, East Pacific Rise. *J. Geophys. Res.* 93: 4522-4536.

Broecker, W. S. and T.-H. Peng. 1982. *Tracers in the Sea*. New York: Eldigio Press.

Bruland, K. W. 1983. Chapter 45: Trace elements in seawater. **In** *Chemical Oceanography, Vol. 8*, J. P. Riley and R. Chester. ed., pp. 157-220. London: Academic Press.

Busenberg, E. and L. N. Plummer. 1985. Kinetic and thermodynamic factors controlling the distribution of SO_4^{2-} and Na^+ in calcites and selected aragonites. *Geochim. Cosmochim. Acta*. 49: 713-726.

Chen, J. H., G. J. Wasserburg, K. L. von Damm and J. M. Edmond. 1986. The U-Th-Pb systematics in hot springs on the East Pacific Rise at 21°N and Guaymas Basin. *Geochim. Cosmochim. Acta*. 50: 2467-2479.

Chester, R., *Marine Geochemistry*, Unwin Hyman, London, 698 p., 1990.

Chester, R., K. J. T. Murphy, F. J. Lin, A. S. Berry, G. A. Bradshaw and P. A. Corcoran. 1993. Factors controlling the solubilities of trace metals from the non-remote aerosols deposited to the sea surface by the 'dry' deposition mode. *Mar. Chem.* 42: 107-126.

Chou, L., R. M. Garrels and R. Wolast. 1989. Comparative study of the kinetics and mechanisms of dissolution of carbonate minerals. *Chem. Geol.* 78: 269-282.

Craig, H. 1974. A scavenging model for trace elements in the deep sea. *Earth Planet. Sci. Lett.* 23: 149-159.

Cronan, D. S. 1980. *Underwater Minerals*. London: Academic Press.

Duce, R. A., P. S. Liss, J. T. Merrill, E. L. Atlas, P. Buat-Menard, B. B. Hicks, J. M. Miller, et al. 1991. The atmospheric input of trace species to the world ocean. *Global Biogeochem. Cycles*. 5: 193-259.

Dymond, J., M. Lyle, B. Finney, D. Z. Piper, K. Murphy, R. Conard and N. Pisias. 1984. Ferromanganese nodules from MANOP Sites H, S, and R — Control of mineralogical and composition by multiple accretionary processes. *Geochim. Cosmochim. Acta*. 48: 931-949.

Dzombak, D. A. and F. M. M. Morel. 1990. *Surface Complexation Modelling: Hydrous Ferric Oxide*. New York: Wiley Interscience.

Eckert, J. M. and E. R. Sholkovitz. 1976. The flocculation of iron, aluminum, and humates from river water by electrolytes. *Geochim. Cosmochim. Acta*. 40: 847-848.

Edmond, J. M., A. Spivack, B. C. Grant, H. Ming-Hui, C. Zexiam, et al., Chemical dynamics of the Changjiang (Yangtze) Estuary, *Cont. Shelf Res.*, 4, 17-36, 1985.

Edmond, J. M., C. Measures, R. E. McDuff, L. H. Chan, R. Collier, et al., Ridge crest hydrothermal activity and the balances of the major and minor elements in the ocean: the Galapagous data, *Earth and Planetary Science Letters*, 46, 1979.

Edmond, J.M., Von Damm, K.L., McDuff, R.E., and Measures, C.I., (1982) Chemistry of hot springs on the East Pacific Rise and their effluent dispersal. *Nature*, **297**: 187-191.

Edmonds, H. N. and J. M. Edmond. 1995. A multicomponent mixing model for ridge-crest hydrothermal fluids. *Earth Planet. Sci. Lett.* 134: 53-67.

Elderfield, H., N. Luedtke, R. J. McCaffrey and M. Bender. 1981. Benthic flux studies in Narragansett Bay. *Am. J. Sci.* 281: 768-787.

Elderfield, H., R. Upstill-Goddard and E. R. Sholkovitz. 1990. The rare earth elements in rivers, estuaries, and coastal seas. *Geochim. Cosmochim. Acta*. 54: 971-992.

Elderfield, H. and A. Schultz. 1996. Mid-ocean ridge hyddrothermal fluxes and the chemical composition of the ocean. *Annu. Rev. Earth Planet. Sci.* 24: 191-224.

Elderfield, H. and E. R. Sholkovitz. 1987. Rare earth elements in the pore waters of reducing nearshore sediments. *Earth Planet. Sci. Lett.* 82: 280-288.

Erel, Y. and J. J. Morgan. 1991. The effect of surface reactions on the relative abundances of trace metals in deep-ocean water. *Geochim. Cosmochim. Acta*. 55: 1807-1813.

Froelich, P. N., G. A. Hambrick, M. O. Andreae, R. A. Mortlock and J. M. Edmond. 1985. The geochemistry of inorganic germanium in natural waters. *J. Geophys. Res.* 90: 1131-1141.

Goldberg, E. D. and G. O. S. Arrhenius. 1958. Chemistry of Pacific pelagic sediments. *Geochim. Cosmochim. Acta*. 13: 153-212.

Greaves, M. J., P. J. Statham and H. Elderfield. 1994. Rare earth element mobilization from marine atmospheric dust into seawater. *Mar. Chem.* 46: 255-260.

Gregory, R. T. and H. P. Taylor, An oxygen isotope profile in a section of Cretaceous oceanic crust, Samail Opiolite, Oman: Evidence for $\delta^{18}O$ buffering of the oceans by deep (>5 km) seawater-hydrothermal circulation at mid-ocean ridges, *J. Geophys. Res.*, 86, 2737-2755, 1981.

Hoyle, J., H. Elderfield, A. Gledhill and M. Greives, The behavior of the rare earth elements during mixing of river and seawaters, *Geochim. Cosmochim. Acta*, 48, 143-149, 1984.

Kadko, D., J. Baross and J. Alt. 1995. The magnitude and global implications of hydrothermal flux. **In** *Seafloor Hydrothermal Systems: Physical, Chemical, Biological and Geological Interactions, Geophysical Monograph Vol. 91*, S. E. Humphris, R. A. Zierenberg, L. S. Mullineaux and R. E. Thomson. ed., pp. 446-466. Washington: AGU.

Kadko, D., E. Baker, J. Alt and J. Baross. 1994. Global impact of submarine hydrothermal processes. *RIDGE Vent Workshop*. 55p.

Keir, R. S. 1980. The dissolution kinetics of biogenic calcium carbonates in seawater. *Geochim. Cosmochim. Acta*. 44: 241-252.

Klinkhammer, G. P. and M. R. Palmer. 1991. Uranium in the oceans: where it goes and why. *Geochim. Cosmochim. Acta*. 55: 1799-1896.

Kraepiel, A. M. L., J.-F. Chiffoleau, J.-M. Martin and F. M. M. Morel. 1997. Geochemistry of trace metals in the Gironde estuary. *Geochim. Cosmochim. Acta*. 61: 1421-1436.

Lilley, M. D., F. R. A. and J. H. Trefry. 1995. Chemical and biochemical transformations in hydrothermal plumes. **In** *Seafloor Hydrothermal Systems: Physical, Chemical, Biological and Geological Interactions, Geophysical Monograph Vol. 91*, S. E. Humphris, R. A. Zierenberg, L. S. Mullineaux and R. E. Thomson. ed., pp. 369-391. Washington: AGU.

Mantoura, R. F. C., A. Dickson and J. P. Riely. 1978. The complexation of metals with humic materials in natural waters. *Estuar. Coastal Shelf Sci.* 6: 367-408.

Martin, J. B., M. Kastner and H. Elderfield. 1991. Lithium: sources in pore fluids of Peru slope sediments and implications for oceanic fluxes. *Mar. Geol.* 102: 281-292.

Martin, J. H. and R. M. Gordon. 1988. Northeast Pacific iron distributions in relation to phytoplankton productivity. *Deep Sea Res.* 35: 177-196.

Martin, J. H., K. H. Coale, K. S. Johnson, S. E. Fitzwater, R. M. Gordon, S. J. Tanner and e. al. 1994. Testing the iron phyothesis in ecosystems of the equatorial Pacific. *Nature*. 371: 123-129.

Measures, C. I., B. Grant, M. Khadem, D. S. Lee and J. M. Edmond. 1984. Distribution of Be, Al, Se and Bi in the surface waters of the western North Atlantic and Carribean. *Earth Planet. Sci. Lett.* 71: 1-12.

Millero, F. J. 1995. Thermodynamics of the carbon dioxide system in seawater. *Geochim. Cosmochim. Acta*. 59: 661-678.

Mucci, A. 1983. The solubility of calcite and aragonite in seawater of various salinities, temperatures, and one atmosphere total pressure. *Am. J. Sci.* 283: 780-799.

Muehlenbachs, K. and R. Clayton, Oxygen isotope geochemistry of submarine greenstones, *Can. J. Earth. Sci.*, 9, 471-478, 1972.

Muehlenbachs, K., Oxygen isotope composition of the oceanic crust and its bearing on seawater, *J. Geophys. Res.*, 81, 4365-4369, 1976.

Nozaki, Y. 1997. A fresh look at element distribution in the North Pacific Ocean. *EOS*. 78: 221. *(Electronic supplement may be foun at: "http://www.agu.org/eos_elec/97025e.html").*

Orians, K. J., E. A. Boyle and K. W. Bruland. 1990. Dissolved titanium in the open ocean. *Nature*. 348: 322-325.

Peterson, M. N. A. 1966. Calcite: rates of dissolution in a vertical profiel in the central Pacific. *Science*. 154: 1542-1544.

Quinby-Hunt, M. S. and K. K. Turekian. 1983. Distribution of elements in sea water. *EOS*. 64: 130-132.

Redfield, A. C. 1958. The biological control of chemical factors in the environment. *Am. J. Sci.* 46: 205-221.

Rudnicki, M. D. and H. Elderfield. 1993. A chemical model of the buoyant and neutrally buoyant plume above the TAG vent field. *Geochim. Cosmochim. Acta*. 57: 2939-2957.

Schaule, B. K. and C. C. Patterson. 1983. Perturbations of the natural lead depth profile in the Sargasso Sea by industrial lead. **In** *Trace metals in Seawater, Vol.* C. S. Wong, E. Boyle, K. W. Bruland, J. D. Burton and E. D. Goldberg. ed., pp. 487-503. New York: Plenum Press.

Seyfried, W. E. J. and K. Ding.1995. Phase equilibria in subseafloor hydrothermal systems: a review of the role of redox, temperature, pH and dissolved Cl on the chemistry of hot spring fluids at mid-ocean ridges. **In** *Seafloor Hydrothermal Systems: Physical, Chemical, Biological and Geological Interactions, Geophysical Monograph Vol. 91*, S. E. Humphris, R. A. Zierenberg, L. S. Mullineaux and R. E. Thomson. ed., pp. 248-272. Washington: AGU.

Shanks, W. C. I., J. K. Böhlke and S. R. R. II. 1995. Stable isotopes in mid-ocean ridge hydrothermal systems: interactions between fluids, minerals, and organisms. **In** *Seafloor Hydrothermal Systems:*

Physical, Chemical, Biological and Geological Interactions, Geophysical Monograph Vol. 91, S. E. Humphris, R. A. Zierenberg, L. S. Mullineaux and R. E. Thomson. ed., pp. 194-221. Washington: AGU.

Sholkovitz, E. R. 1976. Flocculation of dissolved organic and inorganic matter during the mixing of river water and seawater. *Geochim. Cosmochim. Acta*. 40: 831-845.

Sholkovitz, E. R. 1978. The flocculation of dissolved Fe, Mn, Al, Cu, Ni, Co and Cd during estuarine mixing. *Earth Planet. Sci. Lett.* 41: 77-86.

Sholkovitz, E. R. 1992. Chemical evolution of rare earth elements: fractionation between colloidal and solution phases of filtered river water. *Earth Planet. Sci. Lett.* 114: 77-84.

Sholkovitz, E. R., E. A. Boyle and N. B. Price. 1978. The removal of dissolved humic acids and iron during estuarine mixing. *Earth Planet. Sci. Lett.* 40: 130-136.

Sholkovitz, E. and D. Copland. 1981. The coagulation, solubility and adsorption properties of Fe, Mn, Cu, Ni, Cd, and Co and humic acids in river water. *Geochim. Cosmochim. Acta*. 45: 181-189.

Stanley, J. K. and R. H. Byrne. 1990. Inorganic speciation of zinc(II) in seawater. *Geochim. Cosmochim. Acta*. 54: 753-760.

Staudigel, H., T. Plank, W. White and H.-U. Schmincke. 1996. Geochemical fluxes during seafloor alteration of the basaltic upper oceanic crust: DSDP sites 417 and 418. **In** *Subduction: Top to Bottom, Geophysical Monograph Vol. 96*, G. Bebout, D. W. Scholl, S. H. Kirby and J. P. Platt. ed., pp. 19-37. Washington: AGU.

Stumm, W. and J. J. Morgan. 1996. *Aquatic Chemistry*. New York: Wiley Interscience.

Stuvier, M., P. Quay and H. G. Ostland. 1983. Abyssal water carbon-14 distribution and the age of the world oceans. *Science*. 219: 849-851.

Takahashi, T. 1989. The carbon dioxide puzzle. *Oceanus*. 32 (2): 22-29.

Taylor, S. R. and S. M. McLennan. 1985. *The Continental Crust: Its Composition and Evolution*. Oxford: Blackwell Scientific Publications.

Thompson, G. A., Hydrothermal fluxes in the ocean, in *Chemical Oceanography, vol8*, edited by J. P. Riley and C. R., p. 270-337, Academic Press, London, 1983.

Thomson J., M. S. N. Carpenter, S. Colley, T. R. S. Wilson, H. Elderfield, and H. Kennedy. 1984. *Geochim. Cosmochim. Acta*, 48:1935-1948.

Turner, D. R., M. Whitfield and A. G. Dickson. 1981. The equilibrium speciation of dissolved components in freshwater and seawater at 25°C and 1 atm pressure. *Geochim. Cosmochim. Acta*. 45: 855-882.

Von Damm, K. L. 1988. Systematics of and postulated controls on submarine hydrothermal solution chemistry. *J. Geophys. Res.* 93: 4551-4562.

Von Damm, K. L. 1995. Controls on the chemistry and temporal variablility of seafloor hydrothermal systems. **In** *Seafloor Hydrothermal Systems: Physical, Chemical, Biological and Geological Interactions, Geophysical Monograph Vol. 91*, S. E. Humphris, R. A. Zierenberg, L. S. Mullineaux and R. E. Thomson. ed., pp. 222-247. Washington: AGU.

Von Damm, K. L. and J. L. Bischoff. 1987. Chemistry of hydrothermal solutions from the southern Juan de Fuca ridge. *J. of Geophys. Res.* 92: 11334-11346.

Von Damm, K. L., J. M. Edmond, B. Grant and C. K. Measures. 1985. Chemistry of submarine hydrothermal solutions at 21° N, East Pacific Rise *Geochimica et Cosmochimica Acta*. 49: 2197-2220.

Wong, C. S., E. Boyle, K. W. Bruland, J. D. Burton and E. D. Goldberg (ed.), 1983, *Trace Metals in Seawater*, New York: Plenum Press.

Zhong, S. and A. Mucci. 1993. Calcite precipitation in seawater using a constant addition technique: a new overall reaction kinetic expression. *Geochim. Cosmochim. Acta*. 57: 1409-1418.

Zuddas, P. and A. Mucci. 1994. Kinetics of calcite precipitation from seawater: I. a classical chemical description for strong electrolyte solutions. *Geochim. Cosmochim. Acta*. 58: 4353-4352.

CHAPTER 15: OCEANS

PROBLEMS

1. In Figure 15.7, the $\delta^{13}C$ profile shows a pronounced maximum whereas the ΣCO_2 profile does not. Why? (*HINT:* Organic matter is decomposed rapidly in the ocean, calcium carbonate dissolves much more slowly).

2. A number of reaction mechanisms have been proposed for the precipitation of calcite from seawater. These include

$$Ca^{2+} + HCO_3^- \rightleftarrows H^+ + CaCO_3$$
$$Ca^{2+} + CO_3^{2-} \rightleftarrows CaCO_3$$
$$Ca^{2+} + 2HCO_3^- \rightleftarrows H_2CO_3 + CaCO_3$$
$$Ca^{2+} + HCO_3^- + OH^- \rightleftarrows H_2O + CaCO_3$$

Suggest a series of laboratory experiments that you could performed that would enable you to distinguish which of these mechanisms actually occurs. Assume you have a well equiped laboratory in which you can measure all macroscopic properties (i.e., concentrations, partial pressure, pH, carbonate alkalinity). Describe what properties you would measure and how you would use the data you obtained to descriminate between these mechanisms.

3. How does calcite solubility vary with temperature and pressure in the ocean? Assume that temperature can be represented by a simple function of pressure:

$$T = 24\, e^{-P/5} + 1$$

where pressure is in MPa and temperature in °C. Make a plot of the solubility product as a function of depth between 0 and 5000 m using the equations in Examples 15.2 and 15.3. (Hint: remember to use thermodynamic temperature).

4. Composition of seawater
(a.) Calculate the molar concentrations of the major ions in seawater listed in Table 15.2.
(b.) Calculate the ionic strength of this solution.
(c.) Using the equilibrium constants in Table 12.1, calculate the concentration of carbonate ion in equilibrium with this solution at 25°C.
(d.) Calculate the total alkalinity of this solution assuming a pH of 8.1.

CHEMICAL DATA FROM THE NORTH PACIFIC

Depth	Salinity	Cu	Ni	Al
0		0.54	2.49	90
75	33.98	0.69	2.9	88
185	33.92	0.91	3.79	84
375	34.05	1.45	5.26	70
595	34	1.9	7.49	60
780	34.19	2.15	9.07	52
985	34.37	2.38	9.64	48
1505	34.55	2.8	9.79	45
2025	34.61	3.18	10.6	47
2570	34.65	3.46	10.8	50
3055	34.66	3.9	10.9	54
3533	34.66	4.26	10.7	63
4000	34.67	4.57	10.8	66
4635	34.68	5.03	10.3	74
4875	34.68	5.34	10.4	79

Concentrations in nmol/kg; salinity in ppt.

5. Use the *one-dimensional advection diffusion model* in the depth interval of 595m to 4875 m and the chemical data from the North Pacific in the adjacent table to answer the following questions. For this locality, the ratio K was determined to be 2300 and ω to be 4. Is salinity conservative and the one-dimensional model applicable? Make a plot of S vs. $f(z)$ (equation 15.33). Are Cu, Ni, and Al conservative? Are they being produced or scavenged? For each of these elements, find a value of ψ or J to fit the one-dimensional advection-diffusion model to the data.

6. Stanley and Byrne (1990) give the following stability constants for Zn complexes in seawater:

$$Zn^{2+} + Cl^- \rightleftarrows ZnCl^- \qquad \beta^* = -0.40$$
$$Zn^{2+} + HCO_3^- \rightleftarrows ZnHCO_3^+ \qquad \beta^* = 0.83$$

$$Zn^{2+} + CO_3^{2-} \rightleftarrows ZnCO_3 \qquad \beta^* = 2.87$$
$$Zn^{2+} + 2CO_3^{2-} \rightleftarrows Zn(CO_3)_2^{2-} \qquad \beta^* = 4.41$$
$$Zn^{2+} + H_2O \rightleftarrows Zn(OH)^+ + H^+ \qquad \beta^* = -9.25$$
$$Zn^{2+} + SO_4^{2-} \rightleftarrows ZnCO_4 \qquad \beta^* = 0.90$$

Using these stability constants, a pH of 8.1, the ligand concentrations given in Table 15.2 (and the equilibrium concentration of carbonate ion calculated with the equilibrium constant in Table 6.1 for a temperature of 25°C), calculate the fraction of Zn present as each of these species plus free Zn^{2+}.

7. Using the flows of water through mid-ocean ridge crest and flank hydrothermal systems and the mass of the oceans given in Appendix I, how long does it take to cycle the entire ocean through these systems?

8. In the San Clemente Basin, off the southern California coast, Barnes and Cochran (1990) found that U concentrations in sediment pore waters decreased to 3.35 nM/l in the top 7 cm of sediment. Assuming an effective diffusion coefficient (corrected for porosity and tortuosity in the sediment) of 68.1 cm^2/yr, calculate the flux (in nM/cm^2) of U from seawater to sediment in this locality.

9. Using the fluxes of U to the ocean in Table 15.11, estimate the residence time of U in the ocean.